Textural variants of iron ore from Malmberget: characterization, comminution and mineral liberation

Pierre-Henri KOCH

Luleå, June 2013

Presented in partial fulfillment of the requirements for the degree of master in Geology and Mining Engineering

Supervisor: Prof. Pertti Lamberg

Department of Civil, Environmental and Natural Resources Engineering
Division of Sustainable Process Engineering
Luleå University of Technology (LTU)

Department ArGEnCo : Architecture, Géologie, Environnement et Constructions
Division GeMMe : Génie Minéral, Matériaux et Environnement
Université de Liège (ULg)

Abstract

Geometallurgy combines geology and mineral processing into a spatially-based predictive model and is a useful tool that can be used in production management of a mineral processing plant. Two main complementary approaches exist to establish this model. Geometallurgical testing relies on direct measurement of the response of the ore in the processing circuit by conducting several small scale metallurgical tests. The mineralogical approach relies on proper ore characterization and process modeling on mineral basis. Because the latter is generic and applicable to any type of mineral deposit, it was chosen as the main basis of this study and combined with rock mechanics as basic geometallurgical testing.

This work presents comminution characterization of different textural variants of the breccia (semi-massive) iron ore from Malmberget, Northern Sweden. Experimental work includes Point Load Tests, Compressive Tests, comminution as laboratory crushing and grinding, mineralogical characterization and liberation measurements of the products. The results give quantitative information on how physical properties, modal mineralogy and mineral textures are related to comminution and mineral liberation. This work is directly linked with three on-going Ph.D. projects at LTU and contributes to a framework on how mineral textures and liberation information can be included in a geometallurgical model.

Keywords: Geometallurgy, liberation analysis, Malmberget, apatite iron ore, ore breccia

Abstract (Swedish)

Geometallurgi kombinerar geologi och mineralprocesser i en prediktiv rumsligt-baserad modell. Det är ett användbart verktyg som kan användas i produktionsstyrningen vid anriknings- och metallurgiska processer. Huvudsakligen finns det två metoder för att utveckla denna modell. De geometallurgiska testerna, förlitar sig på den direkta metallurgiska responsen som malmen ger från flera småskaliga metallurgiskatester. Det mineralogiska tillvägagångssättet bygger på en korrekt malmkarakterisering och process modellering av fyndighetens kvantitativa mineralogi. Eftersom den senare är mer allmän och är tillämpningsbar för de flesta malmfyndigheterna, valdes den i denna studie.

I detta master arbete presenteras en kross- malbarhetens karakterisering av olika texturella varianter av en malm breccia (semi-massiv malm), från Malmberget apatitjärn fyndighet i norra Sverige. Det experimentella arbetet består utav punktlast-tester, tryckprovning, laborationer, krossning och malningstester med tillhörande frimalningsmätningar av de olika produkterna. Resultatet ger en kvantitativ information om de fysiskaliska egenskaperna, den modala mineralogin och hur mineral texturerna är relaterade till malbarhet och frimalning av olika mineral. Detta arbete är direkt sammankopplat med tre pågående doktorandprojekt vid Luleå Tekniska universitet och bidrar till en struktur om hur information om mineraltexturer och frimalning kan ingå i en geometallurgical modell.

Preface

This is the final report of the master thesis “Textural variants of iron ore from Malmberget : characterization, comminution and mineral liberation“ started in January 2013 and finished in June 2013 at Luleå University of Technology in Luleå, Sweden in the division of Sustainable Process Engineering of Luleå tekniska universitet (LTU), supervised by Prof. Pertti Lamberg. A presentation of this work has been done the 6 of June 2013 at LTU and the 14 of June in Koskullskulle (Malmberget) Research Center for LKAB.

Luossavaara-Kiirunavaara Aktiebolag (LKAB) is gratefully acknowledged for funding this work, providing samples, X-Ray fluorescence analysis and help.

This work would not have been possible without the help and assistance of

- Prof. Pertti Lamberg (LTU), supervisor
- Prof. Jan Rosenkranz (LTU), examiner
- Abdul Mwanga (LTU) PhD, co-supervisor
- Cecilia Lund (LTU) PhD, co-supervisor
- Therese Lindberg (LKAB), Geometallurgy@LKAB
- Prof. Eric Pirard (ULg), home university supervisor

May Coralie, my family and friends also be thanked here for their support.

Table of content

Table of figures

1. Introduction

Malmberget is a large iron ore mine located in northern Sweden (Norrbotten County) operated by LKAB. The deposit has proven reserve of 174 million tons (Mt) at 42.4 % Fe (probably 105 Mt at 41.2 % Fe) and mineral assets besides mineral reserves of 21 Mt measured at 48.9 % Fe , 175 Mt indicated at 45.7 % Fe and 30 Mt inferred at 44.2 % Fe (LKAB 2011). The total size of the deposit is estimated to 840 Mt at 51 to 61 % Fe (Weiheid P 2008).

The total number of iron deposits in northern Norrbotten is about 40, with an iron grade ranging from 30 to 70 %, varying magnetite/hematite ratio, a phosphorus content between 0.05 and 5 and in most of them show strong LREE and moderate Th enrichment.

To enable more effective utilization of the ore body and production management, LKAB is evaluating the feasibility of a geometallurgical program in Kiruna (Niiranen et al. 2012) and Malmberget (Lund et al., in prep)

a. Regional geology

The oldest rocks of the Norrbotten province belong to Archean basement (granitoid-gneiss) ending with intrusive tonalite-granodiorite (2.8 Ga). This first group has been intruded by multiple groups of dykes (mafic).

On top of it comes the Kovo Group (2.5 – 2.3 Ga) ranging from clastic sediments to volcanic rocks in a context of a rift. The following group is the Kiruna Greenstones consisting of a base layer of komatiites and basalts, a middle layer of carbonates and volcaniclastic sediments and the end term with MORB-type lava (Martinsson 1997, Martinsson 2004). This sequence underwent metamorphism and deformation during the Svecokarelian orogen (1.9–1.8 Ga).

The Haparanda Suite is an early orogenic rock series that contains calc-alkaline volcanic rocks dated to 1.9 – 1.88 Ga (Öhlander 1984, Weihed, Arndt et al. 2005). The next sequence is the Perthite monzonite suite (chemically similar to the Kiirunavaara Group and dated from 1.88 to 1.86 Ga) which consists of more alkaline magmatic rocks. Malmberget deposit is linked to the Porphyry Group (cf. Figure 1) and the Kiruna deposit both in space and time with a genesis dated from 1.88 Ga (Romer 1994). From 1.81 to 1.78 Ga, the Lina suite intrusions displayed a magmatic activity linked to the Svencofennian orogen by

the fusion of parts of the middle crust (Weihed, Arndt et al. 2005). A simplified view of these series and events is presented on Figure 1.

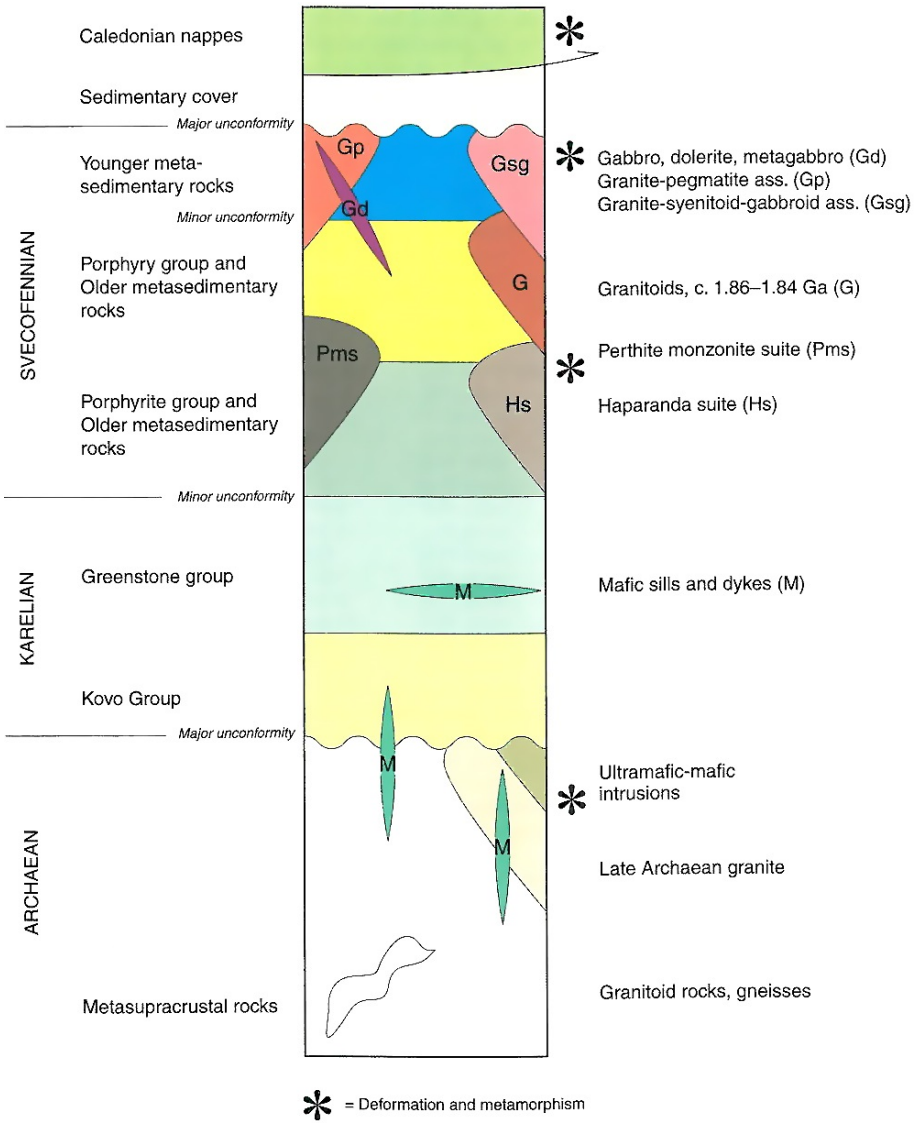

Figure 1 : Main events and series in the northern Norrbotten province (Bergman, Kübler, & Martinsson, 2001), not to scale.

b. Deposit geology

The Malmberget deposit consists of more than 20 iron ore bodies of varying mineralogy. Characteristic for Malmberget is the deformed and metamorphosed nature of the host rocks. Ductile deformation and at least two phases of folding produced the ore lenses, many of which exhibit boudinaged structures along the dipping direction (Bergman 2001). Figure 2 shows the geological setting of the ore in Malmberget with the names of the different ore bodies.

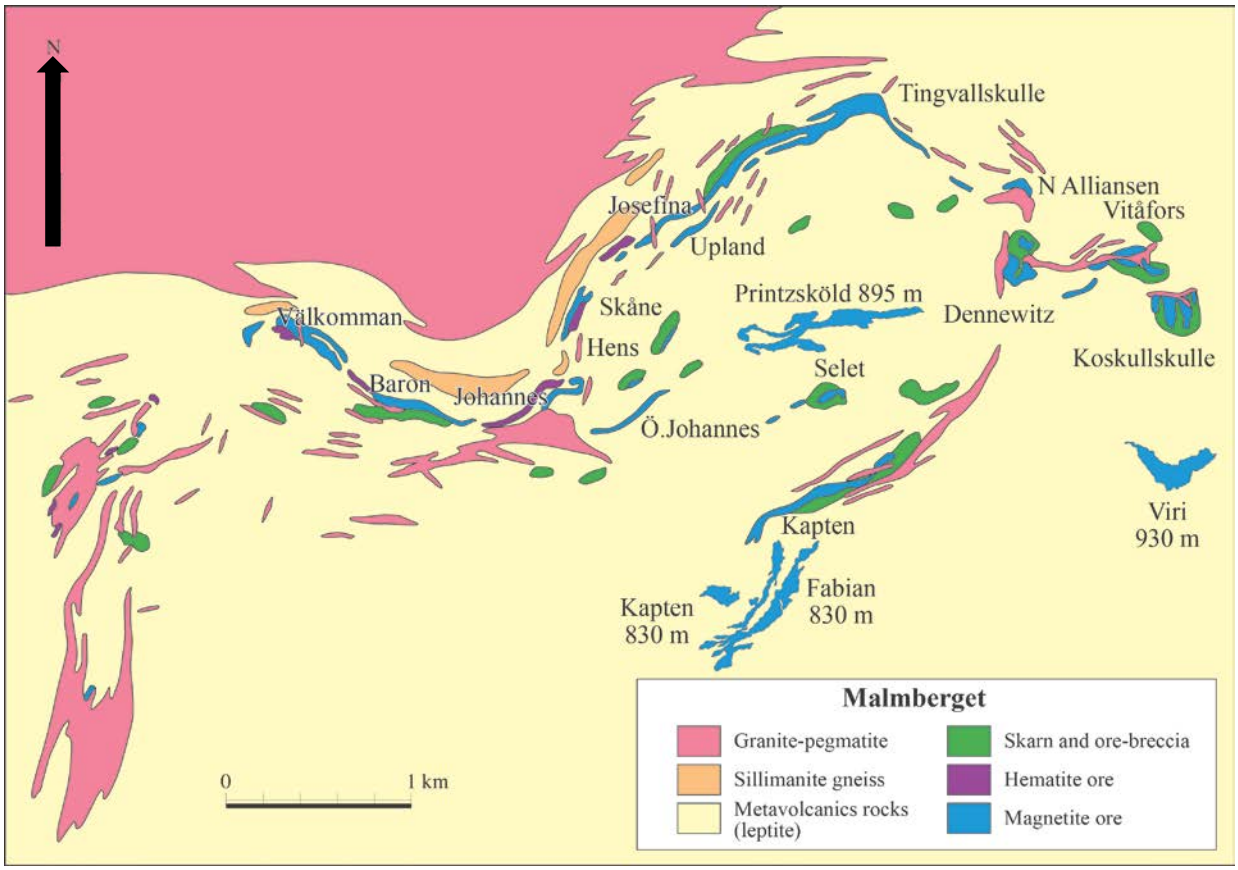

Figure 2 : Geological map of Malmberget area (Lund, Andersen, & Martinsson, 2009, modified)

Iron ore can be divided into massive ore (stratiform-stratabound) and ore breccia (Geijer 1930). The ore breccia is defined as “an irregular network of ore veins which to a varying extent accompany the massive ore” (Geijer 1930, Frietsch 1982). A more generic term semi-massive ore is also used (Lund, in prep). According to (Lund 2009), the massive ore formation can be due to either high temperature hydrothermal fluid circulation or to an iron-enriched magma, whereas the ore breccia mineralization could be caused by low temperature hydrothermal fluid circulation like in the formation of IOCG deposits. The ore breccia samples used in this study cover the Fabian (Fa) and Printzsköld (Pz) ore

bodies as shown on figure 2 and 3. Reference samples of ore come from Hens ore body displayed on figure 2 .

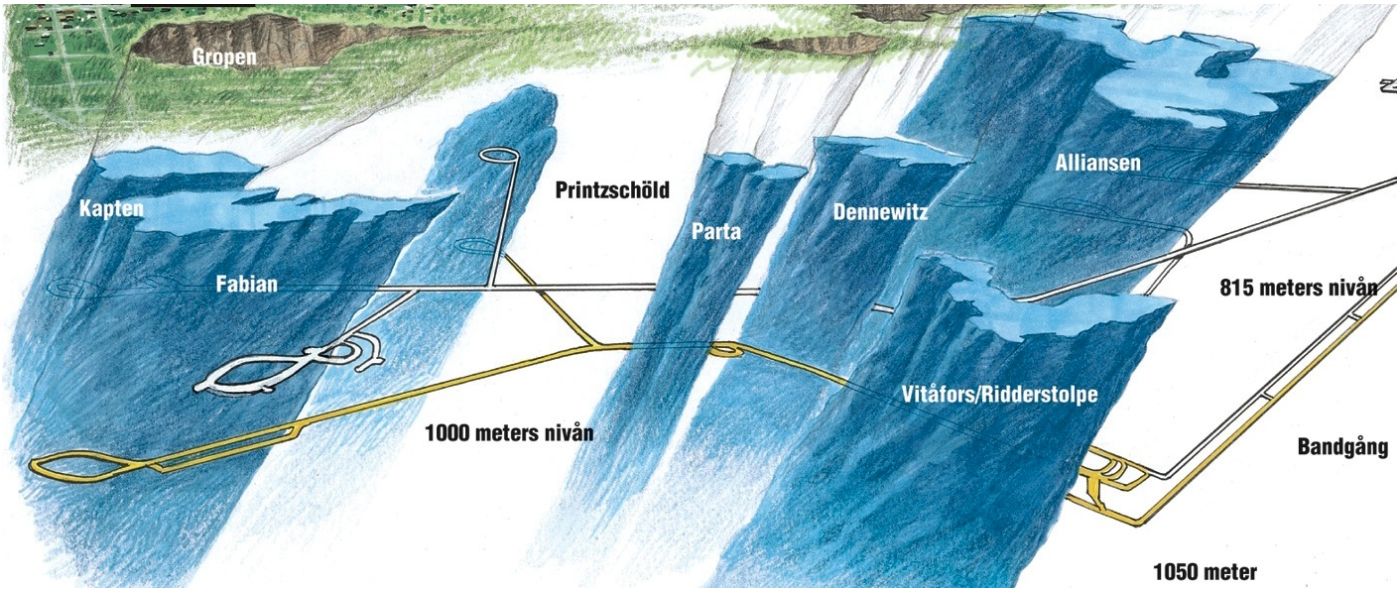

Figure 3 : 3D view of Fabian and Printzsköld ore bodies (LKAB, 2013), modified

c. Mineralogy and chemistry of the ore

i. Fabian magnetite ore

Based on the difference established previously between ore and ore breccia, this section distinguishes between the center of Fabian (ore) and the breccia-style mineralization (ore breccia) that surrounds it.

1. Fabian ore

In Fabian ore, the main iron-containing minerals are

- Magnetite (Mgt) : mineral of the spinel group with chemical formula $Fe^{2+}Fe^{3+}{}_2O_4$
- Ilmenite (Il) : mineral of the ilmenite group with chemical formula $Fe^{2+}TiO_3$

It must be noticed that hematite also exists but does not dominate. Figure 4 shows the whole rock chemical analysis according to data obtained by Cecilia Lund.

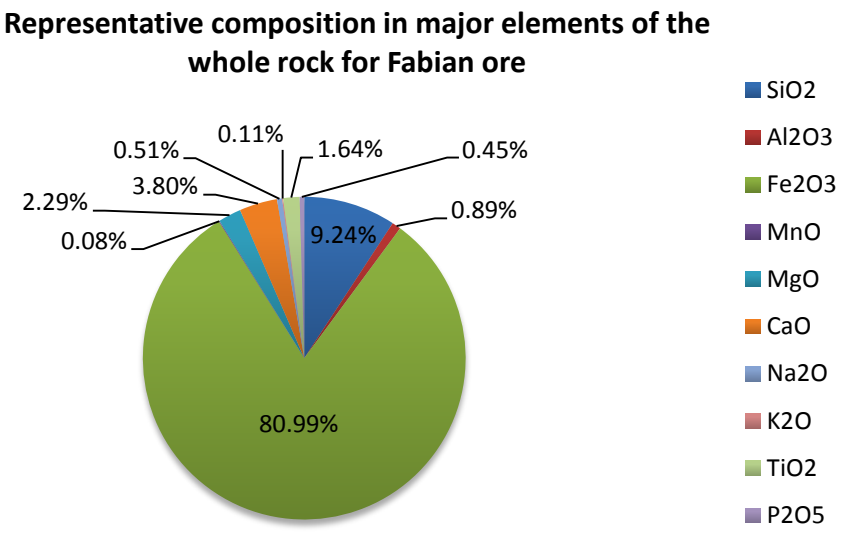

Figure 4 : Typical chemical composition of Fabian ore

Chemical compositions of the main iron containing minerals analyzed by Lund (2012) with electron microprobe are given in Appendix B. The iron (Fe) content in Fabian ore magnetite ranges from 70 % to 72% irrespective of grain size whereas in ilmenite, the total iron content is 42 %.

2. Fabian ore breccia

According to (Lund 2009), the gangue minerals that form the silicate matrix in the breccia ore are albitic plagioclase with K-feldspar and quartz. The iron containing minerals are magnetite and small amounts of Ilmenite. Other minerals include amphibole, pyroxene, biotite, pyrite, anhydrite chalcopyrite and zircon. Figure 5 shows typical chemical composition of ore breccia.

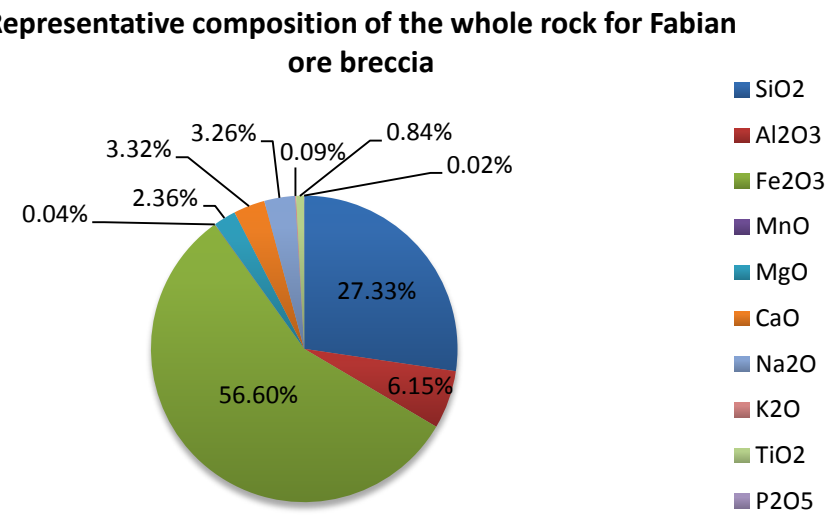

Figure 5 : Typical chemical composition of Fabian ore breccia

Regarding the content of the main iron containing minerals, the microprobe results show a different situation than in the massive ore. Overall, in the breccia ore the ore magnetite is richer in traces elements as seen on table in the Appendix. The fact that the gangue minerals as well as the trace elements in magnetite differs between the massive ore and the ore breccia may indicate a different origin as discussed previously in section 1.b. (Lund 2009)

ii. Printzsköld ore body

1. Printzsköld ore

In Printzsköld ore, the main iron minerals are

- Magnetite (Mgt) : mineral of the spinel group with chemical formula $Fe^{2+}Fe^{3+}{}_2O_4$
- Hematite (Hm) : mineral of the hematite (or corundum) group with chemical formula Fe_2O_3

Figure 6 presents a representative composition of Printzsköld ore.

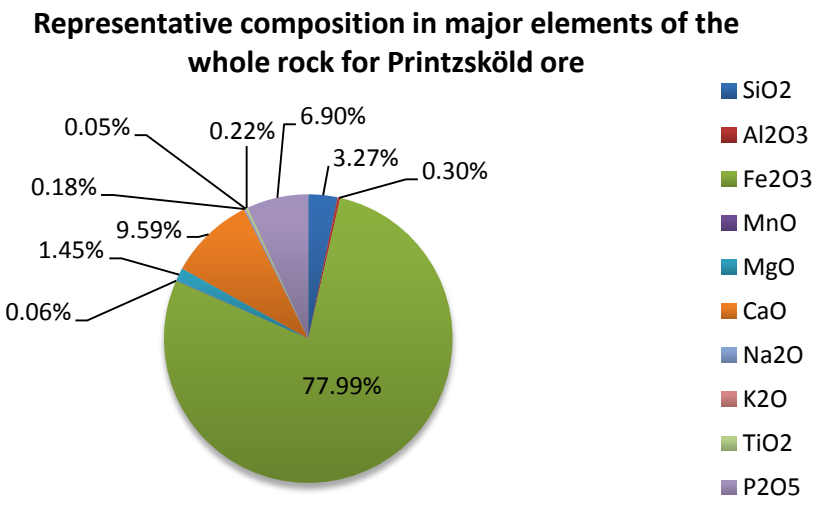

Figure 6 : Typical chemical composition of Printzsköld ore

2. Printzsköld ore breccia

At the hanging wall contact of Printzsköld, ore breccia presents albitisation and includes biotite, anhydrite and amphiboles. At the footwall contact, ore breccia with massive magnetite has been observed that contains biotite and displays some feldspar, amphiboles, pyroxenes as patches (Debras 2010). Figure 7 presents a representative composition of Printzsköld ore breccia.

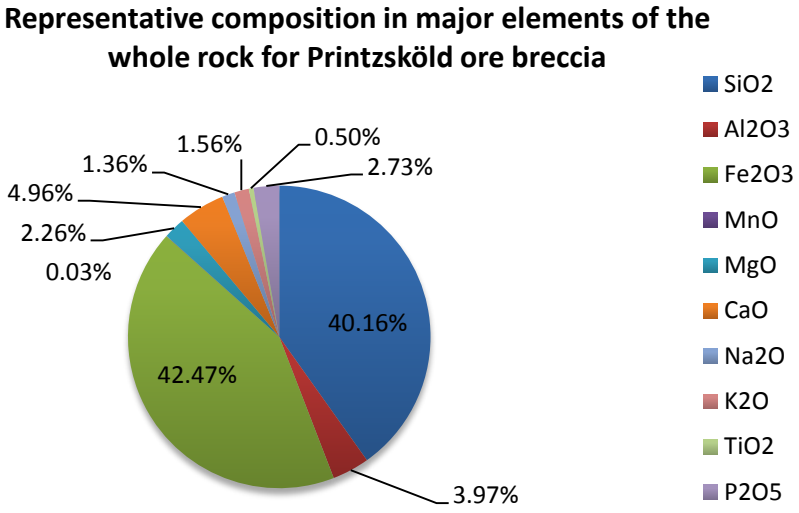

Figure 7 : Typical chemical composition of Printzsköld ore breccia

iii. Relation between ore bodies

According to Lund et al. (2009), the shift from the oxide mineral association magnetite-ilmenite in Fabian to a magnetite-hematite association in Printzsköld shows the existence of different stages of oxidation from the east (Fabian) to the west, with Printzsköld being intermediate caused by the metamorphic events. The description given by Lund et al (2009) includes both homogeneous magnetite and hematite, as well as homogenous magnetite and ilmenite, and proposes lower stratigraphic position to Fabian and ViRi (for example Kiirunavaara) and a higher position to other orebodies such as Välkomma and Hens. However, the intermediate status of Printzsköld does not allow a clear conclusion despite some indication of a structural move. Another fact supporting this proposed stratigraphy is the trend of the curves V_2O_5/TiO_2 that might indicate a different history of ore bodies (Lund 2009).

2. Objectives and working hypothesis

In a geometallurgical context the geological model must give 3D information on ore properties. It has been proposed that information can be compacted to two terms: modal mineralogy and texture (Lamberg 2011). Lund et al. (in prep) showed that in the case of the felspar-rich breccia ore in Malmberget, textures can be simplified into two main types: fine grained and coarse grained. Accordingly all different textures compose of these two end members.

The purpose of the study is to analyze samples of different textural ore types within the felspar-rich breccia ore, by conducting mechanical and mineralogical characterization on them, carrying outcomminution, creating different size fractions by sieving and measuring the modal mineralogy and liberation spectrum of the product for each size fraction. During the tests, special care is taken regarding the samples, given their limited amount and shape.

This work consists of the following steps:

1. Samples description and specific gravity measurements
2. Geo-mechanical tests on the samples and the first classification (clustering) based on physical properties
3. Comminution (crushing and grinding) of the samples and separation into five different size fractions
4. Elemental analysis of the samples by X-Ray fluorescence (XRF) for each size fraction
5. Liberation and modal mineralogy analysis by scanning electron microscope (SEM) of the samples for selected size fractions

6. Use archetypes to describe all the classes and verify the validity of the selected archetypes using the degree of liberation of magnetite and the association index
7. Summarize the characteristics and build predictive empirical models describing all the classes in terms of reduction ratio for jaw crushing, relative work index for ball milling and degree of liberation for magnetite

The hypothesis of the study is that *it should be possible to quantitatively describe the textures of Malmberget feldspar type with two textural archetypes: high graded massive and low graded disseminated*.

A definition for the micro texture (micro fabrics) used here has been developed by Lund and Lamberg (in prep): *two samples are texturally different if their modally refined liberation distribution is different in a given particle size.*

The motivation of this work is based on the need of the industry to predict the throughput, particle size distribution, modal mineralogy by size fraction and liberation distribution based on modal mineralogy, mineral textures and specific energy. The use of archetypes allows to group different kind of iron ore that are similar in terms of particle size distribution and degree of liberation.

3. Literature review

a. Geometallurgy

In mineral processing, there is a need to take into account geology, mineralogy, processing techniques and metallurgy. To achieve this, McQuiston and Bechaud introduced, as early as 1968, the concept of Geometallurgy : *"…geo-metallurgy…since geology is inextricably interwoven with metallurgy in gaining an understanding of the complexities of a deposit, eventually leading to a definition of mineable reserves, with the development of a flowsheet and engineering criteria for the planning of a successful and profitable operation."* (McQuiston 1968)

The concept can thus be defined as the combination of geological and metallurgical (mineral processing) information to create a spatially-based predictive model for mineral processing plant to be used in production management (Lamberg 2011) or as "*the science of integrating geology and mineralogy with resource processing and extraction*" (Hoal 2008).

A geometallurgical program is an industrial application which through different steps leads to a complete geometallurgical model. To achieve this, two approaches should be combined:

- **Geometallurgical testing**: this focuses on the direct measuring metallurgical response of ore samples resulting to a database of parameters that can evaluate how the ore will behave in a treatment plant. This includes a variety of tests in breakage and comminution testing such as JK Bond Ball Lite Test (JKTech, 2013b), Point Load Test, etc or in separation testing, e.g. JKTech Floatability Index (JKFi) (JKTech, 2013a) or Davis tube test (Davis, 1920, 1921).
- **Mineralogy** (Lamberg 2011): this quantitative approach describes the ore and process based on the minerals. The main hypothesis in the process model is that similar particles (mineralogy, size, density) will behave in a similar way regardless of their spatial origin within the ore body (Lund 2013).

One difference between these two approaches is the scale at which samples are studied, geometallurgical testing dealing with macroscopic samples whereas mineralogy focuses on particles and minerals at a microscopic scale. Linking the mineralogical with geometallurgical testing into the geometallurgical program is commonly done through statistics and geometallurgical domains, as shown in Figure 8. In this work, the mineralogy approach mixed with some mechanical tests is studied but only the steps involving ore variability testing and the definition of geometallurgical domains are included.

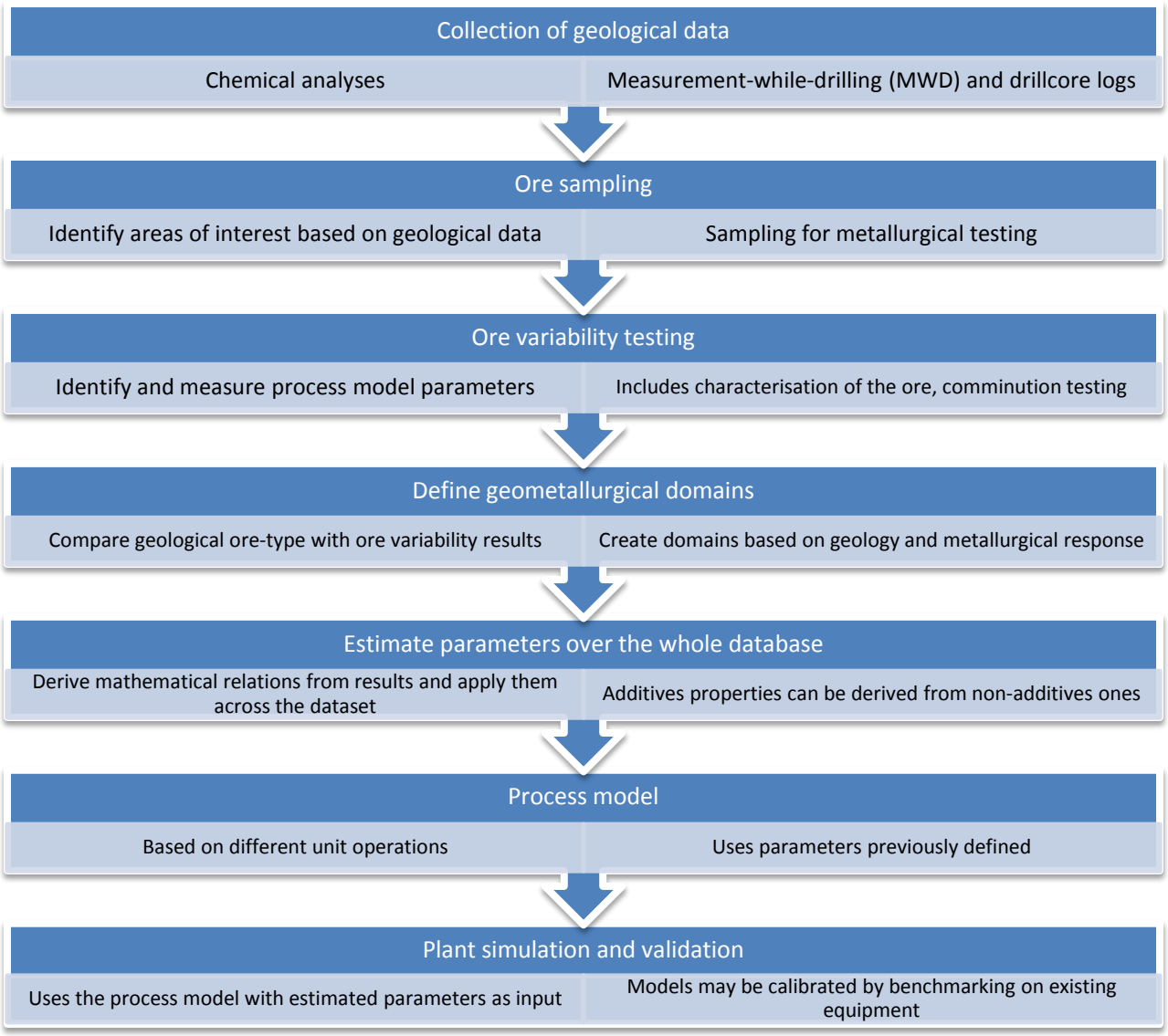

Figure 8 : General geometallurgical program of this work (Lamberg 2011), modified.

b. Physical properties and rock mechanics

To gain knowledge about the physical properties of the ore (in-situ or not), several measurements can be done. This section describes briefly in chronological order (from drilling to the lab) some of them that can be used in a geometallurgical program.

First, information can be obtained by doing measurement while drilling (MWD) or Logging While Drilling (LWD). These techniques are usually used in oil and gas industry but can prove useful in many cases since it yields in-situ or close to in-situ measurements of the rock mass. The properties that can be

measured cover a wide range including gamma ray, induction resistivity , density, neutron porosity, acoustic travel time, pressure sampling, normal and ultrasonic imaging (Trond 2006, Mrozewski 2008).

Some information can be gathered from the visual inspection of drill cores by applying a classification of the rock mass (Charlier 2009) :

- **Rock quality designation (RQD)**: measures the recovery from a drill hole. It is given the ratio between the length of the recovered drill core without parts under 100mm in length and the total length of drilling (Deere and Deere 1988). This measurement can be correlated with seismic speeds (in-situ compression and on non-fractured drill core) and the frequency of discontinuities in drilling (Charlier 2009). The resulting information is the quality of rock mass.

- **Rock Mass Quality (Q**): extension based on RQD and defined by

$$Q = \left(\frac{RQD}{J_n}\right)\left(\frac{J_r}{J_a}\right)\left(\frac{J_w}{SRF}\right) \quad (1)$$

  Where *RQD* is the Rock quality designation, J_n a discontinuity factor, J_r a rugosity factor, J_a a coefficient of alteration in discontinuities, J_w a coefficient accounting for water in discontinuities and *SRF* a reduction factor based on constraints (Barton N 1974). Based on the value of *Q* and using tables, the stability and pressures in excavation works can be deduced (Charlier 2009). This information is useful for stability issues but also allows a clearer view of the main weaknesses within the rock mass.

Other classification systems exist that allow more information to be included but are mostly oriented towards stability and tunnel building. Therefore their description is out of the scope of this study but more information can be found in (Charlier 2009).

While rock mechanics tests are usually part of the geometallurgical testing approach, it makes sense to combine both mineralogy and rock mechanics to define geometallurgical domains. Even though, the physical phenomena governing comminution are complex, there is a need to quantify the mechanical properties of the samples. Special interest is provided by the fact that in comminution, a majority of particles are loaded in compression and fail in tension (Briggs and Bearman 1996). A few tests will be described that can be related to the behavior of samples in comminution steps.

- **Point Load Test (PLT) :** By applying a point load on rock samples and record the breakage pressure, it is possible to get access to the strength of rock materials, particularly the tensile strength (Bieniawski 1975). This test can be conducted on unprepared samples with portable

equipment making it a quick and cheap test. Nevertheless, many samples are required to perform statistical analysis on the results. Figure 9 shows the different settings that can be used for this measurement. In this work, only the axial configuration only was used.

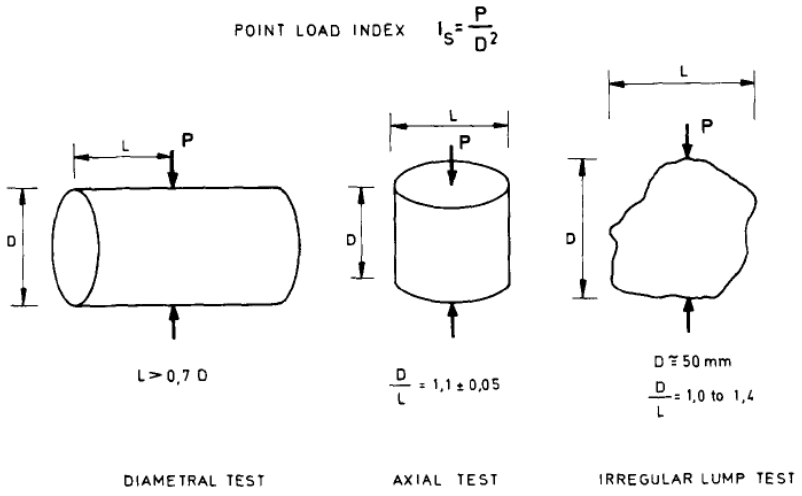

Figure 9 : Different configurations for the Point Load Test (Bieniawski 1975)

The measured value at breakage provides Point Load Index (I_s) that can be correlated to the tensile strength and compressive strength. Since comminution means breakage, this test seems suitable for ore characterization.

The standard measurement is $I_s(50)$, the point load index for an equivalent diameter of 50 mm. This can be linked to the tensile strength given by the Brazilian Test (Charlier 2009) according to

$$I_s(50) = 0.8\sigma_t^{br} \quad (2)$$

Given the anisotropy in rocks, correlation between the point load index and tensile or compressive strength is somehow subject to caution. Whereas earlier works used the following correlation to relate point load index to the compressive strength

$$\sigma_c = 24\, I_s(50) \quad (3)$$

Where $I_s(50)$ is the point load index for a standardized sample size of a 50 mm equivalent diameter. Recent works focus on the study of $I_s(50)$ for itself, given that the correlation can vary between 15 to 50 in the case of anisotropic rocks (Charlier 2009). This test is used in this report, a complete description of the test settings and samples can be found under the experimental work section.

- **Simple compressive test (CT):** The aim of this test is to measure the compressive strength of a rock material. In practice, a sample is placed between two discs of steel while a measured force

is applied on the base disc. The rate of compression must be slow to avoid dynamics effects and constant to build a proper curve linking the stress σ and the deformation ε. The breakage force is recorded to provide an estimate of the compressive strength of the sample (Charlier 2009). It should be noticed however that, despite the name of compressive strength, the mode of failure for rock samples submitted to compressive tests (simple compressive test or uniaxial compressive test) can be tension or shear or a combination of tension and shear (Szwedzicki 2007). This test provides a fast and cheap way to access the compressive strength. The recorded value is the compressive strength (CS) measured in MPa. This test is used in this work, a schematic view is shown on Figure 10 and a complete description of the test settings and samples can be found under the experimental work section.

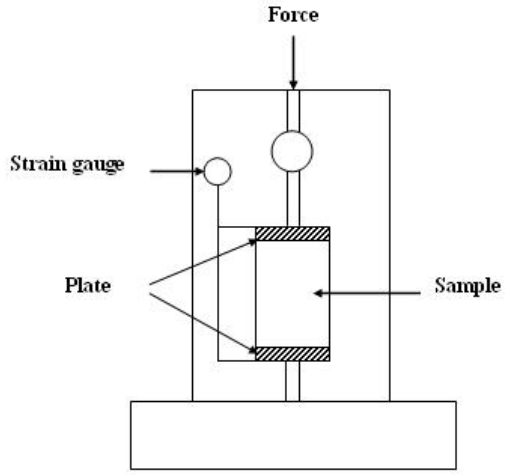

Figure 10 : Typical setting for simple compressive test, (Shosha 2013)

The use of these two tests provides a minimal description of the mechanical properties of the ore: if more extensive testing is required, other tests such as the triaxial test, fracture toughness, Brazilian tensile strength and others can be used as well, depending on the needs of the study and the availability of samples. However, the most relevant correlations between comminution and rock mechanical tests described in this work involve tensile stress as measured by the point load test for example (Bearman, Briggs et al. 1997). It should be noticed that the scale of the rock mechanics tests is similar to the scale used in crushing, where texture and micro cracks have a strong influence on the behavior of the material, making those tests relevant for crushing.

c. Comminution testing

This part will focus on the relation between the energy consumption and the product of comminution (particles). Mwanga et al. (in prep.) provides a review of the different tests for comminution in a geometallurgical context. While the physical mechanism that causes cracks and leads to comminution is studied in theory and may be simulated to some extent (Kou, Liu et al. 2001, Tang 2001b), a more practical approach is often based on Bond theory (Bond 1952) which does not account for all micro-scale phenomena but provides a convenient way to express the link between the energy input of a machine and the breaking of the material (Wills BA 1993, Wills and Napier-Munn 2006).

The formula given by Bond (1952) is the following:

$$W = \frac{10W_i}{\sqrt{P_{80}}} - \frac{10W_i}{\sqrt{F_{80}}} \tag{4}$$

Where W is the work input in [kWh/short ton], P is the diameter which 80% of the product passes in [µm], F is the diameter which 80% of the feed passes in [µm] and W_i is the work index. This index is a property of the rock material that represents its resistance to grinding and crushing (Wills and Napier-Munn 2006).

A way to calculate the work index from a laboratory mill is to use another formula (Magdalinović 1989) :

$$W_i = 1.1 \frac{44.5}{P_c^{0.83} G^{0.82} \left(\frac{10}{\sqrt{P_{80}}} - \frac{10}{\sqrt{F_{80}}} \right)} \tag{5}$$

Where W_i is the work index [kWh/t], P_c the mesh-size of the test-sieve [µm], G the mass of the undersize of the test-sieve per mill revolution [g/min], P_{80} and F_{80} as defined in equation (4).

However, the original method proposed by Bond, without the use of different correction factors, does not describe accurately the whole size range (Bond 1952, Hukki 1961) and prone to error, especially in the case of autogenous (AG) and semi-autogenous (SAG) mills (Morrell 2004) . Moreover, the meaning of the work index is the power draw from the mill to achieve a given P_{80}. By doing so, it assumes that the size distributions for the feed and the product are parallel on a log-log plot, which might not be the case (Morrell and Man 1997). As an alternative, some authors proposed faster tests called simplified versions of Bond ball mill test (Berry and Bruce 1966, Magdalinović 1989), correlations with other rock parameters (Ozkahraman 2005) or revised versions of the Bond equations (Morrell 2004). In a context of

Geometallurgy, Mwanga et al. (in prep.) suggests the use of complementary tests, i.e. the combination of different tests to describe the behavior of rock in comminution more accurately than with a single test. JK Rotary Breakage Test and JK Drop Weight Test are also described as relevant methods (Mwanga et al., in prep.).

d. Liberation analysis using Scanning Electron Microscope (SEM)

Mineral liberation analysis gives the mass proportion of the target mineral occurring as liberated (degree of liberation) and also the association of the target mineral when not liberated. Analysis is performed for particle size fractions and this information is mostly used in defining the required grinding size for the concentration process. Nowadays it is used also for process diagnosis, optimization and development of property based models for mineral processing. Earlier, liberation analysis was usually done with optical microscopes. This process was time-consuming and often produced semi-quantitative results with a small sample size. Recently, advances in computer, microscopy and spectrometry technology made possible the use of scanning electron microscope to produce quantitative results for liberation. Using both Back-Scattered Electrons (BSE) imaging followed by image analysis to de-agglomerate particles and for phases segmentation and Energy-dispersive X-Ray spectrum (EDS or EDX), it is now possible to obtain quickly reliable measurements of mineral liberation size, mineral association and textural parameters (Fandrich 2007).

The acquisition of the energy-dispersive spectrum (EDS) is based on the following simplified mechanism displayed on Figure 11:

1. Emission of an incident radiation by an external source (electron beam for SEM-EDS and X-Ray beam for XRF)
2. Ejection of an electron from the inner shell
3. Filling of the vacancy by an electron from one of the outer shells, emitting a characteristic x-ray

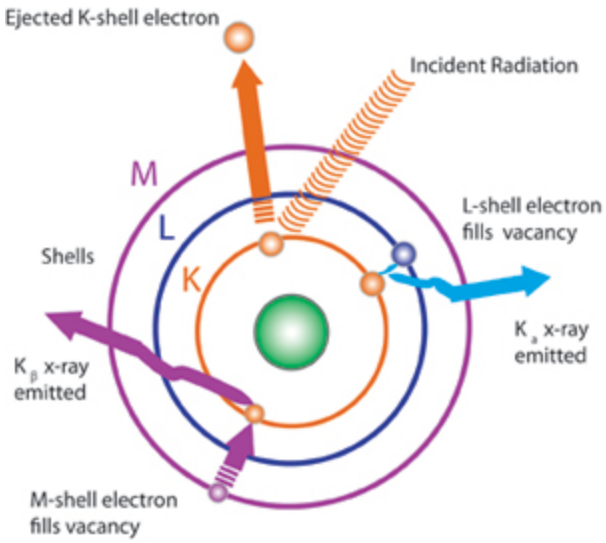

Figure 11 : XRF and EDS simplified mechanism (CLU-IN 2013)

The backscattered electrons come from the electron beam of the microscope and are elastically scattered by the electric field of the nucleus as shown on Figure 12. These electrons provide information on the composition of the mineral grains. Three main components influence the total BSE signal : the mean atomic number (Z), tilt angle and crystallography (Paterson 1989). The most interesting for this study is the Z. A BSE coefficient (η) can be defined as the fraction of electrons that are backscattered. Many different models linking η with the atomic number Z of an element have been proposed (Harding 2002).

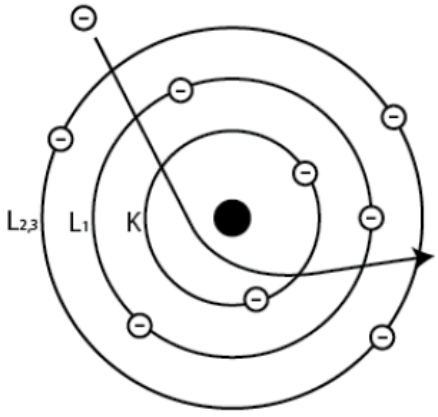

Figure 12 : BSE simplified mechanism (Dewar 2013), modified

Some authors use only the BSE image in grey levels from 1 to 256 citing lower costs, smaller acquisition time and problems that can arise with EDS applied on iron oxides (Harding 2002, Schneider 2004). Figure 13 shows the link between the grey level scale and the atomic number of the sample.

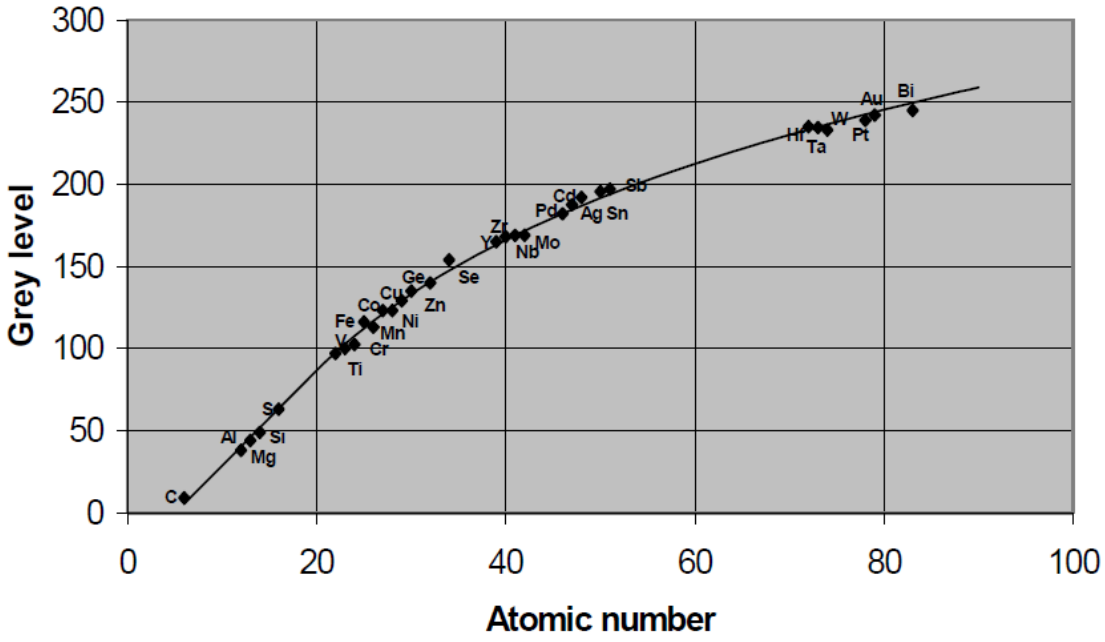

Figure 13 : Relation between mean grey level and atomic number at constant brightness and contrast (Schneider C.L. 2004)

While using both BSE image and EDS measurements, the first step is to adjust the microscope parameters. Before acquisition of a BSE image, some adjustments of brightness and contrast of the image are needed to reach a good contrast between minerals and eliminate noise. To do this, the gray level corresponding to the background is defined as the lowest one, and then different thresholds corresponding to different minerals are interactively defined with INCAMineral through a plug-in.

The next step is the application of particle separation algorithms. The acquired image is processed in order to have well separated particles without touching edges. This is important regarding size and area measurement as well as liberation. When studying magnetite, the presence of micro cracks or grading edges in grey scale picture requires caution while applying segmentation. In Lamberg et al. (in prep.), the effect of this factor is studied because of its impact on the results : a very small minimum grain size will result in artifacts on the grain border leading to misidentification of the minerals whereas large

minimum grain size will properly identify the particle in presence of cracks but might neglect small existing inclusions.

A limitation of this SEM technique is the use of two dimensional sections to quantify three dimensional mineral grains, which could result in an overestimate of liberated particles. To access 3D information, various studies investigated the extrapolation from 2D information to 3D which is limited when more than two mineral phases are present (Lätti 2001, Videla 2007) or the use of X-Ray microtomography (XMT) (Lin 1996, 2002).

e. XRF Analysis and Element to Mineral conversion

The X-Ray Fluorescence allows elemental analysis of rock sample based on the mechanism described on Figure 11. However, one of the limitation of this analysis is the atomic number of the element, for low Z one (Z<14), some modifications are required (Rosenberg 1992). The idea of the element to mineral conversion (EMC) is to convert this elemental analysis results to mineral grades. The problem can be expressed as equation (6).

$$\mathbf{Ax} = \mathbf{b} \tag{6}$$

Where **A** is a matrix containing the weight fraction of the elements in the minerals (from microprobe analysis), **x** an unknown vector containing weight fractions of the minerals in the sample and **b** a vector containing the weight fraction of elements in the sample (from XRF). Using the fact that mineral grades are positive and that the sum of all the mineral grades should be smaller or equal to 100 %, the problem can be solved by minimizing the residuals r in equation (7).

$$r = |\mathbf{b} - \mathbf{Ax}| \tag{7}$$

Over-determined and under-determined problems (more elements than minerals or the opposite) can be solved as well using different methods (Lund 2013). This approach has been successfully used by several authors these last forty years (Wright 1970, Banks 1979, Lund 2013).

f. Liberation models

A geometallurgical program reduces risk in operation, gives tools for production management and gives on daily basis realistic production goals in terms of throughput and recovery (Alruiz 2009). As plants operate with more or less fixed flow sheets, there are only limited amounts of tools to adjust the process to the variation in the feed. Commonly, reagent addition rates are adjusted with the flow rates of minerals. In comminution, prevailing practice is to grind the material into fixed target fineness with maximal throughput. If the ore is hard, then the feed rate is lowered and in the case of soft ore, the plant operates with higher throughput. However, every ore shows variation in the mineral grain size and in other textural properties. As a result, fixed particle size distribution will produce different liberation degree for the valuable mineral(s). Optimally, all the following parameters: the liberation degree, mineral association (of locked particles), overall particle size distribution and plant throughput should be optimized thorough an economic function. On-line measurements exist for throughput and particle size distribution but not for liberation. Therefore, it would be important to include this kind of information in the geometallurgical model to enabling such an optimization. Therefore, it is important to study how particles with different texture and composition break as comminution includes both size reduction and liberation aspects.

Regarding the mathematical description of size reduction, a common approach is the population balance models. These models are based on equation (8).

$$\frac{dn(d,t)}{dt} = [Inflow] - [Outflow] + [Creation] - [Disappearance] \quad (8)$$

Where *n(d,t)* is the amount of particles within the d size fraction at the time t, [Inflow] and [Outflow] are the amount of particles respectively entering and leaving the system and [Creation] and [Disappearance] terms account respectively for the creation of new particles in the d size fraction through breakage, attrition, or the disappearance of particles in the d size fraction due to agglomeration for example (Mishra 2000).

Based on equation (8) it is possible to link the product and the feed with a matrix equation.

$$\mathrm{P} = \mathrm{Kf} \quad (9)$$

If i and j are size fractions, a way to compute the elements of the product array P is given by equation (10).

$$p_{ij} = \mathrm{k}_{ij}\mathrm{f}_j \quad (10)$$

Where

- *P* is the product array of (i,j) elements
- *f* the feed as a vector of j elements
- *K* a matrix in which the ij th element (k_{ij}) is the mass fraction of a particle of the i range falling in the j range in the product

Defining *S* , the selection function describing the probability for a particle to be selected for breakage and *B*, the breakage function describing the distribution of breakage fragments, **Sf** represents the fraction of the feed selected for breakage and **(1-S)f** is the fraction of not broken feed. This approach derives from the population balance equation (8) and several authors studied it (Bass 1954, Gardner, Austin et al. 1961, Gardner and Austin 1962, Reid 1965). With *S* and *B*, the process for a primary breakage can be written as equation (11).

$$\mathrm{P} = \mathrm{BSf} + (1 - \mathrm{S})\mathrm{f} \quad (11)$$

While much work has been done regarding the size reduction side, only recently a few models including mineral liberation in the size reduction process have been proposed (Wills and Napier-Munn 2006).

In order to investigate and predict the result of comminution, models (called liberation models or particle breakage models) have been previously developed, mainly based on the following concepts (Lamberg 2012) :

1. **Probability-based models**

   - *Random breakage model*: By applying grids (deriving from linear-intercept lengths) to polished sections of a rock and under the main hypothesis that particles will randomly break, breakage models have been developed (King 1979, Leigh 1996, Fandrich 1997, Gay 2004b). Despite giving some information about non-random breakage, in most real-life cases the random breakage assumption is invalid (Gay 2004b).

   - *Kernel model:* This approach is based on Equation (8) and focus on the expression of the parameter K. A way to describe K is to use Andrews-Mika diagrams (A-M) which represent

what kind of progeny particles can be produced from a single feed particle in a comminution environment (Andrews and Mika 1975, Lamberg 2012). Gay gives an extension to multiphase particles based on probability theory (Gay 2004). In the case of complex multi-components systems, the formulation becomes increasingly complex and leads to the resolution of a multi-dimensional differential equation. However, the cost in terms of complexity has some advantages such as providing a way to simulate non-random fractures (King and Schneider 1999).

2. **Empirical liberation measurements**

   Using automatic mineral identification and simulated fragmentation (based on a chessboard algorithm), processing of samples can be ranked (Hunt 2011) and with scanning electron microscopy (SEM) combined with image processing techniques, quantified textural information can be obtained and integrated in a model (Bonnici, Hunt et al. 2008).

Despite complexity and limitations, probabilistic models are useful for simulation needs, however while following a metallurgical program, actual measurements of liberation can be done. A problem with the last approach is that, as it is not feasible to do the measurements for all the collected samples, how to define which samples should be measured and how to populate the liberation distribution for the samples not analyzed. The idea proposed by (Lamberg P. 2012) is to define archetypes which represent samples producing similar compositionally refined liberation distribution. From any ore block, for each textural type, the particle population will be established based on those archetypes.

To develop a library of archetypes for a given ore body, the following instructions should be followed (Lamberg 2007,2012, Lund 2013) :

- Representative samples are collected from each textural type
- Samples are ground to the processing fineness, sized and resin mounts are prepared.
- Liberation measurement is done by size and in the case of fines or coarse fraction, extrapolation is applicable.
- The classification of the particles resulting from the liberation analysis on each sample is done according to the method developed in (Lamberg 2007).
- By doing so, the only difference between two samples will be the relative abundance of each particle type in a given archetype.
- Using a refinement procedure, an archetype can be converted to liberation distribution for any given modal composition. This is called modally refined liberation distribution.

- If two samples have different modally refined liberation distribution they represent different textural types and should have a corresponding archetype in the library.

4. Experimental work

a. Classification of samples

The samples used in this study come from LKAB' mine in Malmberget and were classified earlier in eight classes as shown on figure 17 (Lund, in prep.). In order to classify and manage information, a database is built based on three following data structures described on figure 14.

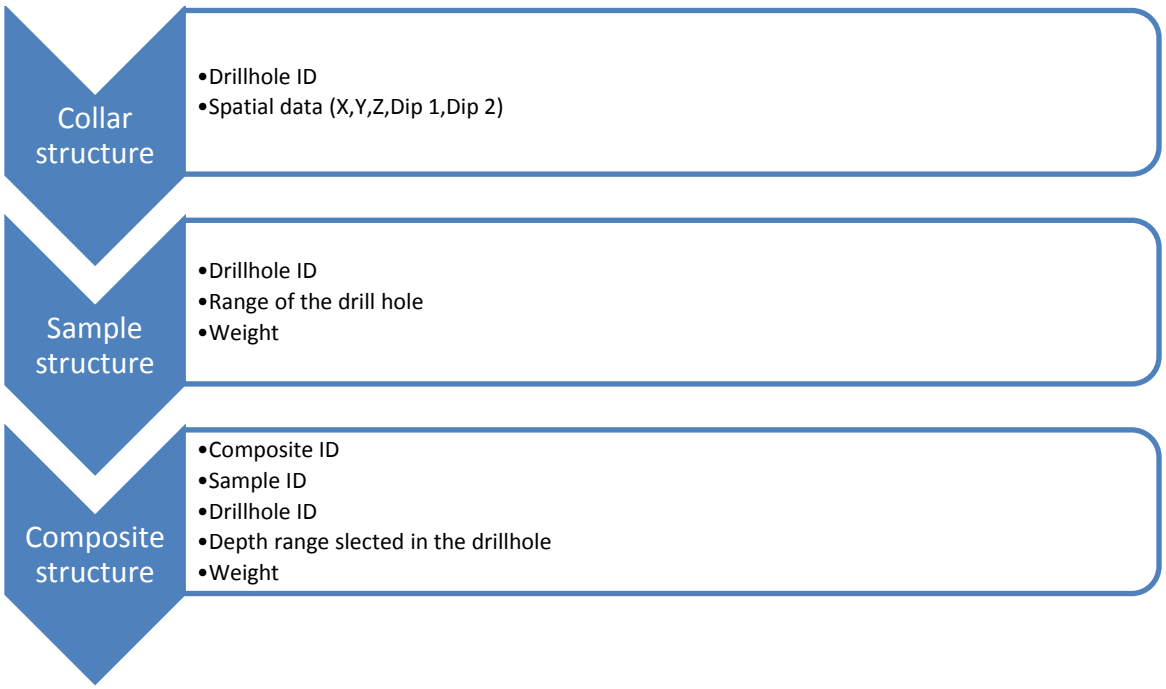

Figure 14 : Data structures used to classify the samples

The collar structure is the raw information from the drill core. It includes the spatial coordinates and an identification code (ID). On the sample level, adjacent sections of the drill core of the same kind of rock are selected. The composite structure will classify different samples into groups that have similar geometallurgical properties. The composite table is presented in appendix B.

The samples received were already composites in limited amount, so that a selection was made in order to ensure that a sufficient and representative quantity of material was tested. The samples include 10 different classes based on the mineralogy of the gangue and textural properties and classified by (Lund 2013) as shown on Figure 15. The approach is to analyze the response in terms of physical properties,

crushability, grindability and degree of liberation of the classes defined from CF1 to CF8 for feldspar-rich samples and CRC or CRF for amphibole-rich high grade ore samples from rock mechanics tests at a milimetric scale down to liberation analysis at a micrometric scale.

CRC and CRF are used as reference samples for liberation but are not included in the clustering process since they represent a different rock material with rather different modal composition and texture. The main purpose of having those classes is to provide information about how the grain size influences the liberation.

CF1 to CF8 are composites mostly from Fabian and some from Printzsköld ore bodies whereas CRC and CRF come from Hens.

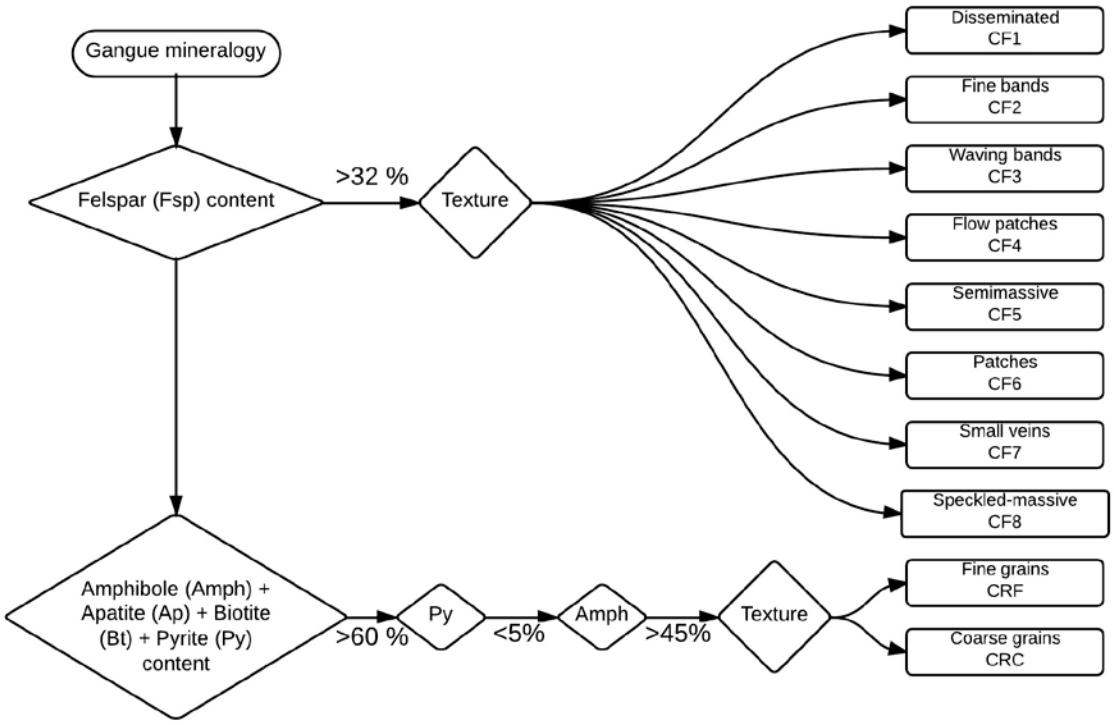

Figure 15 : Samples classification system (Lund C. 2013), modified

Sample material was first used for mechanical tests, then underwent comminution and was split according to size fraction for both SEM analysis and XRF analysis as shown on Figure 16 .

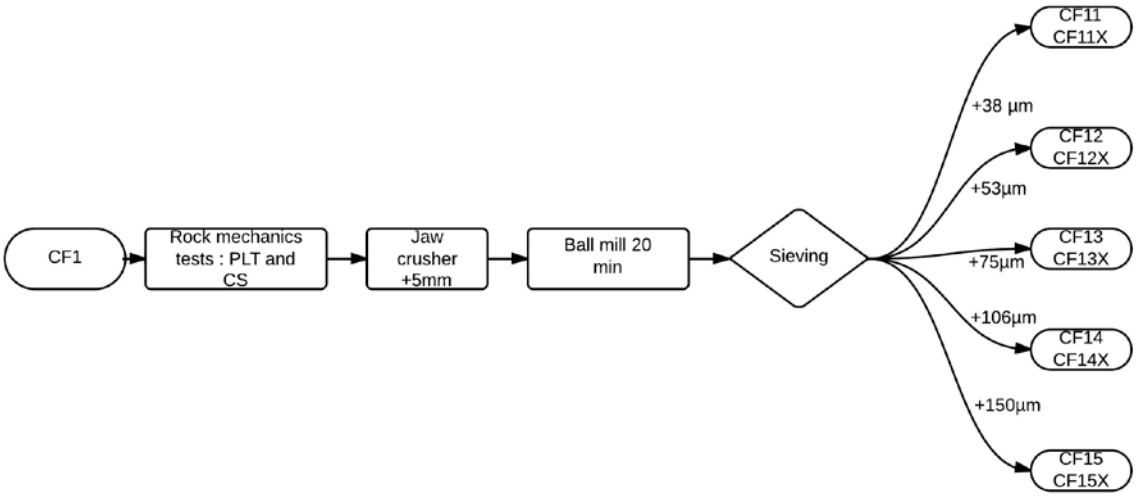

Figure 16 : Sample preparation for CF1

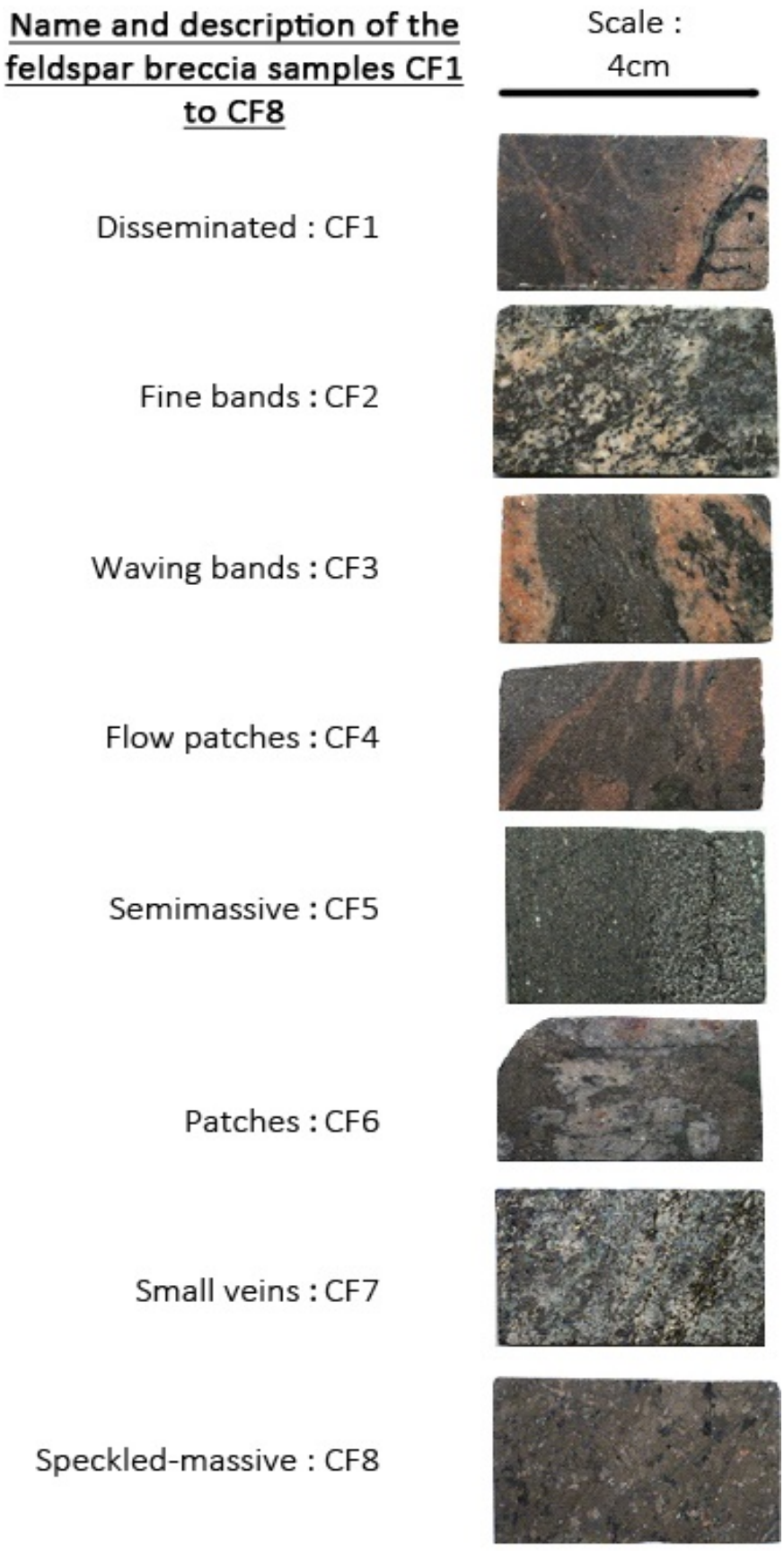

Figure 17 : Name, description and pictures of feldspar breccia samples CF1 to CF8 (Lund C. 2013)

b. Rock mechanics material and methods

i. Point load test (PLT)

The received material consisted of quarters of drill cores with a radius between 15 and 20 mm and a length between 10 mm and 200 mm. Unified dimensions of a 15 mm radius (L) and 30mm (D) length were chosen. Afterwards, each sample has been measured and weighted to obtain an estimated specific gravity for the rock material.

According to the D5731-08 standard ((ASTM) 2011), the following conditions should be respected:

- 30 to 85 mm test diameter for irregular lumps, rock cores or blocks : verified with D=30 mm
- At least 10 samples for core or block samples: verified initially, though some of them were categorized as invalid.
- Controlled water content: verified since all the samples were stored in the same conditions.
- 10 to 60s before failure : verified
- 0.3L<D<L as on Figure 9 : not verified, a D/L ratio of 2 was chosen due to the available material

Given the limited availability of sample materials in terms of shape, those tests were conducted in conditions as similar as possible to these standards. In particular, a test is regarded as valid only if the fracture is continuous from the top contact point between the test machine and the sample to the bottom contact point as shown on Figure 18.

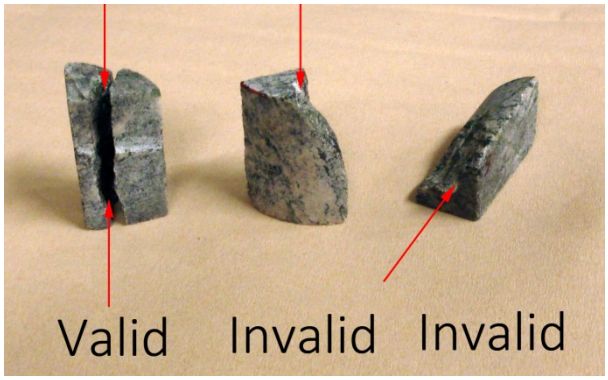

Figure 18 : PLT validity criterion adapted to non-standard samples

As a result of this validity requirement, some test results have been dropped out and are referred to as invalid in the data file. The number of tests varied according to the initial total mass of material, the behavior during the test, notably for CF6 which displayed some heterogeneity reflected directly by a high rate of invalid point load tests.

Table 1 : Sample material properties and number of valid mechanical tests per class

Class	Mean specific gravity []	Total mass [g]	Valid PLT	Valid CT
CF1	2.525	626	8	9
CF2	2.658	840	13	13
CF3	2.992	537	15	13
CF4	3.500	1585	12	12
CF5	2.717	626	10	11
CF6	3.561	1021	6	13
CF7	3.505	720	11	10
CF8	4.203	782	10	11
CRC	4.307	2339	13	15
CRF	4.659	1470	14	15

ii. Simple compressive test (CT)

Simple compressive tests were conducted in the mineral processing lab at LTU, with samples of same size and shape as for the point load test. To be as close as possible to an uniaxial test : the speed of charge was kept low to avoid as much as possible dynamic effects (time of load between 1 and 4 minutes), the samples had a D/L ratio of 2 to avoid instabilities or overestimation of the strength and the samples were stored in the same conditions (room temperature close to 20°C, relative humidity of 70%)(Charlier 2009).

c. Comminution material and method

In this work, the comminution test includes a first run in a jaw crusher with a 5 mm opening to produce sample material below 3.5 mm. The second step consists of a ball mill running for 20 minutes with 1L of water for 1.2 kg of solid material. The energy drawn by the mill was recorded and a sieving curve has been established for each class after each step. This work was done in the mineral processing laboratory at LTU.

The grinding step was used to study the behavior of different mineral textures during comminution and link it to liberation characteristics.

d. XRF analysis and element-to-mineral conversion material and method

XRF analysis was used to compare and validate the results from the SEM but also to get modal analysis for all size fractions. The analysis in itself was carried on by LKAB at Malmberget and included Fe(II) for all samples in all the size fractions except CF65X, CRC5X and CRF5X for which the amount of sample was not sufficient for a proper Fe(II) measurement.

In this study, XRF was used to validate the results from the EDS acquired with the Merlin SEM. Given that XRF provides elemental analysis whereas INCA gives mineral grades, an operation of mass-balancing called Element to Mineral conversion (EMC) was applied as described in (Lund 2013).

The EMC was done in three rounds, the first one using a normal least squares method (LS) and the two next rounds using a non-negative least square (NNLS) method to solve the minimization problem described in section c. Regarding Fe (II), it has been assigned to magnetite, resulting in an overestimation of hematite when no measurement of Fe (II) was available. In table 2, mineral names are abbreviated according to this list:

- Magnetite : Mgt
- Hematite : Hem
- Ilmenite : Ilm
- Albite : Ab
- Apatite : Ap
- Tremolite : Tr (no distinction within the tremolite-actinolite solid-solution)
- Orthoclase : Or
- Biotite : Bt
- Quartz: Qtz

Table 2 : Settings for the element to mineral conversion

Round	Minerals	Elements	Method
1	M/Ab/46 M/Ap/504	P XRF Na XRF	LS
2	M/Bt/1721 M/Tr/447 M/Or/3594 M/Qtz/53	K XRF Mg XRF Ca XRF Al XRF Si XRF	NNLS
3	M/Hem/79 M/Mgt/80 M/Ilm/837	Fe XRF Fe II Ti XRF	NNLS

Since it is difficult to make a difference between iron oxides on the SEM, all the iron oxides have been measured as magnetite which in fact covers magnetite but also hematite and possibly other iron oxides.

To account for this effect, all the iron oxides given by the element-to-mineral conversion have been summed up and then compared to the magnetite grade obtained by the SEM.

e. SEM liberation material and method

The liberation analysis was carried using a Merlin High-Resolution FEG-SEM available at LTU using the following detectors:

- InLens-backscattered electrons (BSE) detectors
- Energy-dispersive spectrometry (EDS) detector

The column itself is presented on figure 19.

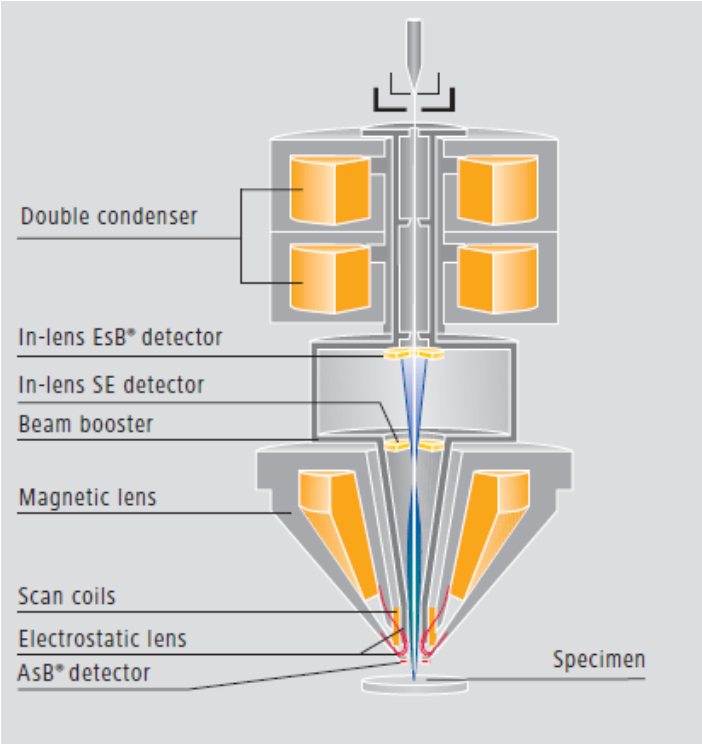

Figure 19 : Merlin SEM column schematic (Zeiss 2011)

The liberation analysis involved a quantitative study of minerals with measurements by a SEM and processing by INCAMineral software (INCA 2011) . Based on the liberation data , the determination of the association index (AI) was done with HSC Geo (Lamberg 2011). The association index gives a criterion to categorize textural archetypes and is discussed in a later section.

Samples for liberation analysis consisted of cylindrical epoxy-resin mounts (prepared at Oulu University) coated with carbon (done at LTU). A first test was run with CF61 to compare the liberation results obtained by backscattered electrons (BSE) only and BSE-imaging with energy-dispersive spectrograph (EDS). A motivation for this was the time needed, given that BSE-only measurements are much faster than EDS. The two techniques show a clear difference both in terms of modal mineralogy and liberation of magnetite (EDS gave 80 % liberated magnetite whereas only BSE gave 60 %), these results are displayed in the appendix. As a result, all samples have been processed with EDS measurements to ensure the quality of the data.

The main measurement settings for the microscope were a magnification of 400x for fine grains samples and 200x for coarse grain in order to have enough particles within the sample. INCAMineral provides one file per sample, which includes modal composition for each particle, particles count, shape and area of each particle and statistics. The general process to produce these files is the following (OxfordInstruments 2012) :

- Subdivide the whole measurement area into smaller fields
- Acquire BSE image of the field and apply morphological operations to obtain separated particles. This step is important because some problems may arise from incorrectly de-agglomerated particles like two nearby particles to be counted as one
- Perform an EDS measurement on each grain to identify and quantify the mineral phases of the grain, based on either full-spectrum rules or simple ones (Lamberg 2013)
- Store all the measurements in the file for further processing

The minerals identified by rules were magnetite (Mgt), albite (Ab), orthoclase (Or), apatite (Ap), biotite (Bt) and tremolite (Tr). In this work, no distinction is made within the actinolite-tremolite solid-solution terms so the term tremolite is used to describe anything between actinolite and tremolite end-members. If the identification fails, it will be labeled as unknown or “others”. The fact that no distinction was made between different iron oxides and that Ilmenite was not included will result in the classification of all these iron-containing phases as magnetite.

The first step was to treat the particles files obtained by the SEM (and INCAMineral software) to obtain a file where all the particles and their properties are included for all size fractions for a given sample. After that, using a binning algorithm on the particles for each size fraction, useful graphs are constructed such as liberation curves per element for each size fraction, mineral composition of each size fraction and the mode of occurrence of magnetite which describes the amount binaries or ternaries of magnetite with gangue minerals with the Geo module of the HSC Chemistry software.

f. Liberation model by archetypes material and method

The use of archetypes to describe the liberation is the main hypothesis of this work. This has been done by processing the data from SEM and INCAMineral with HSC Geo 7.18 (Lamberg 2011).

A first technique is available to validate the archetype: iterative rebalance. In this process, we will use the liberation data of the first sample (archetype) but replace the modal composition by the one of another sample. The assumption is that grade by size will follow the trend observed in the archetype. By doing this, particles of the archetype will be rebalanced to match the modal composition of the second sample. The liberation key figures, degree of liberation and association index for magnetite, are calculated for the rebalanced product. This process is based on iterative formulas described by (Lamberg 2012) in equations (12) and (13).

For each mineral i in a given size fraction, the mineral grade in the sample for the current size fraction ($M(i)_{fraction}$) is compared to the sum of the product of the mass proportion of particle in the current size fraction ($p(j)_{fraction}$) multiplied by the mass proportion of mineral i in a particle ($x(i)_p$). This sum is the mineral grade calculated from the liberation of the archetype.

$$k_{i,fraction} = \frac{M(i)_{fraction}}{\sum_{j=1}^{n}(p(j)_{fraction}x(i)_p)} \quad (12)$$

For each iterative step, the mass proportion of particle j in the current size fraction ($p_{j,fraction}$) is then corrected with the correction factor $k_{i,fraction}$.

$$p_{j,fraction} = p_{j,fraction}\sum_{j=1}^{L}(x(i)_j k_{i,fraction}) \quad (13)$$

With this iterative process, the modal composition of a sample is used to generate a new particle population based on an archetype. This population will be compared to the measured population in terms of liberation and association index to verify the ability of the chosen archetype to describe the sample.

If the difference between the initial liberation key figures and the rebalanced is small, it means that, despite different modal compositions, the samples are texturally similar, i.e. the other sample shows similar liberation distribution when compensated against modal mineralogy. If the difference is high, the second sample represents another texture class and cannot be used as an archetype for the first sample.

In this case, the +53 µm size fraction (containing CF22, CF42, CF62, CRC2 and CRF2) was chosen since it had been completely analyzed and that each SEM measurement includes a sufficient number of particles.

A second tool to evaluate if a given sample class can be used as an archetype, is to use the Association Index (AI). It is defined for a target mineral (here, magnetite) and a given gangue mineral (i) as

$$AI(i, target) = \frac{association(i,target)}{grade(i)} \quad (14)$$

The grade in mineral I is known by modal mineralogy and association (i,target) is obtained by summing the proportion of binaries “mineral i –target mineral” and ternaries “mineral i – mineral j – target”, divide it by (100-Liberated magnetite-association(others, magnetite) and multiply the whole by 100. An example is displayed on figure 20.

This value can be calculated for each mineral pair but here it was calculated only for each mineral associating with magnetite (i.e. magnetite-albite, magnetite-tremolite, magnetite-apatite, …). It is a non-dimensional measure of the affinity for magnetite to be associated with the gangue minerals as a binary or ternary with the target mineral. To calculate AI, only the modal composition and the mode of occurrence of magnetite (association) are needed.

For every gangue material we can evaluate the association of it with magnetite by summing the amount of binary and ternary associations of magnetite with this given gangue mineral and divide it by the total amount of the gangue mineral (when magnetite is excluded). This will give the mass of locked magnetite associated with that given gangue material. If we divide this quantity by the modal composition in that gangue mineral, normalized to exclude magnetite, we get a ratio of the weight of magnetite associated with that given gangue material and the grade of that gangue material.

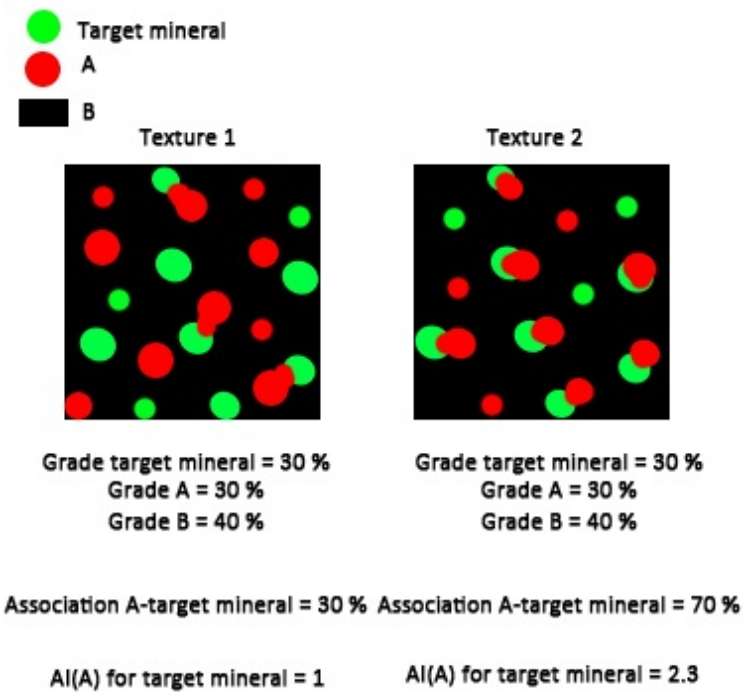

Figure 20 : Simple example of association index (AI)

This means that

- If AI = 1, association of magnetite with the gangue mineral is expected by the gangue grade; i.e. AI indicates random texture and breakage for magnetite and gangue.
- If AI > 1, association of the magnetite with gangue mineral is preferential. This can be due to non-random, preferential texture or preferential breakage or both.
- If AI < 1 then magnetite association with the gangue mineral in particulate material is non-preferential. This may be due to texture or preferential breakage or both.

For each size fraction and for each gangue mineral an association index can be calculated. By its definition, if we assume an equal distribution of gangue minerals in all size fractions, AI should be independent of the size fraction. If some variation of AI across different size fractions is observed, that means that preferential breakage occurred for that gangue mineral.

Thus, the second step is to calculate an initial AI for each sample class and compare the values of AI for the main gangue minerals between different sample classes.

If for a given class, the degree of liberation and AI for gangue minerals does not change much when using an archetype, then that archetype is valid and can be used to describe that given class.

5. Results

a. Rock mechanics analysis

i. Point load test (PLT)

The results of the PLT for the whole population let appear a multimodal distribution on the normal probability plot as shown on Figure 21. Therefore, it makes sense to analyze the data per class, based on the mean of each class. Moreover, since the sample size in each class is small, a Student's-t distribution is used instead of a normal distribution. As an effect of this hypothesis, the formula to evaluate the confidence interval (*CI*) for the mean is given by equation (15).

$$CI = \overline{x_n} \pm t_{\frac{\alpha}{2},n-1} \frac{S_n}{\sqrt{n}} \quad (15)$$

Where x_n is the sample's mean, t the Student's t value found in tables, S_n the standard deviation of the sample and n the size of the sample.

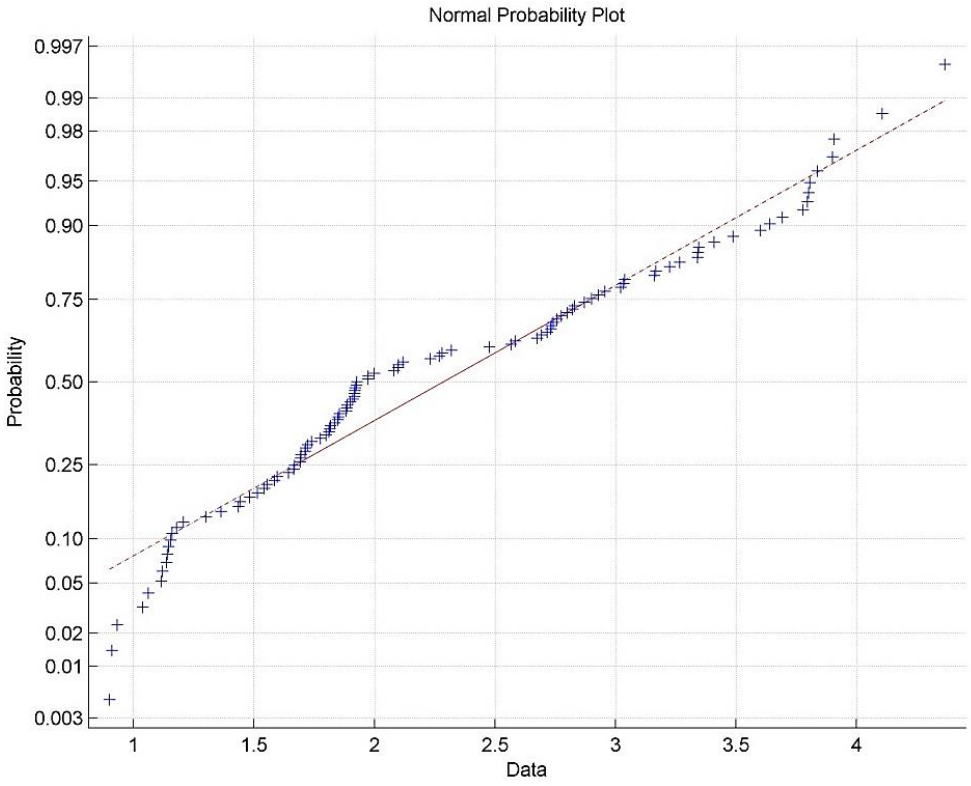

Figure 21 : normal probability plot for PLT values of the whole population

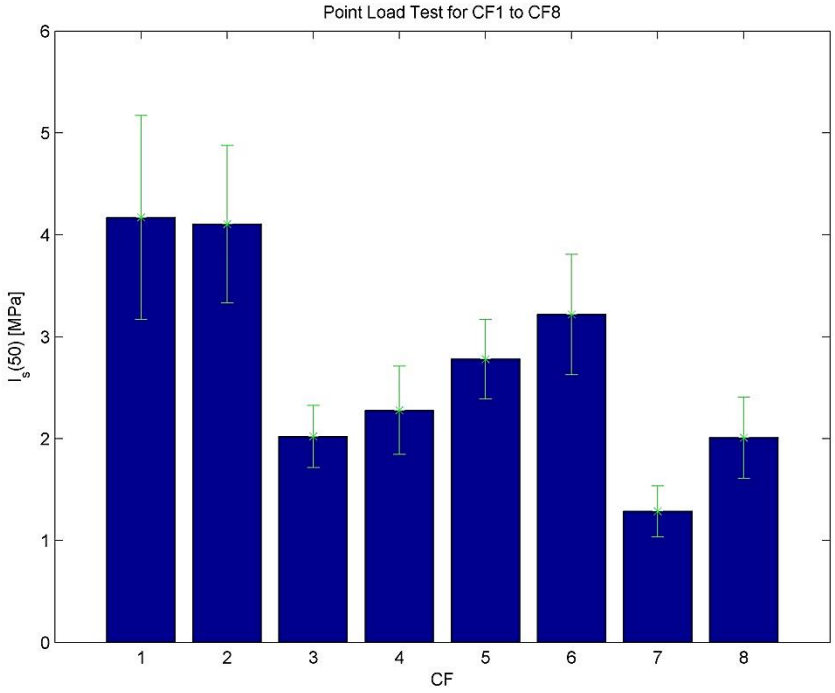

Figure 22 : $I_s(50)$ mean values and 95 % CI bars for CF1 to CF8

No continuous trend is seen for the $I_s(50)$ values despite an overall decrease from CF1 to CF8. This can be understood given the heterogeneity of the rock material: iron ore breccia composite samples. However, CF1 and CF2 have higher mean values whereas CF7 and CF8 form a lower-valued group. Caution is required for CF1, CF2 and CF6 given the large confidence interval resulting of a small sample size (CF6) or ore breccia natural heterogeneity.

The Point Load Test results for each class may be found in a graphical form the Appendix A and as a table in Appendix B.

ii. Simple compressive test (CT)

One of the expected results from the compressive test is a correlation with the Point Load Test with a linear correlation coefficient within the interval [15;50] as seen on equation (3). As shown on Figure 23, a good approximation (norm of residuals = 22.39) is given by equation 16

$$CS = 18.69 I_s(50) - 0.59 \quad (16)$$

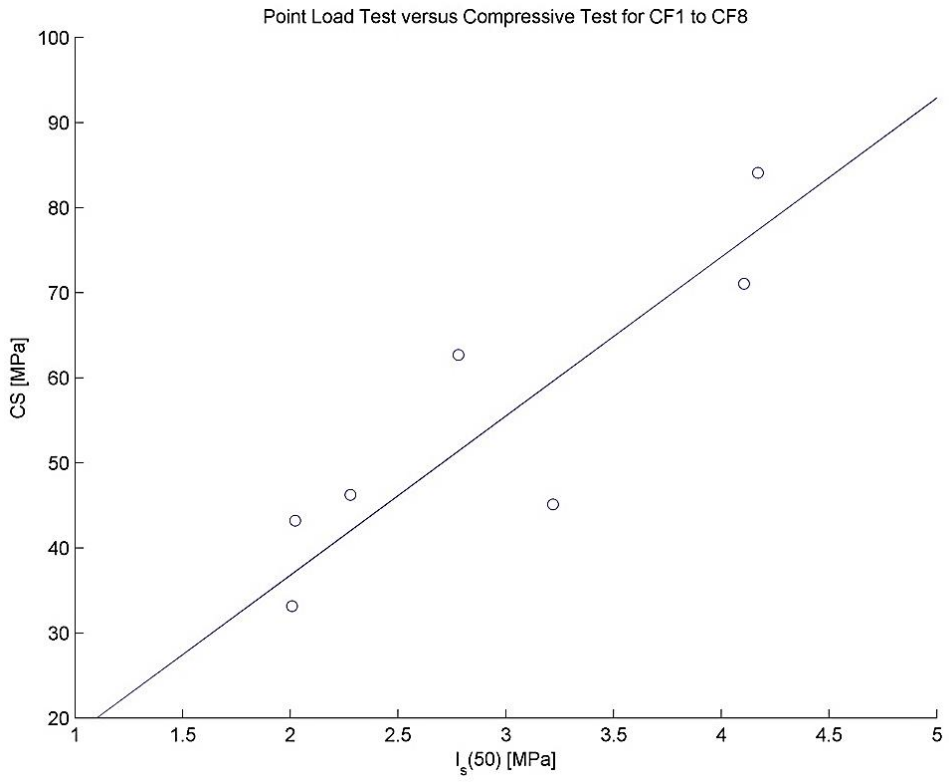

Figure 23 : Correlation between Is(50) and compressive strength

Given the correlation, the general trend of the mean compressive strength displayed on Figure 24 is the same as for $I_s(50)$. A difference lies in the fact that despite a similar decreasing trend from CF1 to CF8, the confidence intervals are much larger.

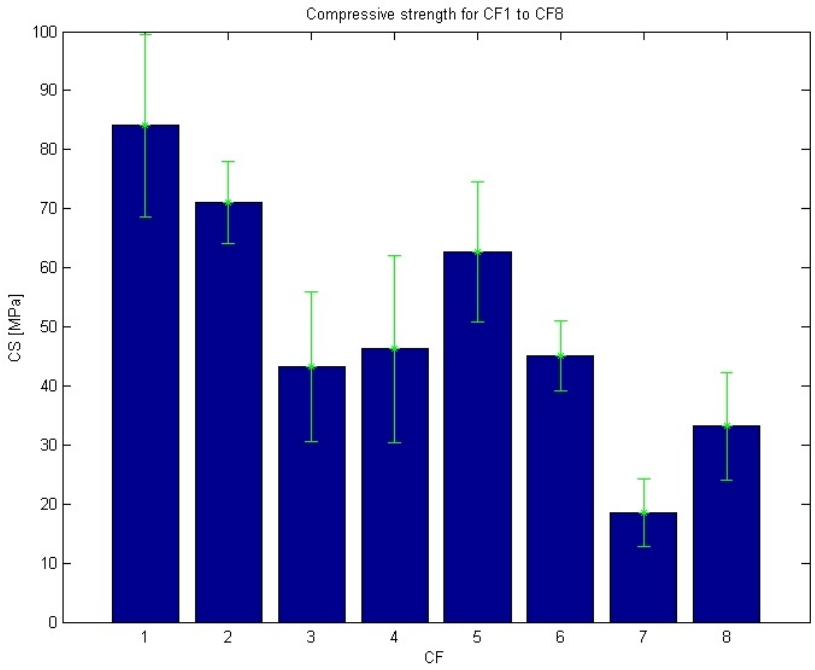

Figure 24 : Compressive strength mean values and 95 % CI bars for CF1 to CF8

The compressive test results for each class may be found in a graphical form in Appendix A or as a table in Appendix B.

iii. Statistical treatment of the results

The aims of the statistical treatment of the results are multiple:

- Get a better understanding of the properties of the ore breccia
- Track potential correlations between parameters
- Find an objective method to group the eight classes in two or three clusters according to their physical properties and test the validity of the quantitative description of the texture of Malmberget felspar type with only high graded massive and low graded disseminated archetypes. This clustering approach has been used in another context by (Anderson 1971) and the general
- Determine classes of different properties to select representative samples for the SEM imaging and EDS analysis as well as XRF.

However, the relatively limited number of samples used in this study must be noticed. Therefore, one must be cautious about the interpretation of statistical results and keep in mind its physical meaning. Specifically, the link between mechanical tests and behavior in comminution as well as degree of liberation is not established here. This first classification is an attempt to see if the differences observed in terms of iron content and grain size can be related to mechanical properties and density. A motivation

for this is some knowledge of the modal mineralogy of the samples. The macroscopic texture of the samples, the analysis of the gangue minerals done by Cecilia Lund and the hypothesis of two end-members able to describe liberation in other classes are a first basis of classification.

Data normalization formula, given by equation 17, was applied to be able to compare different kinds of data and allow a better visualization.

$$x_{i,norm} = \frac{(x_i - \overline{x_n})}{S_n} \tag{17}$$

To each class were associated 5 different properties or attributes:

1. Average specific gravity [] (direct measurement)
2. Average $I_s(50)$ [MPa] (measured by PLT)
3. Average CS [MPa] (measured by SCT)
4. Average iron grade [%] from (Lund 2013)
5. Average grain size [µm] from (Lund 2013)

This numbering is used again on Figure 25.

Table 3 displays the formed matrix of dimensionless (normalized) values. This can be seen as 8 different points in a 5-dimensionnal space or as 8 different vectors that might be correlated. The first step is to compute the Pearson's correlation coefficients and p-values to evaluate if any linear correlation may be found and how statistically significant they are. Based on that, the least correlated parameters will be chosen as a basis to form the clusters.

Table 3 : Standardized attributes matrix

	Specific gravity	Is(50)	CS	Iron grade	Grain size
CF1	-1.179	1.385	1.585	-1.235	-1.821
CF2	-0.949	1.323	0.970	-1.060	0.516
CF3	-0.373	-0.648	-0.327	-0.592	-0.507
CF4	0.505	-0.494	-0.200	-0.358	-0.552
CF5	-0.848	0.056	0.589	0.110	-0.220
CF6	0.610	0.477	-0.282	0.772	0.458
CF7	0.515	-1.394	-1.519	0.694	0.651
CF8	1.720	-0.703	-0.815	1.668	1.475

Based on the p-values ($p<0.05$), the most significant correlated attributes for Fabian ore breccia are

- Average iron grade and average specific gravity
- $I_s(50)$ and CS as shown on Figure 23
- Average grain size and average iron grade

The selected attributes for clustering are average $I_s(50)$ and average iron grade. In hierarchical clustering, the main challenges are the choice of the attributes (how many attributes used for classification and which ones) and the number of clusters that has to be known in advance. Literature suggests the use of maximum k attributes for classification of 2^k elements samples (Formann 1984, Mooi 2011). By using hierarchical clustering with centroid linkage (a way to define the distance between two clusters as the distance between their means (Flach 2012)) and two clusters representing the two end members of archetypes: high graded massive and low graded disseminated, CF1 CF2 CF3 CF4 CF5 were grouped in cluster 1 , whereas CF6 CF7 and CF8 were put in cluster 2. However, this classification cannot be fully justified by a look at all the five normalized attributes presented on Figure 25. CF1 to CF5 samples seem to vary a lot and the overall difference between CF2 and CF3 is large. Some trends can be seen on figure 26: iron grade, grain size and specific gravity show the same increasing trend towards CF8

whereas the rock mechanics properties show a decreasing trend towards CF8. This indicates that the magnetite-rich ore breccia has a weaker mechanical resistance. However, these trends reflect the correlation and do not imply any causal link.

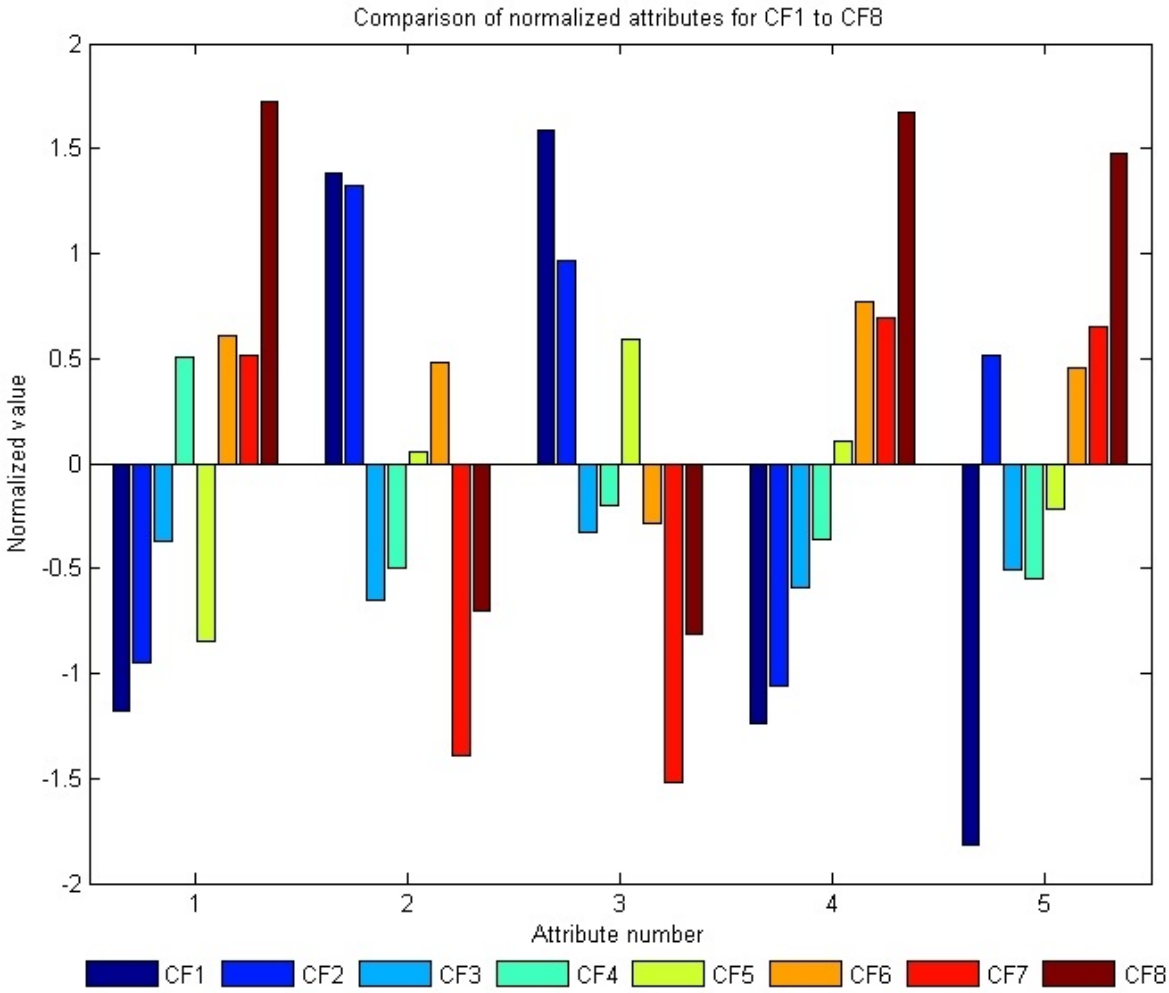

Figure 25 : Comparison of normalized attributes for samples CF1 to CF8

Legend for attribute number

1. Normalized specific gravity
2. Normalized $I_s(50)$
3. Normalized CS
4. Normalized iron grade
5. Normalized grain size

Based on these observations, the number of clusters was extended to three. Even though this classification is not perfect, it allows refining the first hypothesis of the two end-members (from fine grains with low iron content to coarse grains with high iron content) with the introduction of an intermediate class in terms of mechanical properties. Figure 26 shows the three new clusters:

- Cluster 1 (blue) includes CF7 and CF8
- Cluster 2 (green) includes CF6, CF5,CF4 and CF3
- Cluster 3 (brown) includes CF1 and CF2.

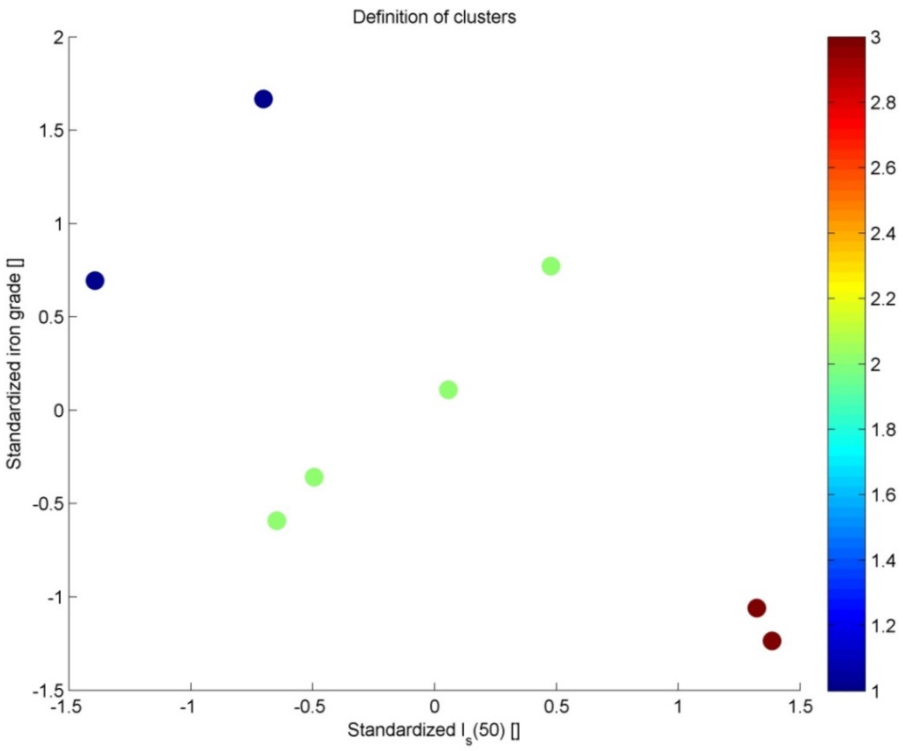

Figure 26 : Classification of the samples into three clusters

Three classes of ore breccia were selected for the liberation study: CF2, CF4, CF6 along with CRC and CRF as reference samples.

b. Comminution analysis

Figure 27 displays the sieving curves established for both comminution steps. As expected, between the jaw crusher series and the ball mill ones, the curve shifts upwards and to the left as a result of the size reduction process. Some facts should be noticed:

- CF2 class (low magnetite grade, high feldspar content) shows in both cases as a higher resistance to comminution than other materials.
- CRF (fine grain reference sample) shows a lower resistance both to the jaw crusher and to the ball mill than any other samples
- CF4 and CF6 (grouped together in cluster 2) display a similar behavior in both steps

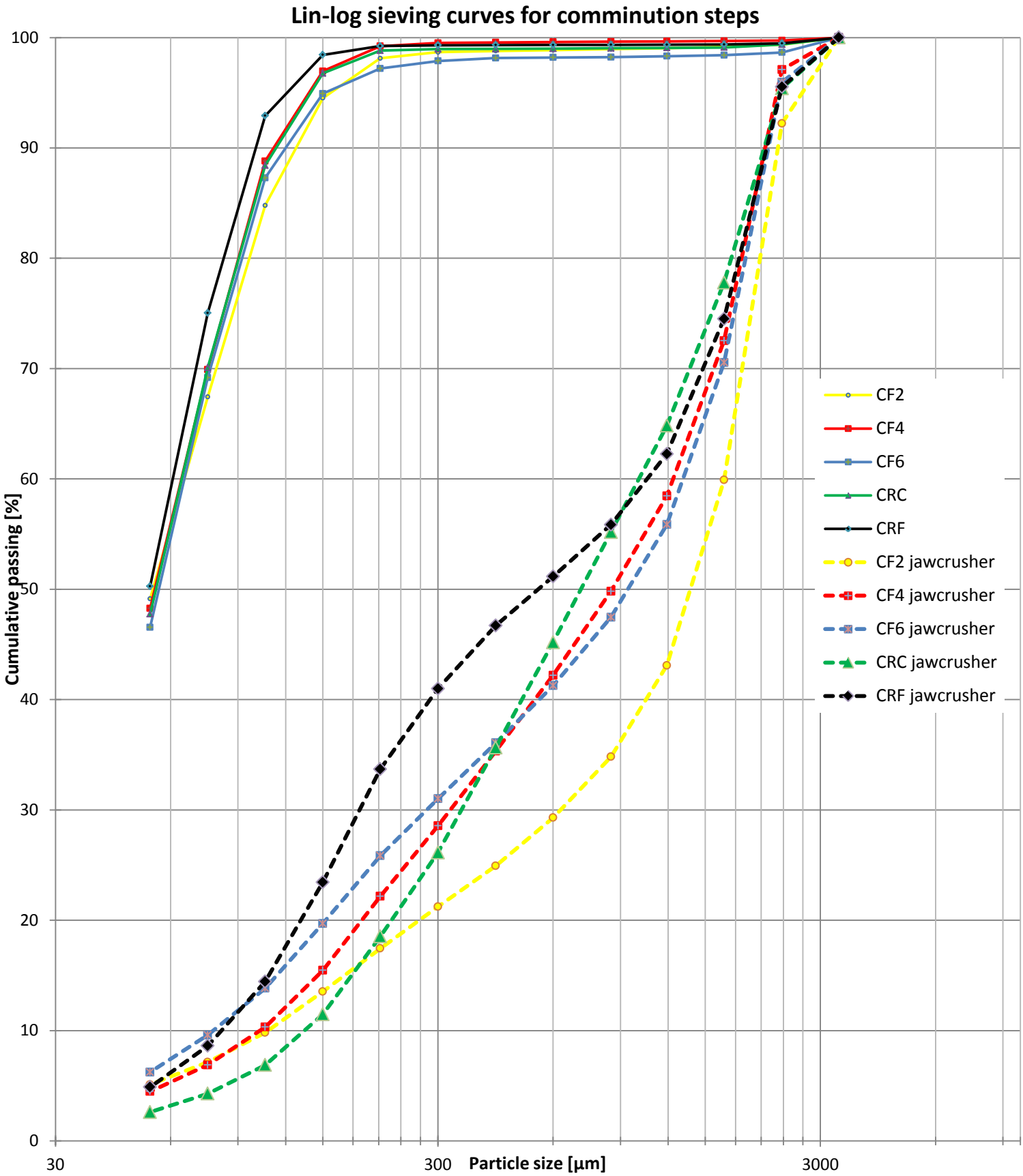

Figure 27 : Lin-log sieving curve for comminution steps

Regarding the reduction ratio, the definition of equation (18) is used

$$R = \frac{f_{80}}{p_{80}} \tag{18}$$

Where f_{80} is the size to which 80 % in mass of the feed is inferior and p_{80} the size to which 80 % in mass of the particles produced after comminution is inferior. In the case of the jaw crusher, p_{50} provides a better indication but p_{80} was still used to compute the reduction ratio. As f_{80} in the jaw crusher step, an average size of 17.3 mm based on the drill cores was chosen, whereas in the ball mill step the feed was the particles produced by the jaw crusher. As seen on the sieving curves, CF2 has always the highest d_{80}, CRF has always the lowest and there is no significant difference between CF4 and CF6 for the crushing step. However, some difference is observed during the grinding step in terms of d_{80}: CF6 has a higher value and CRC gets closer to CF4. As a conclusion, the classification in three clusters with CF2 in the first, CF4 and CF6 in the intermediate one seems to be valid for both comminution steps. CRC shows a different behavior than CRF in terms of comminution. Since their modal mineralogy is the same, this could be explained by their different grain size.

Table 4 : Computation of the reduction ratio for comminution steps (f80 for feed and p80 for product)

Class	Grinding p80 [mm]	Crushing p80 [mm]	Crusher feed f80[mm]	R for crushing	R for grinding
CF 2	0.097	2.115	17.300	8.178	21.709
CF 4	0.092	1.893	17.300	9.139	20.676
CF 6	0.094	1.941	17.300	8.914	20.751
CRC	0.092	1.863	17.300	9.286	20.302
CRF	0.084	1.768	17.300	9.785	21.147

c. Liberation analysis

i. XRF analysis and Element to mineral conversion

The SEM versus EMC magnetite content in weight follows a straight line as shown on figure 28. To test if the averages were significantly different in paired samples (CF2 SEM and CF2 EMC), a paired t-test was run and shown that there is no significant difference between the SEM results and the EMC calculations for magnetite content. The relative standard deviation is 5 % which allows us to use both methods in this work. Some statistics and the result of the t-test can be found in Appendix B.

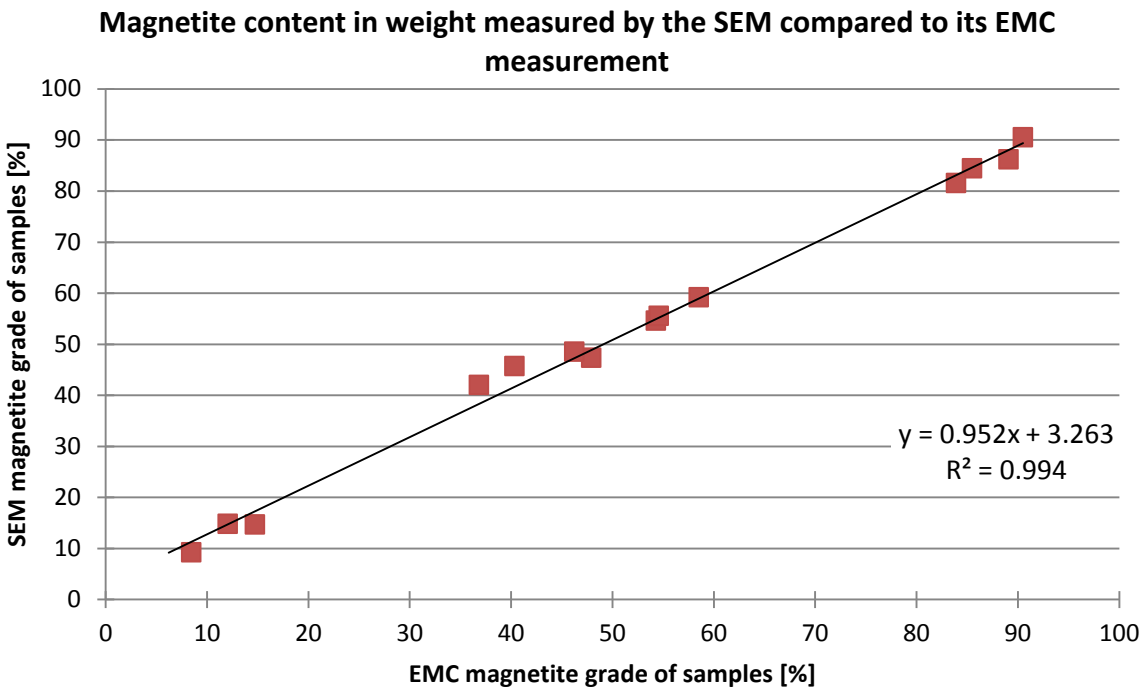

Figure 28 : Magnetite content in weight measured by the SEM compared to its EMC measurement

Another interesting result is the validation of the lab measurements of specific gravity. The direct measurement in the lab is very sensitive to variation in dimensions of the sample as shown on figure 29.

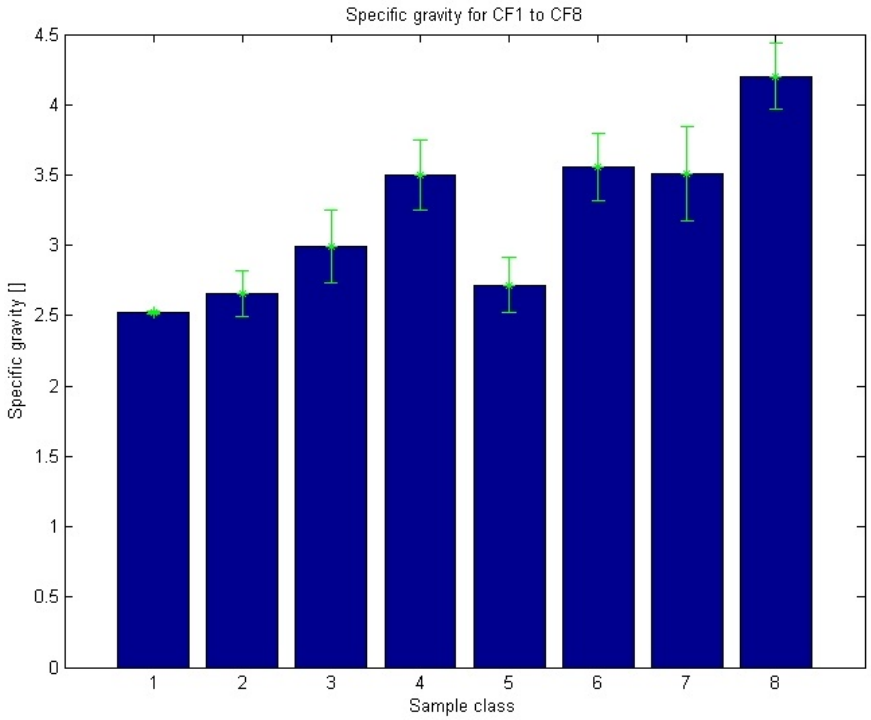

Figure 29 : Specific gravity measurement with 95 % CI

As for the magnetite grain, a paired t-test was run and shown that there is no significant difference between the specific gravity measured in laboratory and calculated from the modal mineralogy after EMC calculation. Some statistics and the results of the paired t-test can be found in Appendix B. As observed earlier, CF4 and CF6 have very close average specific gravity whereas CF2 is distinct.

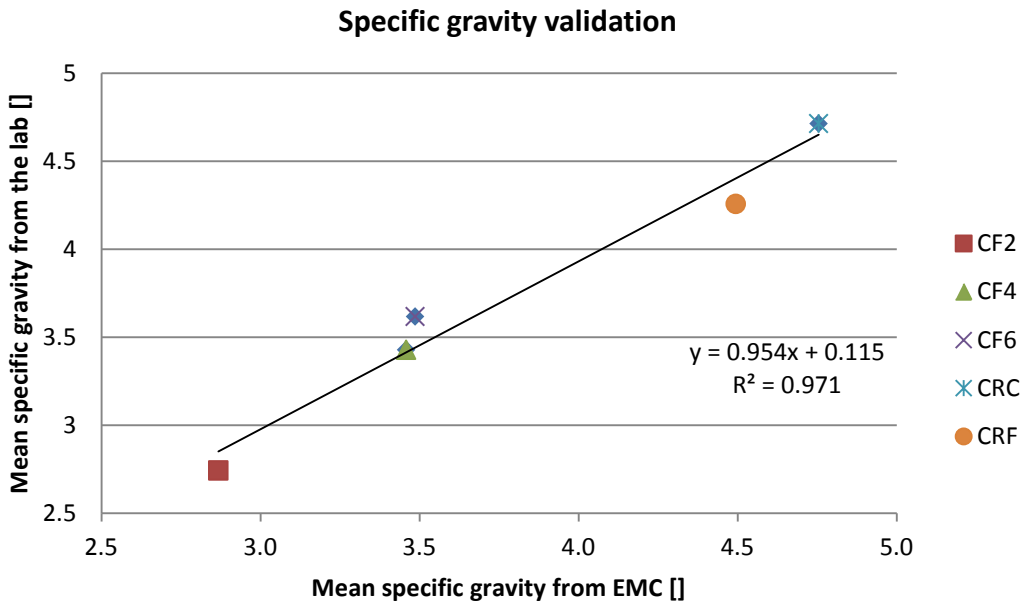

Figure 30 : Specific gravity measured by the SEM compared to its EMC measurement

Some additional information about the modal composition of each sample class is provided by both SEM and EMC. Figure 31 shows the modal mineralogy for one size fraction with the magnetite content decreasing towards CF2 and the similar composition of CF4 and CF6 which follows the same trend again. The clear relation between magnetite and apatite can be seen on figure 32.

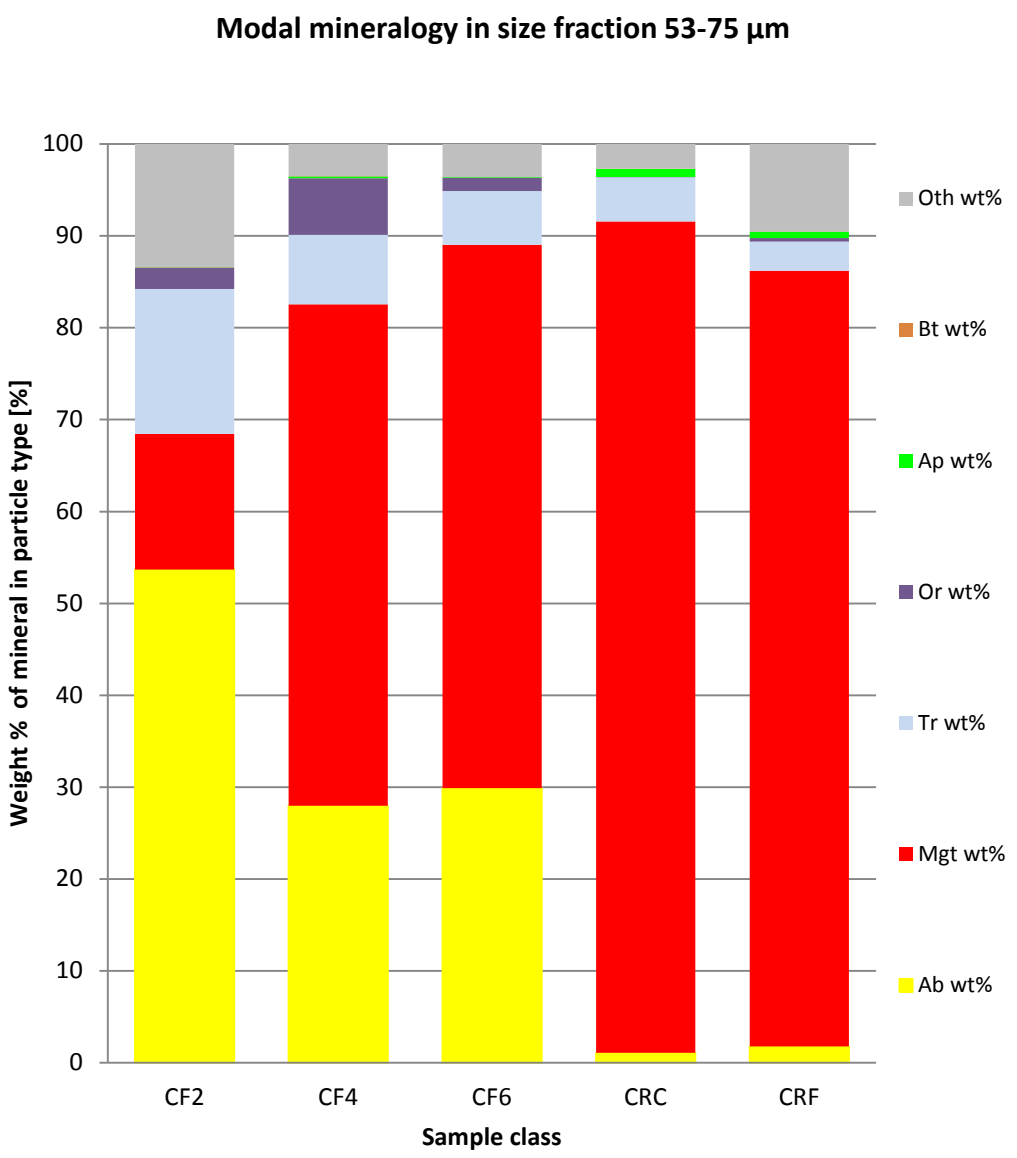

Figure 31 : Modal mineralogy in size fraction 53-75 µm

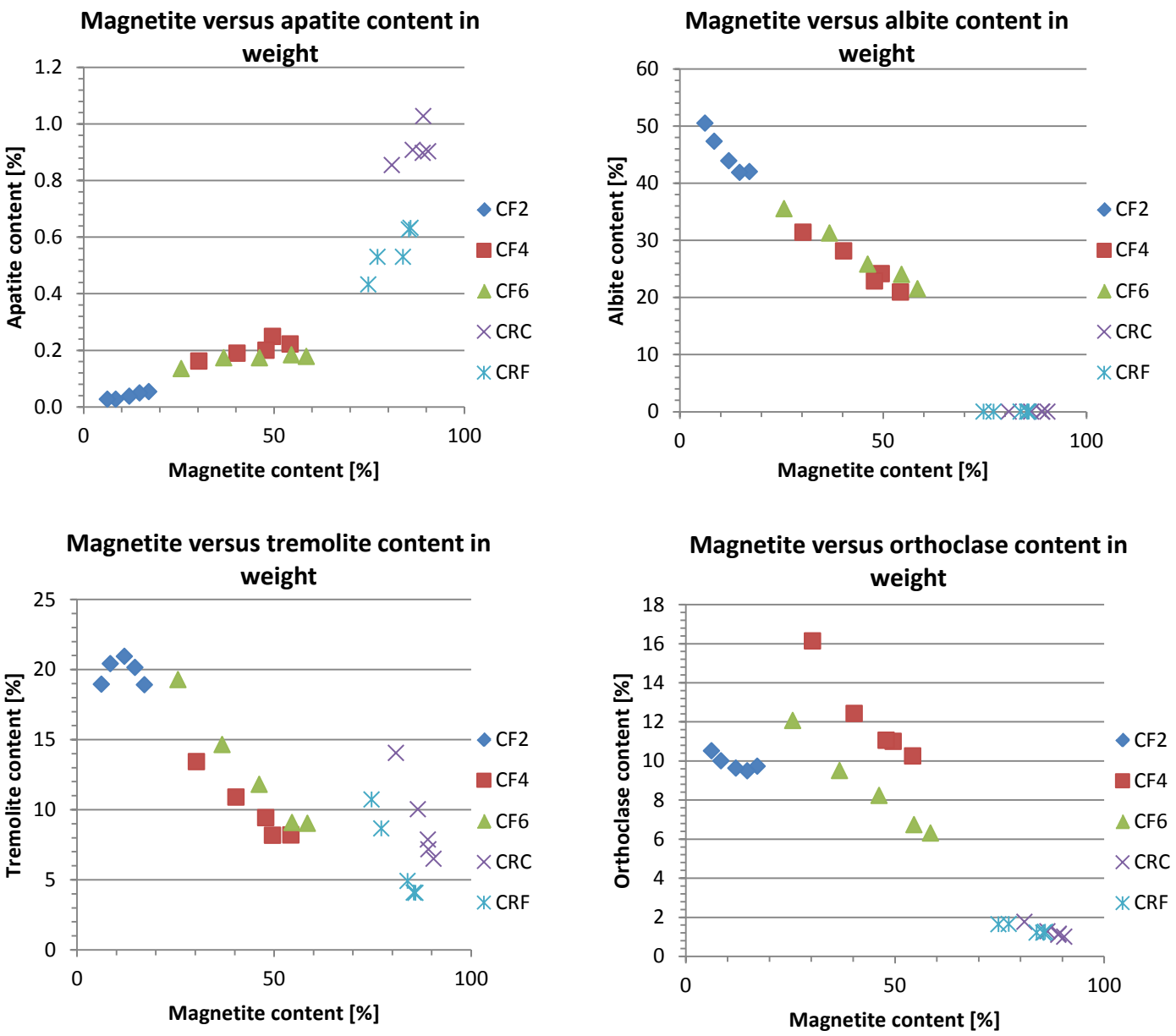

Figure 32 : Magnetite versus apatite, albite, tremolite and orthoclase contents in weight in size fractions of the samples.

The modal composition shows that for most of the minerals CF2, CF4 and CF6 form continuous trend. CF4 is, however richer in orthoclase than the other samples. Reference samples, massive coarse and fine grained magnetite differ from the breccia ore samples by showing lower albite and orthoclase content as the extrapolation would suggest and higher apatite and tremolite content, respectively.

ii. SEM Liberation analysis

Due to a technical problem with scanning electron microscope, not all size fractions could be analyzed for liberation. However, all different textures and reference samples were analyzed for the size fractions 53-75 µm and 75-106 µm. Interpolation could have provided information for all size fractions. As an example, extrapolated CF2 data is displayed on figure 33 and 34.

However, it was decided not to rely on interpolated data to draw conclusions but rather use the 53-75 µm fraction for which a sufficient number of particles were measured with the SEM and for which all samples have been fully analyzed. For each sample, the mode of occurrence of magnetite will be displayed and the liberation curve will be presented in Appendix A.

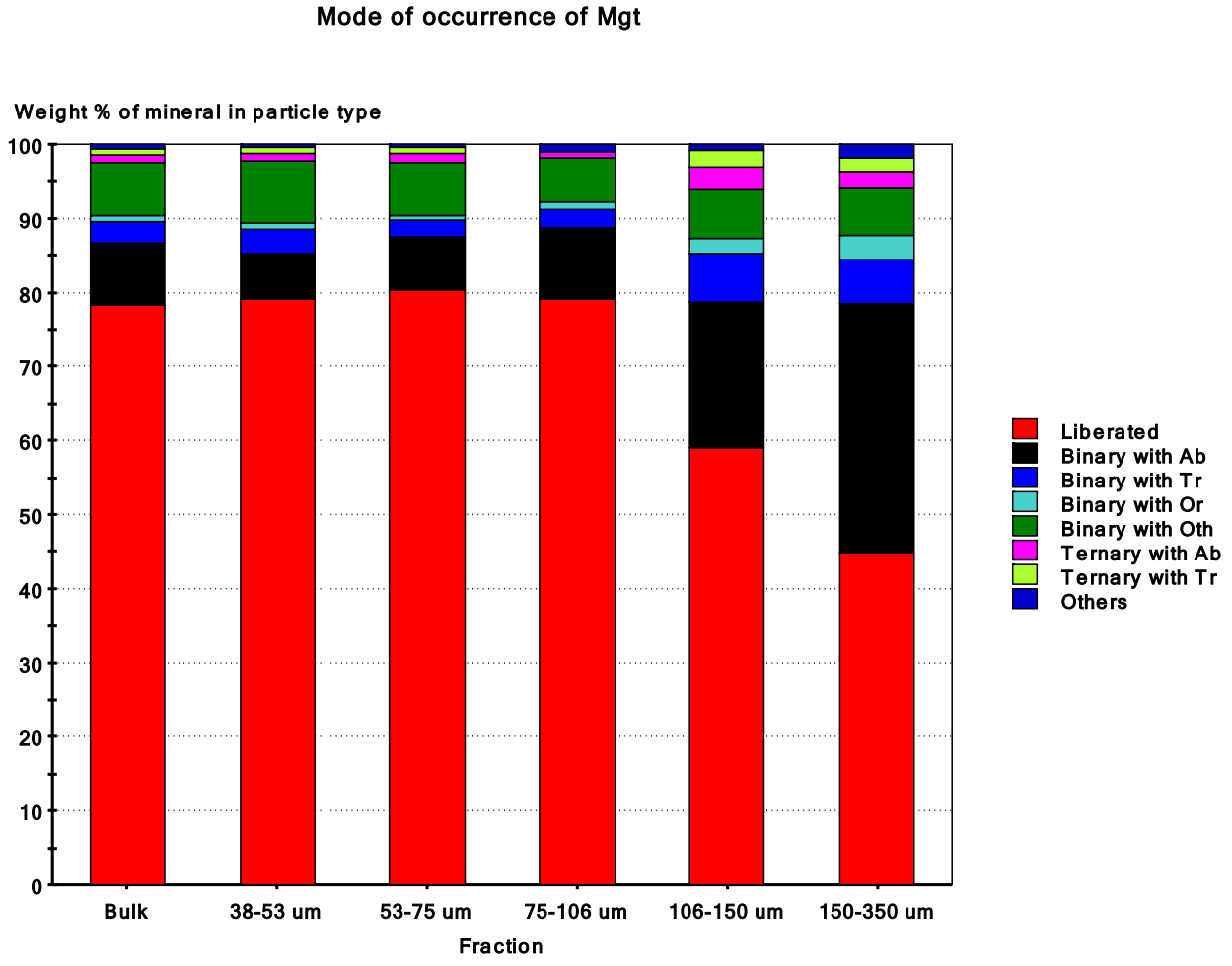

Figure 33 : Mode of occurrence of magnetite in CF2 with interpolated data

The liberation of magnetite increases by decrease in particle size while the mass proportion for the magnetite binaries with albite and tremolite follow the opposite trend. This result is as expected for the magnetite liberation. Another interesting feature is that for 53-75 µm size fraction, the liberation of magnetite seems to be a little higher than in finer particle size, 38-53 µm. This could lead to think of an

optimal liberation size for magnetite in CF2 but these results come from extrapolation and the overall difference is small so that no clear conclusion regarding this hypothesis can be drawn.

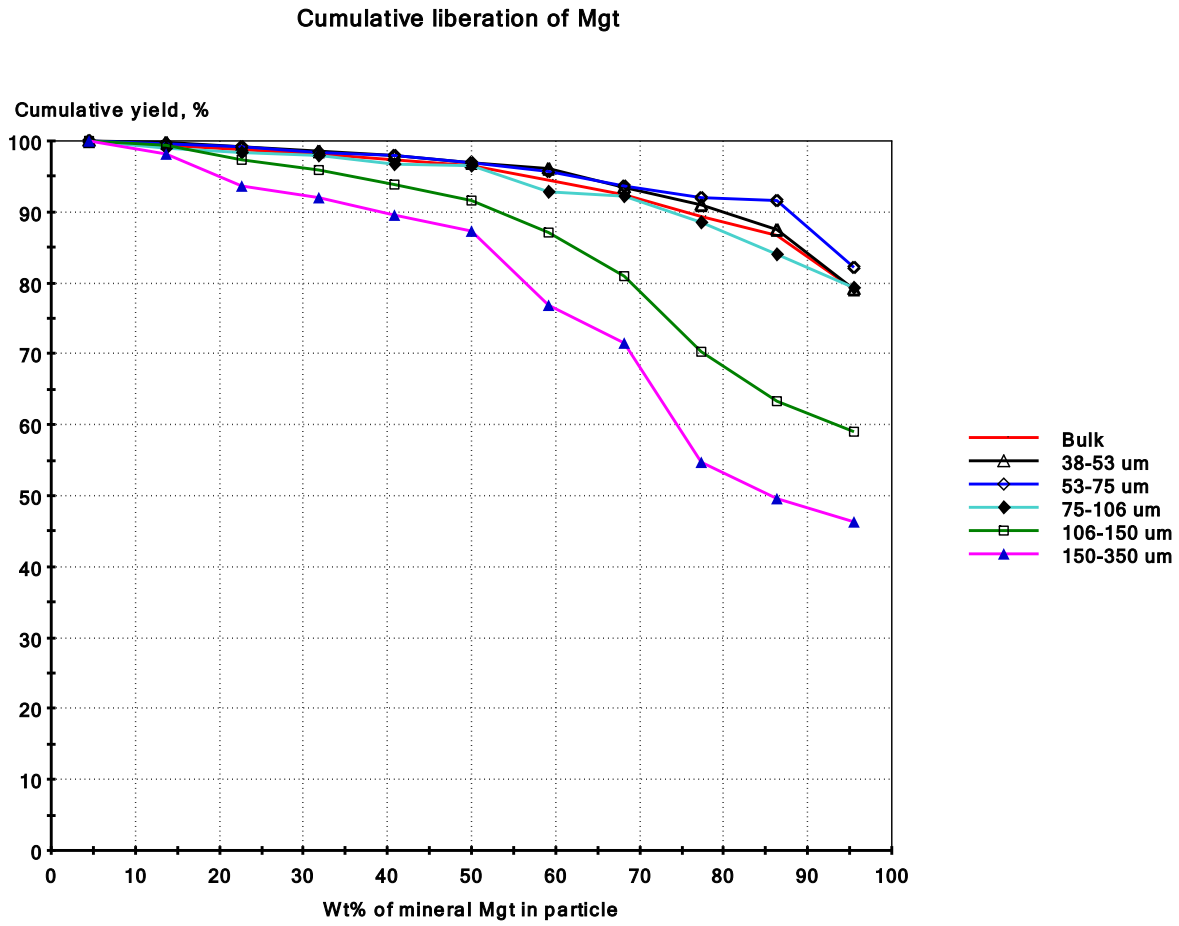

Figure 34 : Cumulative liberation curve of magnetite in CF2 for all size fractions with interpolated data

On Figure 35, in the cumulative liberation curve, the same trend of an increase in the degree of liberation towards the smaller size fractions is observed.

The next part focuses on the 53-75 µm size fraction. On all figures, mineral names are abbreviated according to this list:

- Magnetite : Mgt
- Albite : Ab
- Apatite : Ap
- Amphiboles : Tr (no distinction made in the tremolite-actinolite solid-solution)
- Orthoclase : Or
- Biotite : Bt
- Other minerals : Oth

Figure 35 shows how magnetite is liberated or associated in binaries, ternaries or more complex assemblages in the different classes.

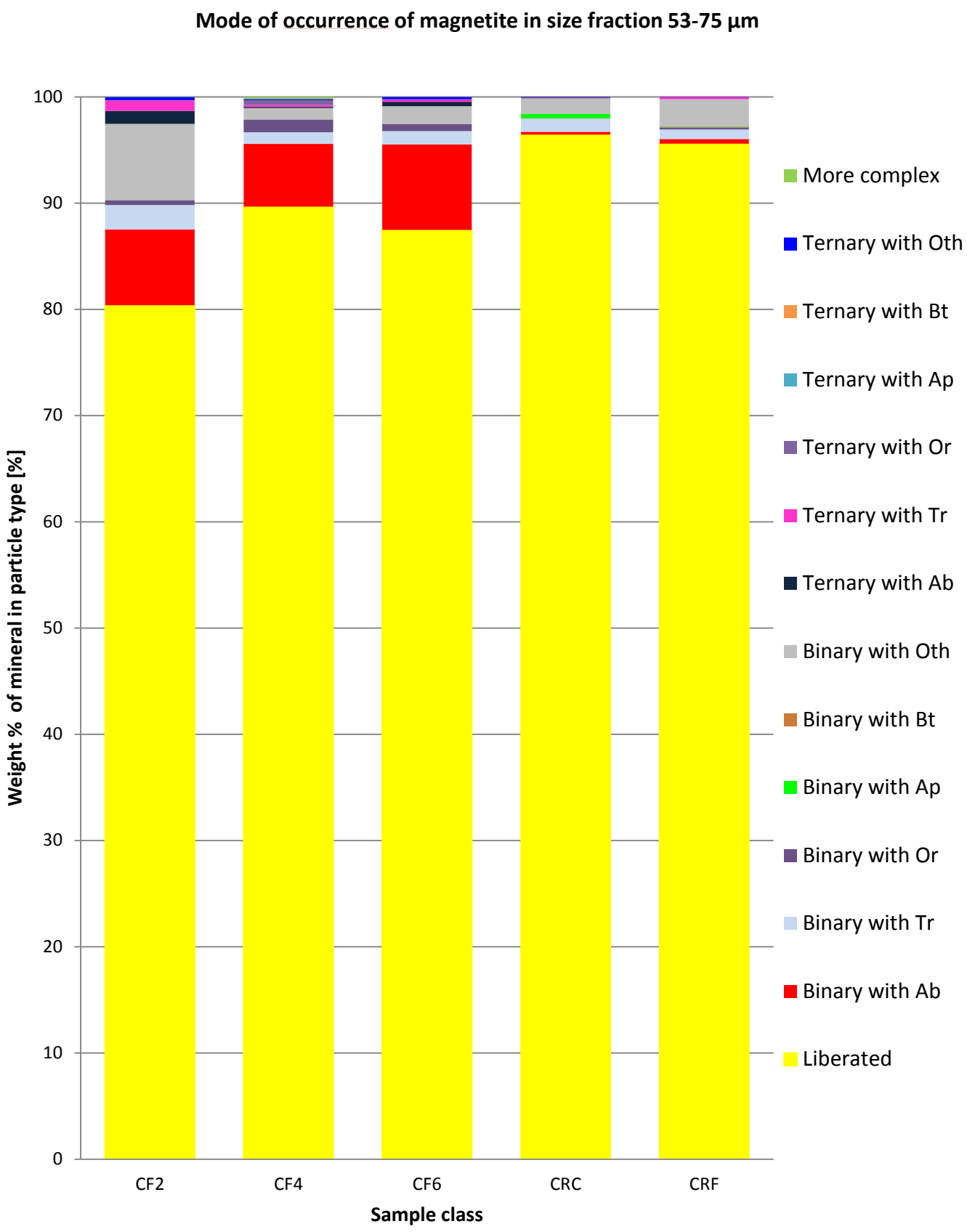

Figure 35 : Mode of occurrence of magnetite in size fraction 53-75 µm for all samples classes

The first striking fact is the relatively high degree of liberation, most notably in the reference samples. As in other results, CF2 shows different association for magnetite and is characterized by a low degree of liberation. In CF2, the proportion of ternaries is higher as well as the magnetite associated with other minerals. CF4 and CF6 are comparable but CF4 has a higher degree of liberation that could be due to the tendency of CF6 not to liberate as easily from albite binaries and ternaries or from binaries with other minerals. Another explanation could be the slightly different modal composition between those classes as displayed in Appendix A. The reference samples both display a high degree of liberation.

iii. Liberation model by archetypes

The first way to check if a given class could be used as an archetype or not, is to compare the measured degree of liberation (DOL) with the rebalanced degree of liberation.

Table 5 : Degree of liberation of magnetite, i.e. mass proportion of fully liberated magnetite

Weight % of fully liberated magnetite	CF2	CF4	CF6	CRC	CRF
Measured	80.4	89.7	87.5	96.4	95.6
Using CF2 as archetype	80.4	85.1	85.3	89.4	87.8
Using CF4 as archetype	89.7	89.7	90.3	94.3	93.2
Using CF6 as archetype	64.4	86.8	87.5	92.9	91.5
Using CRC as archetype	60.2	89.5	91.7	96.4	95.6
Using CRF as archetype	66.8	88.6	91.5	96.3	95.6

As seen on table 5, some values highlighted in green and orange have only a small difference between their original values and the ones generated by the archetype. Therefore, the following archetypes could be possible: CF6 for CF4 or CRC or CRF, CF6 for CF2 or CRC for CRF but these should also keep a similar association index while using an archetype.

The fact that the weight of liberated in CF2 goes down a lot when using CRF as an archetype discards the option of using CRF as an archetype for CF2 .

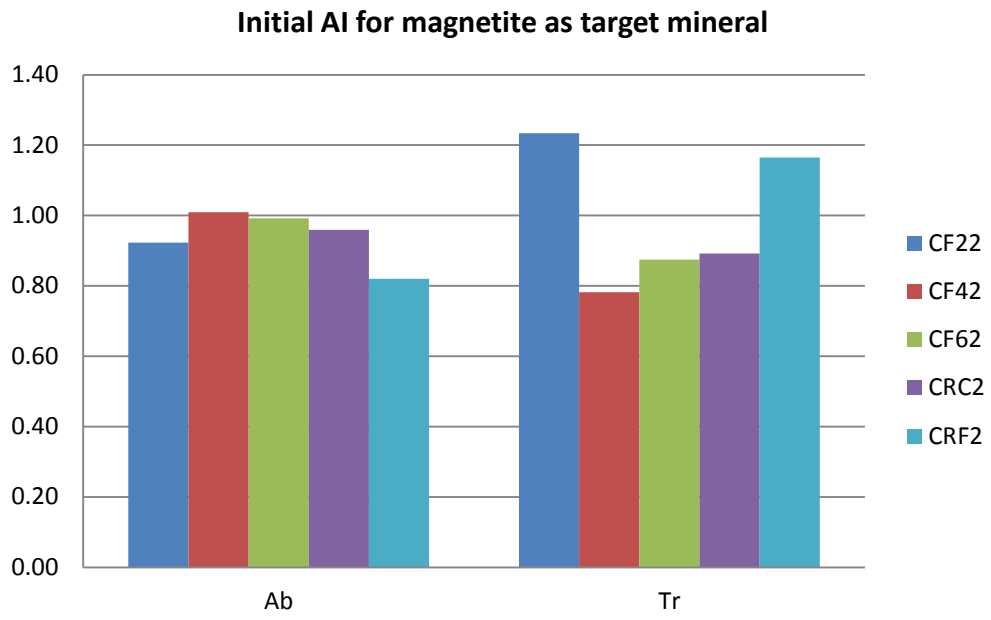

Figure 36 : Initial AI for magnetite as target mineral

On figure 36 it seems likely that CF4 could be used as an archetype to describe CF6. CF2 does not behave similarly to the others so should not be described by CF4 archetype but CRC could be described by CF4 as well since its AI values are close to the CF4 and CF6 ones. This figure will be the basis to which all other rebalanced AI results will be compared: if the difference is big then the choice of archetype was bad, if the difference is small, then the archetype can be used provided the degree of liberation is close enough.

From the figure one could deduce that CF2 could be used as an archetype to describe CRF since their AI is similar, especially in tremolite. But in fact, liberation data shows big differences in their behavior as shown on table 5.

Figure 37 and 38 show that neither CRC nor CRF can be used to describe CF4 or CF6: the rebalanced AI differs too much from the initial one.

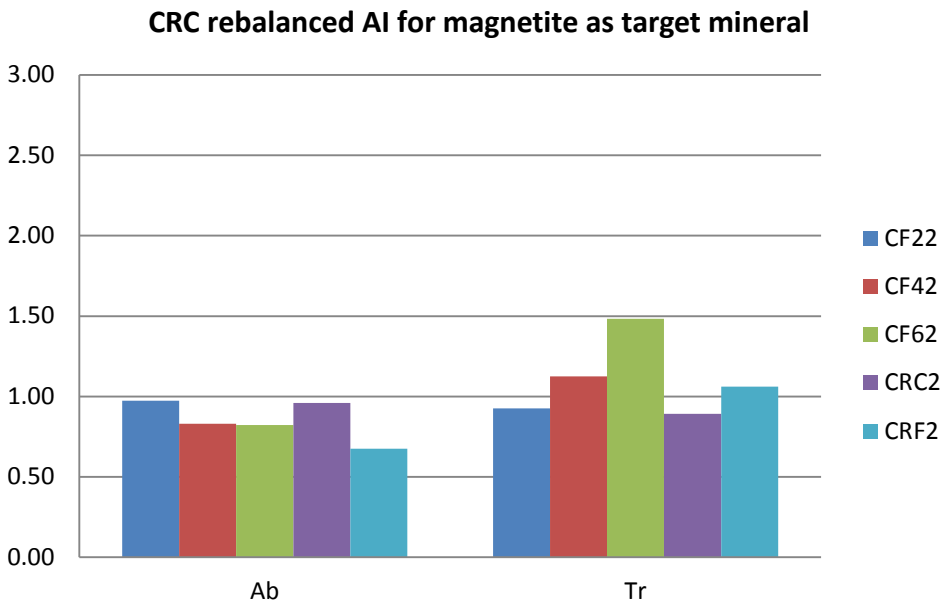

Figure 37 : CRC rebalanced AI for magnetite as target mineral

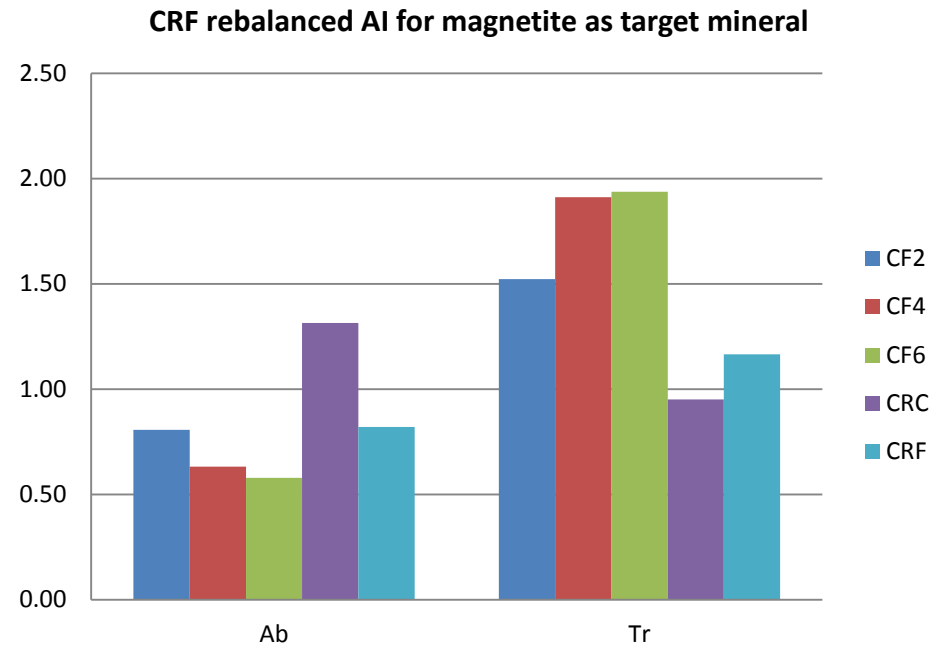

Figure 38 : CRF rebalanced AI for magnetite as target mineral

By applying the rebalance operation with CF4 as archetype and calculating the rebalanced AI we obtain the results shown on figure 39.

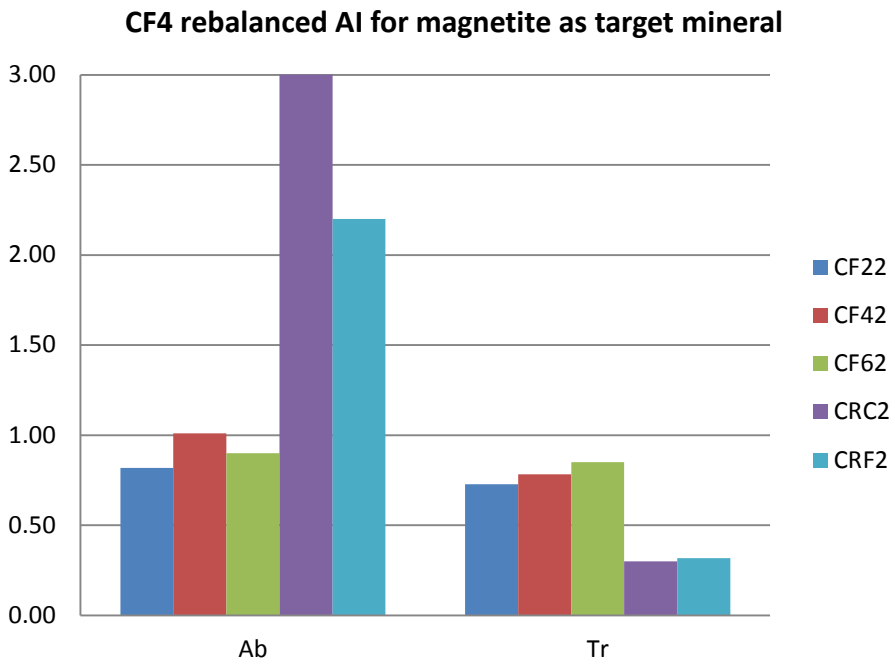

Figure 39 : CF4 rebalanced AI for magnetite as target mineral

These results show that the association index is almost similar for CF6 while using CF4 as an archetype. This suggests that CF4 can be used as an archetype to describe the texture of CF6. On the other hand, CRC cannot be used as an archetype for CF4. Another observation is the clear distinction between the iron ore breccia CF2, CF4 and CF6 compared to the reference ore samples CRC and CRF.

These results suggest that there are three archetypes and they can be used in reconstructing the liberation distribution of samples modally close to these ones as displayed in Table 6.

Table 6 : Similarities between classes

Archetype	Samples similar in texture, tested with liberation measurement	Samples similar in texture suggested by similarity in modal composition
CF2		CF1
CF4	CF6	CF3, CF5
CRC		CRF,CF7,CF8

d. Empirical linear models

i. Method

As stated in the motivations of this study there is an interest for prediction of

1. The reduction ratio for jaw crushing (R_c)
2. The Work Index for grinding (W_i)
3. Degree of liberation of magnetite (Lib)

In this section, empirical linear models based either on rock mechanics and physical properties or modal mineralogy are studied. This work was done by using HSC Data which provides a convenient framework to test different models.

Due to a low number of measurements (five classes only) , a limited number of parameters should be used to forecast classes CF2, CF4, CF6, CRC and CRF since the data to predict consists only of five values. Regarding W_i, since it is an intrinsic property of the material, information from the previous comminution step (jaw crusher) was not taken into account for the models. The available data is shown in table 7.

Table 7 : Data used to build the models

	g [µm]	Mgt wt%	Ab wt%	Tr wt%	Ap wt%	Or wt%	Bt wt%	PLT [Mpa]	CS [MPa]	Rc	Wi[kWh/t]	Lib %
CF2	102.840	11.707	45.111	19.878	0.039	9.871	0.033	4.105	71.075	8.178	5.243	80.386
CF4	75.944	44.474	25.500	10.030	0.204	6.153	0.013	2.220	46.344	9.139	5.085	89.662
CF6	101.391	44.349	27.627	12.766	0.169	8.571	0.020	3.227	44.625	8.914	5.139	87.482
CRC	180.000	87.239	1.176	4.793	0.918	1.263	0.028	1.677	16.430	9.286	5.092	96.445
CRF	32.000	74.776	1.677	6.484	0.550	1.396	0.003	1.734	32.898	9.785	4.858	92.666

The first column is named g for the average mineral grain size that comes from earlier measurements done by Cecilia Lund. The following columns show the modal composition in weight percentage of a representative size fraction (53-75 µm). The two new columns reflect the mechanical test (PLT and CS as described previously). The three last columns are the parameters to forecast. The reduction ratio for the jaw crusher $\mathbf{R_c}$ has been modified to include the d_{max} instead of the d_{80} value. The values $\mathbf{W_i}$ represent the relative work index (it is called relative since the efficiency of the laboratory ball mill is not known and therefore it cannot be used to compare against other comminution circuits) to which was applied a correction factor for the experimental results, more information is provided in appendix B. **Lib %** refers to the degree of liberation for magnetite.

ii. Results

1. Model 1 : Reduction ratio for jaw crusher described by grain size and CS

A model based on the grain size and compressive strength is able to explain 95.76 % of the variance for R_c. In this case, PLT could also be used since CS and PLT are correlated as explained earlier. A detailed table for this model can be found in Appendix B.

$$R_c = -0.0237CS - 0.0060g + 10.6555 \quad (19)$$

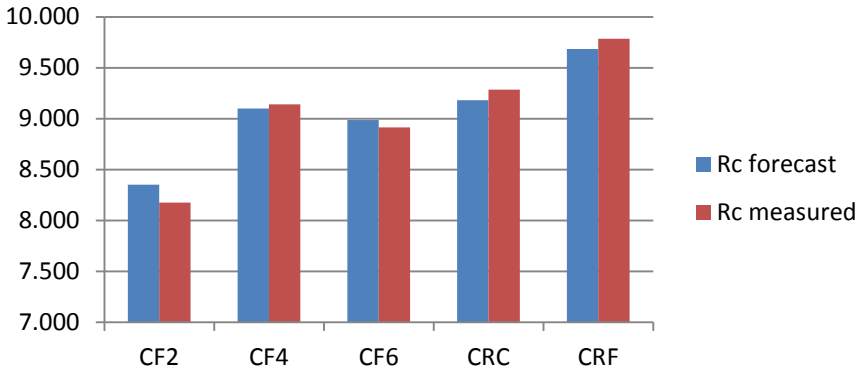

Figure 40 : Predicted versus measured values for model 1

Table 8 : Model 1 values and error

Grain size [µm]	CS [MPa]	Rc forecast	Rc measured	Rel. error [%]	SSQ	RMSD
102.840	71.075	8.352	8.178	2.129	0.030	0.012
75.944	46.344	9.100	9.139	0.433	0.002	
101.391	44.625	8.987	8.914	0.815	0.005	
180.000	16.430	9.180	9.286	1.138	0.011	
32.000	32.898	9.683	9.785	1.038	0.010	

The relative error is low enough to consider the model as properly describing the reduction ratio for the jaw crusher. This indicates that for the five selected classes, compressive test results can be combined with grain size information to provide a good estimate of the reduction ratio on the jaw crusher. Concerning the effect of grain size on R_c, it should be noticed that the grain size only explains about 30 % of the variance. Moreover, these models fit the measured data and do not provide any explanation about the precise effect of a parameter nor of physical mechanisms on the

value of R_c. The only intent is to provide a way to forecast the value of R_c, not to identify the physical phenomena that influence it.

2. Model 2 : Reduction ratio for jaw crusher described by modal mineralogy

A model based on the gangue minerals is able to explain 87.76 % of the variance for R_c. A detailed table for this model can be found in Appendix B.

$$R_c = -0.0907\,Tr - 0.2024\,Ap - 0.0044\,Ab + 10.2047 \quad (20)$$

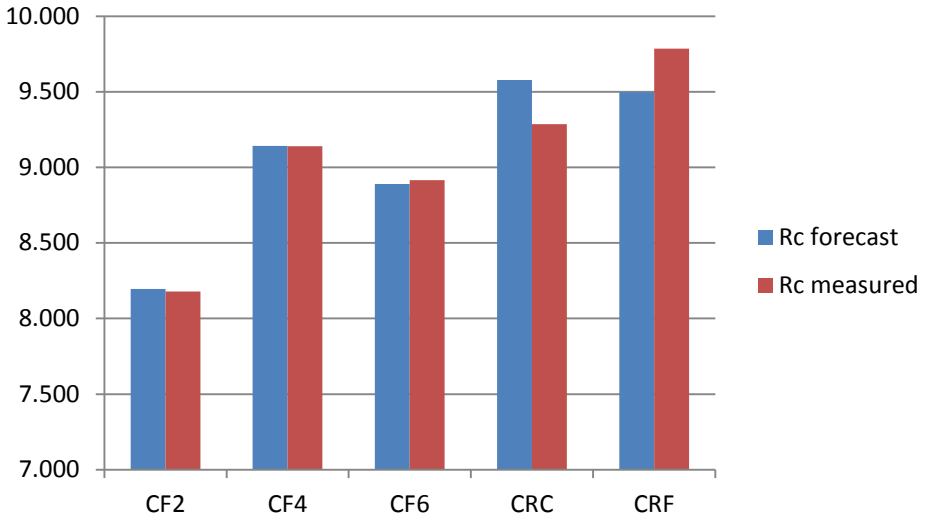

Figure 41 : Predicted versus measured values for model 2

Table 9 : Model 2 values and error

Ab wt%	Tr wt%	Ap wt%	Rc forecast	Rc measured	Rel error [%]	SSQ	RMSD
45.111	19.878	0.039	8.195	8.178	0.205	0.000	0.034
25.500	10.030	0.204	9.141	9.139	0.017	0.000	
27.627	12.766	0.169	8.891	8.914	0.267	0.001	
1.176	4.793	0.918	9.579	9.286	3.153	0.086	
1.677	6.484	0.550	9.498	9.785	2.936	0.083	

The relative error is low enough to consider the model as properly describing the reduction ratio for the jaw crusher. This indicates that for the five selected classes, modal mineralogy and more specifically of the gangue minerals could provide a good estimate of the reduction ratio on the jaw crusher.

3. Model 3 : Work index for ball mill described by PLT and grain size

A model based on the point load test and grain size is able to explain 90.76 % of the variance for W_i. A detailed table for this model can be found in Appendix B. As stated earlier, a model for Wi should only include intrinsic properties, so the use of mechanical resistance (CS or PLT since they are heavily correlated) or grain size makes sense.

$$W_i = 0.1048\, PLT + 0.0014\, g + 4.6709 \qquad (21)$$

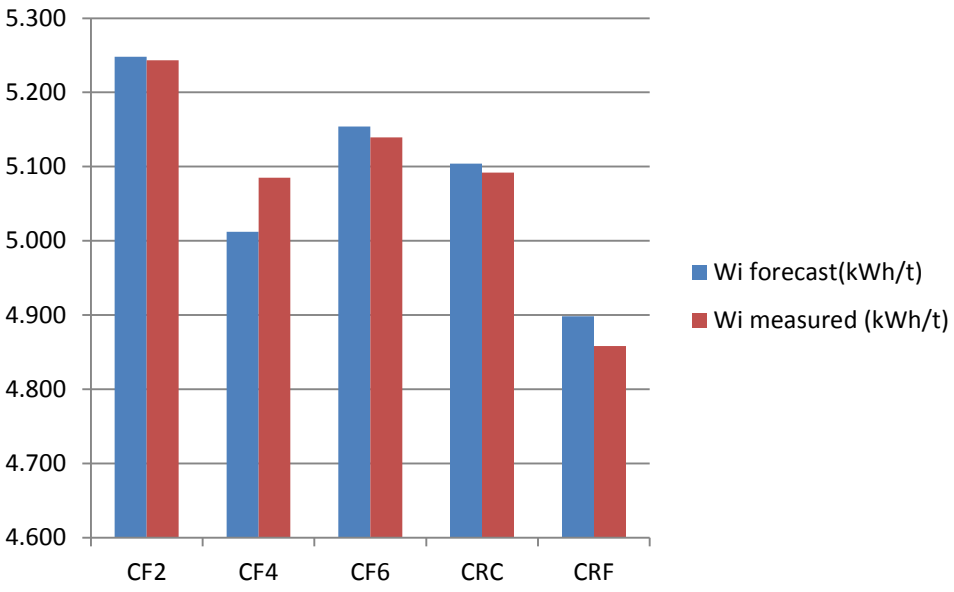

Figure 42 : Predicted versus measured values for model 3

Table 10 : Model 3 values and error

Grain size µm	PLT	Wi forecast(kWh/t)	Wi measured (kWh/t)	Rel error [%]	SSQ	RMSD
102.840	4.105	5.248	5.243	0.091	0.000	0.001
75.944	2.220	5.012	5.085	1.434	0.005	
101.391	3.227	5.154	5.139	0.288	0.000	
180.000	1.677	5.104	5.092	0.234	0.000	
32.000	1.734	4.898	4.858	0.826	0.002	

This model tends to slightly overestimate W_i.

4. Model 4 : Work index for Ball Mill described by modal mineralogy

A model based on the gangue minerals is able to explain 72.81 % of the variance for W_i. A detailed table for this model can be found in the appendix 2.

$$W_i = 0.006\,Ab + 0.888\,Ap - 0.0075\,Or + 4.8816 \quad (22)$$

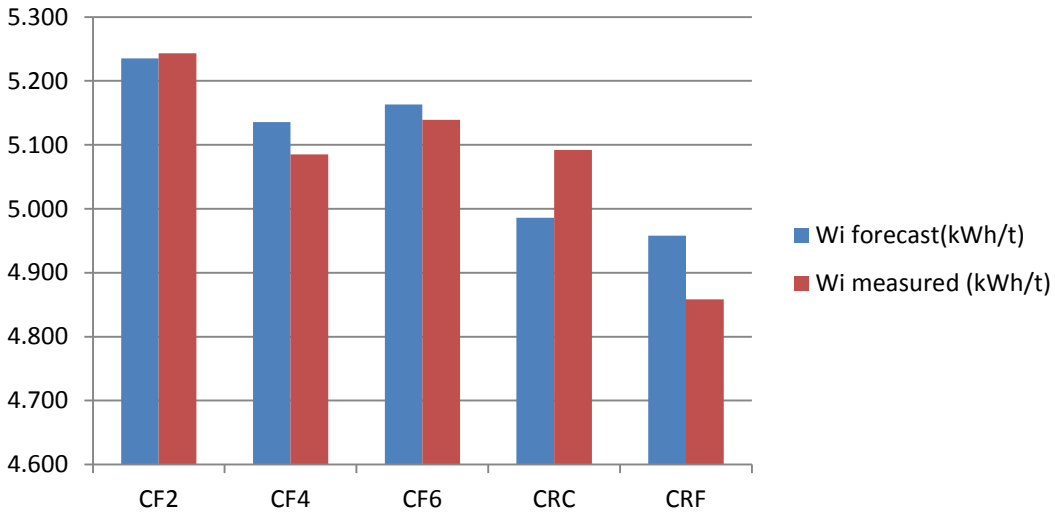

Figure 43 : Predicted versus measured values for model 4

Table 11 : Model 4 values and error

Ab wt%	Or wt%	Ap wt%	Wi forecast(kWh/t)	Wi measured (kWh/t)	Rel error [%]	SSQ	RMSD
45.111	9.871	0.039	5.235	5.243	0.153	0.000	0.005
25.500	6.153	0.204	5.136	5.085	0.993	0.003	
27.627	8.571	0.169	5.163	5.139	0.459	0.001	
1.176	1.263	0.918	4.986	5.092	2.082	0.011	
1.677	1.396	0.550	4.958	4.858	2.053	0.010	

The relative error is low enough to consider the model as properly describing the relative Work Index for the ball mill. This indicates that for the five selected classes, the modal mineralogy provides a good estimate of the Work Index of the ball mill.

5. Model 5 : Liberation described by modal mineralogy

A model based on the gangue minerals is able to explain 99.84 % of the variance for the degree of liberation. The choice here was to focus on gangue minerals instead of magnetite which can be used also since its content is directly correlated to the sum of the gangue mineral content. A detailed table for this model can be found in the appendix 2.

$$Lib = 0.0705\ Or + \ 0.7878\ Ap - 1.0045\ Tr + 99.4826 \qquad (23)$$

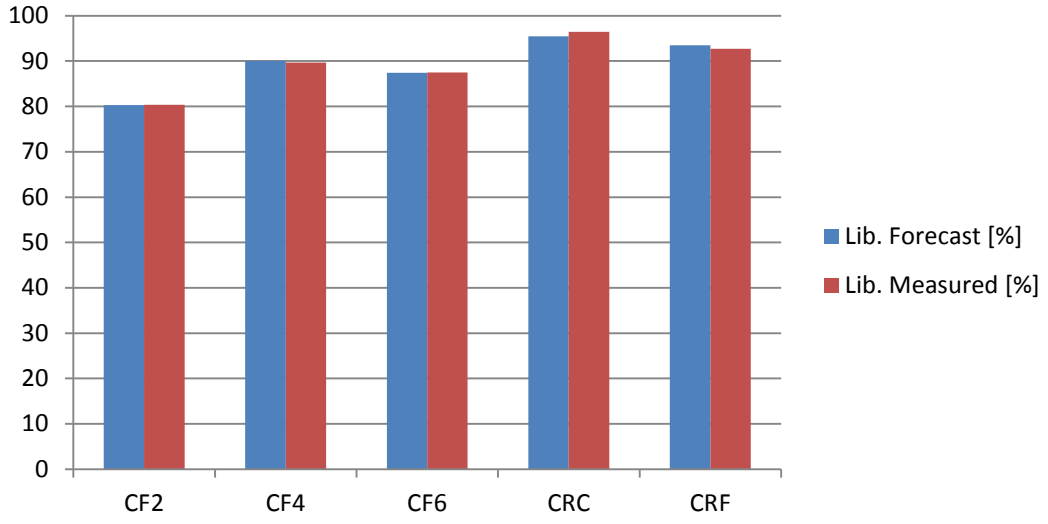

Figure 44 : Predicted versus measured values for model 5

Table 12 : Model 5 values and error

Tr wt%	Ap wt%	Or wt%	Lib. Forecast [%]	Lib. Measured [%]	Rel error [%]	SSQ	RMSD
19.878	0.039	9.871	80.248	80.39	0.172	0.019	0.355
10.030	0.204	6.153	90.006	89.66	0.384	0.118	
12.766	0.169	8.571	87.400	87.48	0.093	0.007	
4.793	0.918	1.263	95.482	96.44	0.999	0.927	
6.484	0.550	1.396	93.504	92.67	0.904	0.701	

The relative error is low enough to consider the model as properly describing the degree of liberation of magnetite. This indicates that for the five selected classes, the modal mineralogy provides a good estimate of the degree of liberation of magnetite.

Despite limitations in terms of statistical quality and applicability, predictive models can be built and used to predict comminution parameters and liberation. For prediction of W_i and R_c, modal mineralogy limited to three minerals seems not able to explain as much variance as mechanical parameters. This is due to the choice of keeping a low number of parameters in the model. By including more gangue minerals, the amount of variance explained can be increased. Future work on these kinds of models should include the combination of mechanical and modal composition models within a single predictive model, trying to keep a low number of parameters.

6. Summary and conclusion

The critical parameters in this case are the modal mineralogy and texture. Rock mechanics helps to classify and provides some additional information on the system. Prediction of rock mass parameters is complex and the tests performed in this study did not allow to fully linking modal composition with the mechanical strength of the samples even if some indication is provided: as a general trend from both point load and compressive tests, the higher the feldspar content the higher the mechanical resistance. Since the feldspar content itself is correlated to magnetite or iron grade and average grain size and that breakage mechanism also depends on cracks and micro cracks in the sample, the real cause of this change of resistance was not clearly identified.

In this work, a procedure applicable with limited sample availability but still gives quantitative results has been developed.

The main results of this work were:

- An increased knowledge on how feldspar breccia from Malmberget behaves in terms of mechanical properties, comminution and liberation.
- The linear models indicate that, based on texture information (grain size) and rock mechanics (PLT/CS), forecasting W_i and R_c for iron ore breccia from Malmberget is possible.
- The linear models indicate also that, based on modal mineralogy (gangue) forecasting the degree of liberation of magnetite for iron ore breccia from Malmberget is possible.
- The effective use of archetypes discarded the possibility to describe all the samples with only two end-members (high graded coarse grains and low graded fine grains). More specifically, CRF and CF2 cannot be grouped together and use one another as archetype. The use of archetype should always go with a good knowledge of the modal composition so not to try describing too different samples with the same archetype. The combination of modal

mineralogy information and the use of archetypes suggest the use of three classes instead of eight initially defined.

- Both modal mineralogy and texture are governing factors in comminution and liberation.

7. Limitations of the study and further work

- The linear models are based on limited data, not validated yet and might be ore-specific.
- Non-standard and limited rock mechanic testing but it still proved useful and help to a first classification of samples
- Unable to build a liberation model for all fraction sizes because not all samples have been analyzed due to a technical problem
- Different thresholds could be used to differentiate the iron oxides with the scanning electron microscope
- CF7 and CF8 have not been fully studied

In the future, some interesting questions remain that are linked to this study:

- Is there any other method to evaluate or measure the association index and how to use it for prediction?
- Can the linear models be used for other samples from Malmberget?
- What would be the result of the blend of different ore breccia classes in the feed? What would be the impact of it on energy consumption and liberation?
- Which mechanical test is the more relevant and feasible in a context of geometallurgy?
- Would mechanical tests be valuable information in the final model of an ore body?

8. References

ASTM 2011. D5731 Standard test method for determination of the point load strength index of rock and application to rock strength classifications. West Conshohocken, Pennsylvania, USA, ASTM International: 11.

Alruiz, OM., M. S., Suazo CJ, Naranjo A (2009). "A novel approach to the geometallurgical modelling of the Collahuasi grinding circuit." Minerals Engineering 22(12): 1060-1067.

Anderson, A. (1971). "Numeric examination of multivariate soil samples." Journal of the International Association for Mathematical Geology 3(1): 1-14.

Andrews, J. and Mika, T. (1975). Comminution of a heterogeneous material: development of a model for liberation phenomena. Proceedings of the XI International Mineral Processing Congress, Cagliari, Italy.

Banks, R. (1979). "The use of linear programming in the analysis of petrological mixing problems." Contributions to Mineralogy and Petrology 70(3): 237-244.

Barton, N., L. R., Lunde J. (1974). "Engineering classification of rock masses for the design of tunnel support." Rock Mechanics and Rock Engineering 6(4): 189-236.

Bass, L. (1954). "Zur Theorie der Mahlvorgänge." Zeitschrift für angewandte Mathematik und Physik ZAMP 5(4): 283-292.

Bearman, R., et al. (1997). "The applications of rock mechanics parameters to the prediction of comminution behaviour." Minerals Engineering 10(3): 255-264.

Bergman, S., Kübler, L. and Martinsson, O., 2001, Description of regional geological and geophysical maps of northern Norrbotten County (east of Caledonian orogen): SGU Geological Survey of Sweden, v. Ba 56, p. 110.

Berry, T. and Bruce, R. (1966). "A simple method of determining the grindability of ores." Can. Min. J 87: 63-65.

Bieniawski, Z. (1975). "The point-load test in geotechnical practice." Engineering Geology 9(1): 1-11.

Bond, F. (1952). "Mathematics of Crushing and Grinding." Recent Developments in Mineral Dressing: 101-115.

Bond, F. (1952). "The third theory of comminution." Trans. AIME 193(2): 484-494.

Bonnici, N., et al. (2008). Relating textural attributes to mineral processing: Developing a more effective approach for the Cadia East Cu-Au porphyry deposit. ICAM Australia 2008, AusIMM.

Briggs, C. A. and Bearman, R. A. (1996). "An investigation of rock breakage and damage in comminution equipment." Minerals Engineering 9(5): 489-497.

Charlier, R. , Bolle F. (2009). Mécanique des roches et des massifs rocheux. Liège, Centrale des cours (CdC) de l'AEES.

CLU-IN (2013, 23/04/2013). "X-Ray Fluorescence." Retrieved 20/05, 2013, from http://www.clu-in.org/characterization/technologies/xrf.cfm

Davis, E. (1920). Patent : Process for the magnetic sizing and grading of ore, retrieved via Google Patents.

Davis, E. (1921). Magnetic concentration of iron ore, University of Minnesota.

Debras, C. (2010). "Petrology, geochemistry and structure of the host rock for the Printzsköld ore body in the Malmberget deposit."

Deere, D. and Deere, D. (1988). The rock quality designation (RQD) index in practice. Symposium on Rock Classification Systems for Engineering Purposes, 1987, Cincinnati, Ohio, USA.

Dewar, M. (2013). Characterization and Evaluation of Aged 20Cr32Ni1Nb Stainless Steels Department of Chemical and Materials Engineering. Edmonton, Alberta, University of Alberta. Master of Science in Materials Engineering.

Fandrich, R.G., Y., Burrows D, Moeller K (2007). "Modern SEM-based mineral liberation analysis." International Journal of Mineral Processing 84(1): 310-320.

Fandrich, R.G. , B. R. A., Boland J., W. Lim (1997). "Mineral liberation by particle bed breakage." Minerals Engineering 10(2): 175-187.

Flach, P. (2012). Machine learning: the art and science of algorithms that make sense of data, Cambridge University Press.

Formann, A. (1984). Die Latent-Class-Analyse: Einführung in Theorie und Anwendung, Beltz.

Frietsch, R. (1982). "On the chemical composition of the ore breccia at Luossavaara, northern Sweden." Mineralium Deposita 17(2): 239-243.

Trond, G., H. B. I. (2006). Logging Demonstrating Capability. Geo ExPro: 24 - 26.

Gardner, R. and Austin, L. (1962). "A chemical engineering treatment of batch grinding." Zerkleinern Symposion. Dusseldorf: Verlag Chemie.

Gardner, R. et al. (1961). Phenomenological approach to the batch grinding of coals: Medium: X; Size: Pages: 150.

Gay, S. (2004). "A liberation model for comminution based on probability theory." Minerals Engineering 17(4): 525-534.

Gay, S. (2004b). "Simple texture-based liberation modelling of ores." Minerals Engineering 17(11-12): 1209-1216.

Geijer, P. (1930). "Geology of the Gällivare Iron Ore field." Geological Survey of Sweden Ca 22: 115. not consulted.

Harding, D. (2002). "Mineral identification using a scanning electron microscope." Minerals and Metallurgical Processing 19(4): 215-219.

Hoal, K. O. (2008). "Getting the Geo into Geomet." SEG Newsletter(73): 52.

Hukki, R. (1961). "Proposal for a solomonic settlement between the theories of von Rittinger, Kick, and Bond." Trans. AIME 220: 403-408.

Hunt, J. , B. R., Bradshaw, D. (2011). "Characterising chalcopyrite liberation and flotation potential: Examples from an IOCG deposit." Minerals Engineering 24(12): 1271-1276.

INCA (2011). INCAMineral software, Oxford Instruments.

JKTech (2013). "Comminution testing." Retrieved 27/02, 2013, from http://www.jktech.com.au/comminution-testing.

JKTech (2013). " JK Bond Ball Lite (JK BBL)." Retrieved 27/02, 2013, from http://www.jktech.com.au/jk-bond-ball-lite-test-jk-bbl.

King, R. (1979). "A model for the quantitative estimation of mineral liberation by grinding." International Journal of Mineral Processing(6): 207-220.

King, R. and Schneider , C. (1999). "Mineral liberation and the batch comminution equation." Minerals Engineering 12(5): 579-580.

Kou, S. et al. (2001). "Numerical investigation of particle breakage as applied to mechanical crushing—Part II: Interparticle breakage." International journal of rock mechanics and mining sciences 38(8): 1163-1172.

Lamberg, P. (2011). Particles, the bridge between geology and metallurgy. Luleå, Sweden, Luleå University of Technology: 16.

Lamberg, P. and Lund, C., 2012, Taking liberation information into a geometallurgical model-case study, Malmberget, Northern Sweden: Process Mineralogy'12 , Cape Town, South Africa, 7-9 November, Proceedings, p. 1-13

Lamberg, P. and Mwanga, A. (2013). Mineral liberation analysis of Malmberget ore – Finding the right analysis conditions in INCAMineral.

Lamberg, P. and Vianna, S. (2007). "A technique for tracking multiphase mineral particles in flotation circuits." XXII ENTMME / VII MSHMT.

Lamberg, P. and Y. I. (2011). HSC Geo, Outotec.

Lätti, D. , A. B. J. I. (2001). "An assessment of stereological adjustment procedures." Minerals Engineering 14(12): 1579-1587.

Leigh G. , L. G., Gottlieb P. (1996). "Stereological estimates of liberation from mineral section measurements : a rederivation of Barbery's formulae with extensions." Powder Technology(87): 141-152.

Lin CL. , M. J. (1996). "Cone beam X-ray microtomography for three-dimensional liberation analysis in the 21st century." International Journal of Mineral Processing 47(1–2): 61-73.

Lin CL. , M. J. (2002). "Cone beam X-ray microtomography-a new facility for three-dimensional analysis of multiphase materials." Minerals and Metallurgical Processing 19(2): 65-71.

Lund, C. (2013). Whole rock chemical analysis from Fabian and Printzschöld ore bodies in Malmberget, Sweden. W. r. d. Fa&Pz.

Lund, C. , A. J., Martinsson, O. (2009). Magnetite chemistry, textural and mineralogical aspects of the metamorphosed apatite iron ore, Malmberget, Sweden, Luleå University of Technology: 30.

Lund, C., 2009, Mineralogical, chemical and textural properties of the Malmberget iron deposit, a process mineralogically characterisation: Licentiate thesis, Luleå University of Technology, Department of Civil, Environmental and Natural resources engineering, 100 p.

Lund, C., Lamberg, P. and Lindberg, T., 2013, Practical way to quantify minerals from chemical assays at Malmberget iron ore operations – An important tool for the geometallurgical program: Minerals Engineering, v. 49, p. 7-16.

Magdalinović, N. (1989). "A procedure for rapid determination of the Bond work index." International Journal of Mineral Processing 27(1): 125-132.

Martinsson, O. (1997). "Paleoproterozoic greenstones at Kiruna in northern Sweden: a product of continental rifting and associated mafic-ultramafic volcanism." O. Martinsson: Tectonic setting and metallogeny of the Kiruna Greenstones. Ph. D. Thesis 19.

Martinsson, O. (2004). "Metallogeny of the northern Norrbotten Fe-Cu-Au-ore province." CTMG (Centrer for applied ore studies).

McQuiston F.W. Jr. , B. L. J. J. (1968). Metallurgical sampling and testing, The American Institute of Mining, Metallurgical, and Petroleum Engineers. Surface mining: New York: 103−121.

Mishra, B. (2000). "Monte Carlo simulation of particle breakage process during grinding." Powder Technology 110(3): 246-252.

Mooi E., S. M. (2011). A concise guide to market research: The process, data, and methods using IBM SPSS statistics, Springerverlag Berlin Heidelberg.

Morrell, S. (2004). "An alternative energy–size relationship to that proposed by Bond for the design and optimisation of grinding circuits." International Journal of Mineral Processing 74(1–4): 133-141.

Morrell, S. and Man, Y.(1997). "Using modelling and simulation for the design of full scale ball mill circuits." Minerals Engineering 10(12): 1311-1327.

Mrozewski, S. (2008). An Introduction to Logging While Drilling, Columbia University, Lamont - Doherty Drill hole research, Lamont - Doherty Earth observatory.

Öhlander, B. (1984). "Geochemical analyses of rocks of the Haparanda suite, northern Sweden." GFF 106(2): 167-169.

Oxford Instruments (2012). INCAMineral Brochure: Automated mineral liberation analysis for multipurpose SEMs, Oxford Instruments.

Ozkahraman, H. (2005). "A meaningful expression between bond work index, grindability index and friability value." Minerals Engineering 18(10): 1057-1059.

Paterson BA, S. W., Herd, DA (1989). "Zoning in granitoid accessory minerals as revealed by backscattered electron imagery." Mineral Mag 53: 55-61.

Reid, K. (1965). "A solution to the batch grinding equation." Chemical Engineering Science 20(11): 953-963.

Romer R.L. , M. O., Perdahl , J.A. (1994). "Geochronology of the Kiruna iron ores and hydrothermal alterations." Economic Geology 89(6): 1249-1261.

Rosenberg R.A., S. J. K., Frigo S.P., Tan K., Chen J.M. (1992). "X-ray fluorescence detection of low-Z elements using a microchannel plate detector." Review of scientific instruments 63(4): 2193-2194.

Schneider C.L. , N., Reiner N., Neto A.A. (2004). "Automated, adaptive thresholding procedure for mineral sample images generated by BSE detector."

Shosha, M. R. H. (2013, 06/15/2011). "Classification of soil." Retrieved 03/03, 2013, from http://osp.mans.edu.eg/geotechnical/Ch1C.htm.

Szwedzicki, T. (2007). "A hypothesis on modes of failure of rock samples tested in uniaxial compression." Rock Mechanics and Rock Engineering 40(1): 97-104.

Tang, C., Xu XH, Kou SQ, Lindqvist P-A, Liu HY (2001b). "Numerical investigation of particle breakage as applied to mechanical crushing—Part I: Single-particle breakage." International journal of rock mechanics and mining sciences 38(8): 1147-1162.

Videla, A. R., Lin C. L., Miller J. D. (2007). "3D characterization of individual multiphase particles in packed particle beds by X-ray microtomography (XMT)." International Journal of Mineral Processing 84(1–4): 321-326.

Weihed, P. et al. (2005). "8: Precambrian geodynamics and ore formation: The Fennoscandian Shield." Ore Geology Reviews 27(1–4): 273-322.

Weiheid, P., E. P., Larsen R ,Stendal H, Tontti M (2008). "Metallic mineral deposits in the Nordic countries." Episodes 31(1): 131.

Wills, B. and T. Napier-Munn (2006). Mineral Processing Technology : an introduction to the practical aspects of ore treatment and mineral recovery, Elsevier.

Wills, B., A. K. (1993). "Some observations on the fracture and liberation of mineral assemblies." Minerals Engineering 6(7): 697-706.

Wright TL, D. P. (1970). "A linear programming and least squares computer method for solving petrologic mixing problems." Geological Society of America Bulletin 81(7): 1995-2008.

Zeiss (2011). MERLIN Brochure, Carl Zeiss Microscopy: 12-13.

9. Appendices

a. Appendix A: additional figures

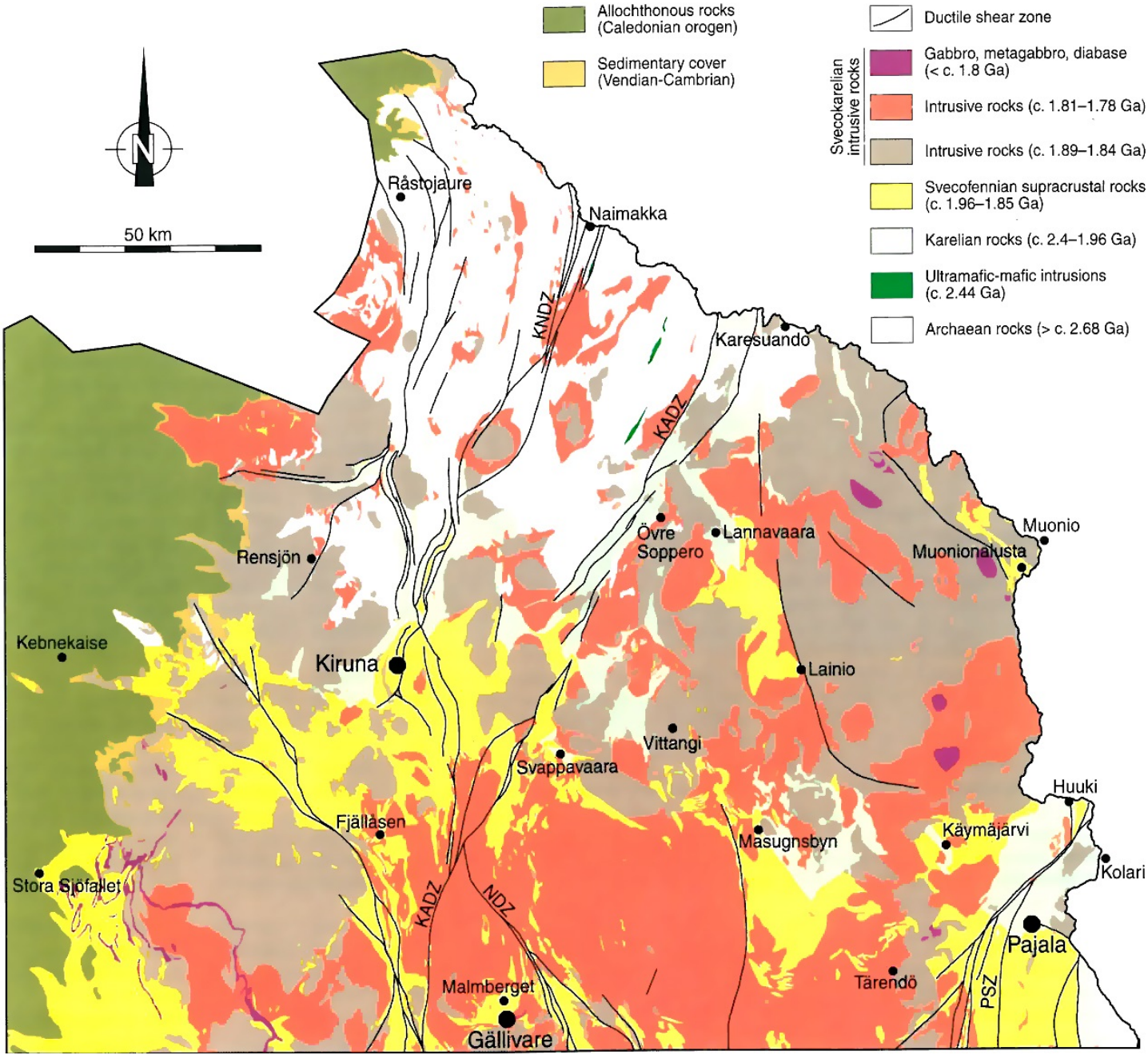

Figure 45 : Geological map of northern Norrbotten county, Sweden (Bergman S. 2001)

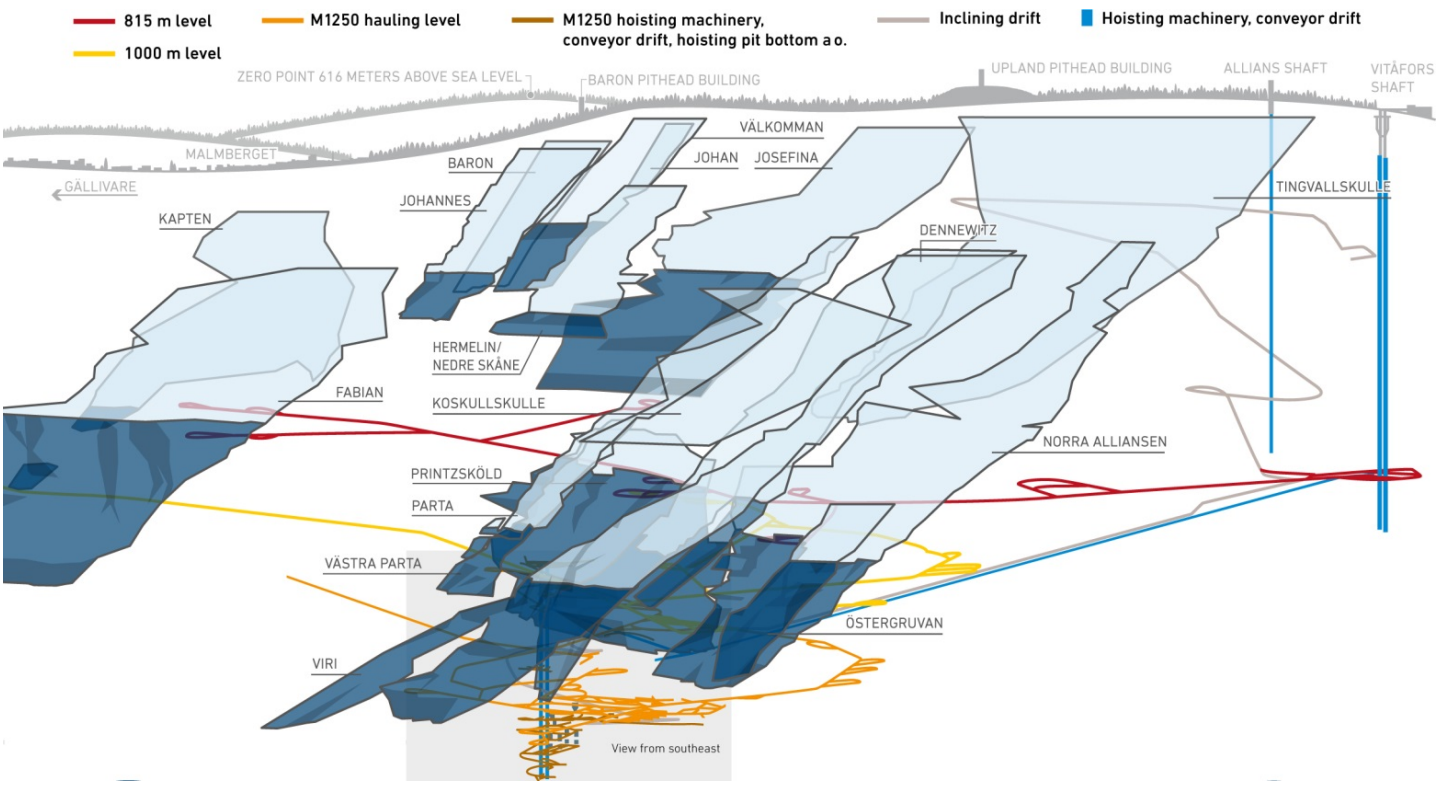

Figure 46 : Malmberget's mine plan (LKAB 2011)

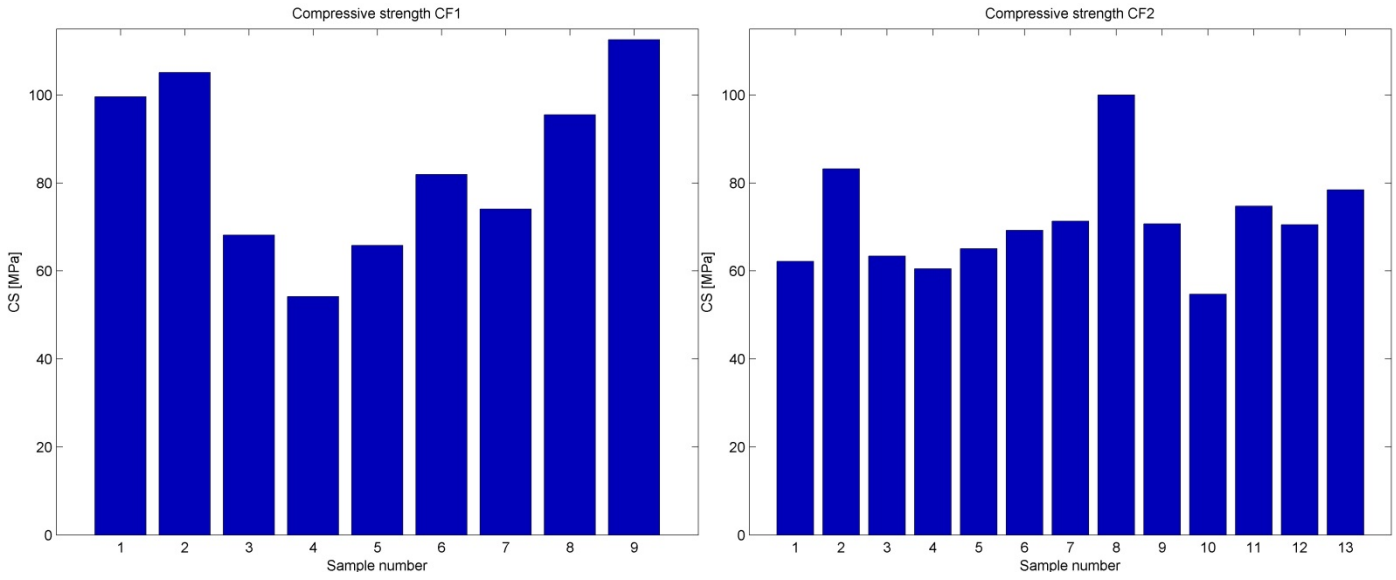

Figure 47 : Compressive strength of CF1 and CF2 samples

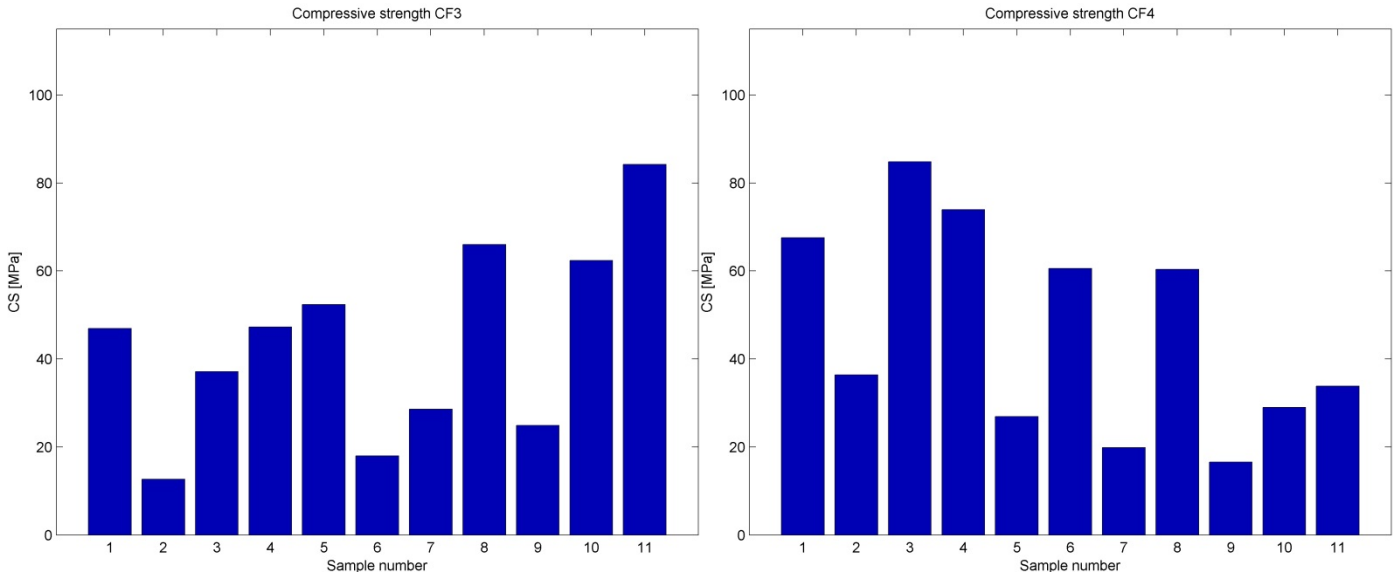

Figure 48 : Compressive strength of CF3 and CF4 samples

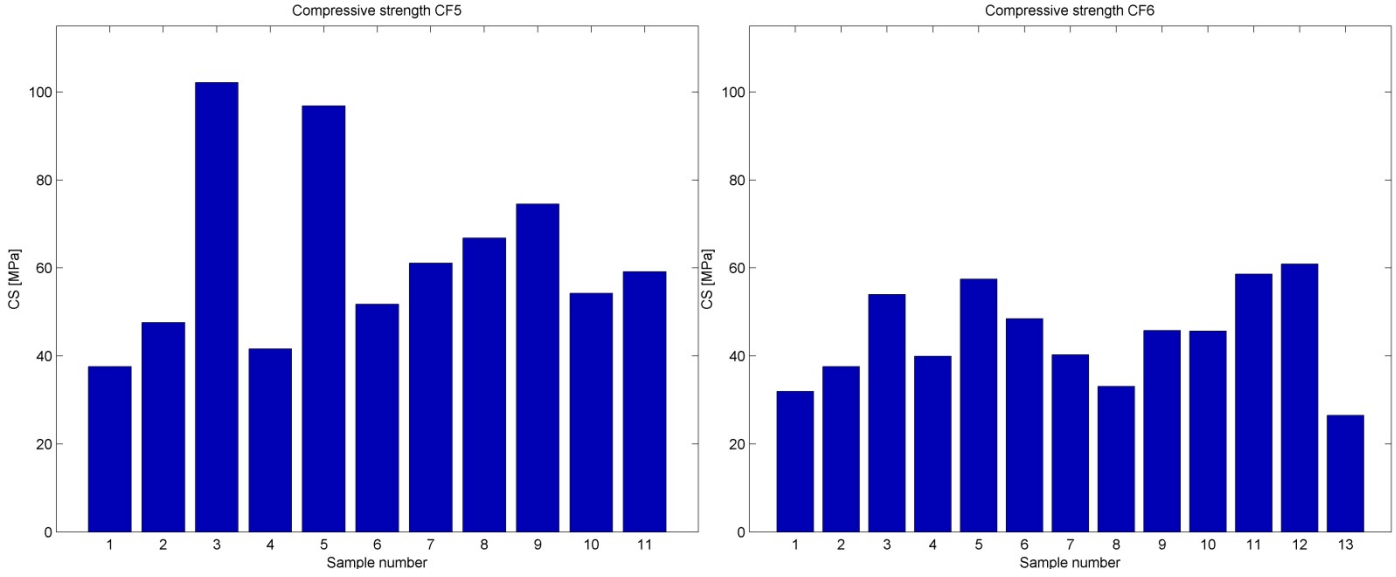

Figure 49 : Compressive strength of CF5 and CF6 samples

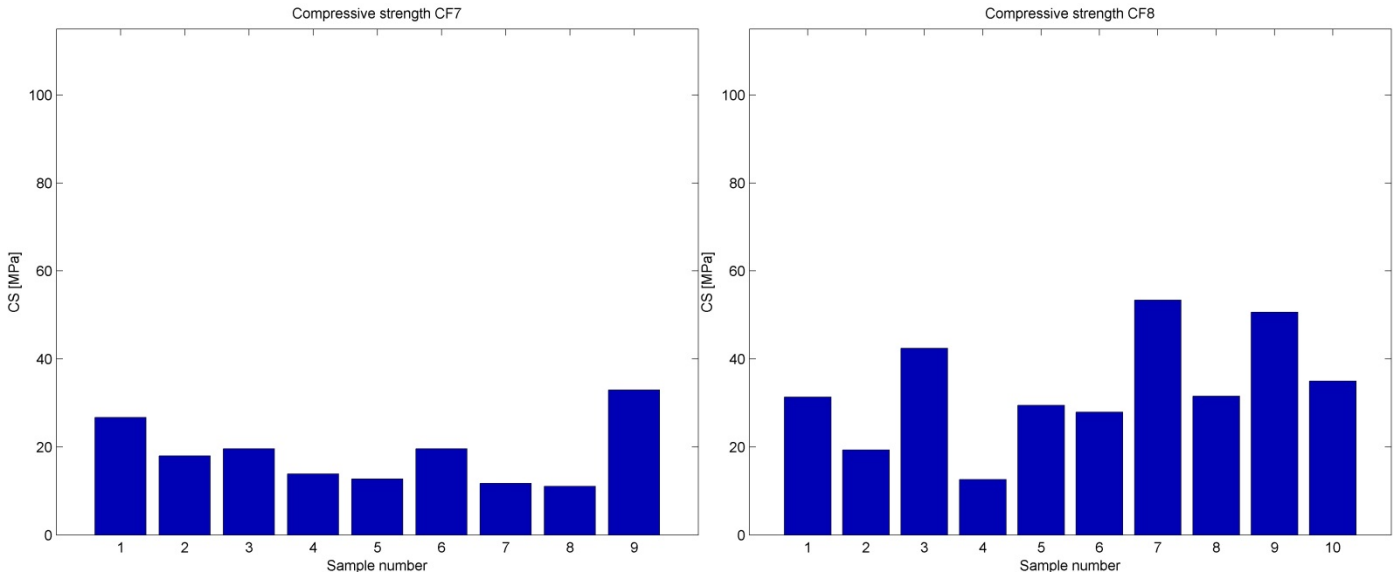

Figure 50 : Compressive strength of CF7 and CF8 samples

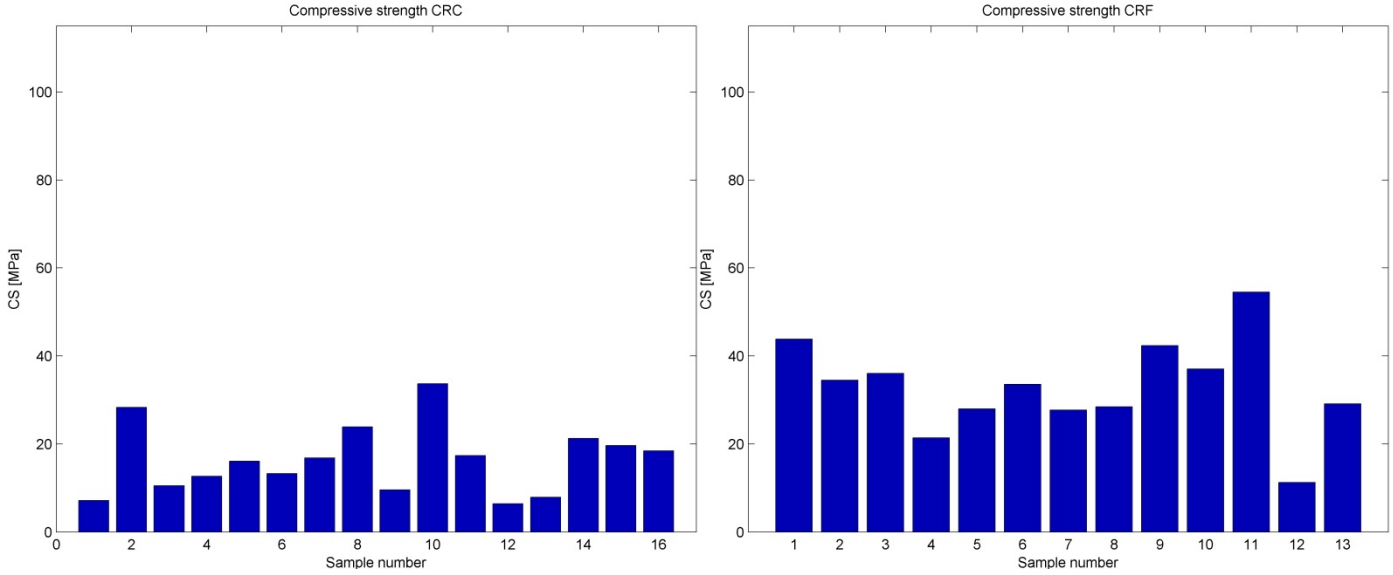

Figure 51 : Compressive strength of CRC and CRF samples

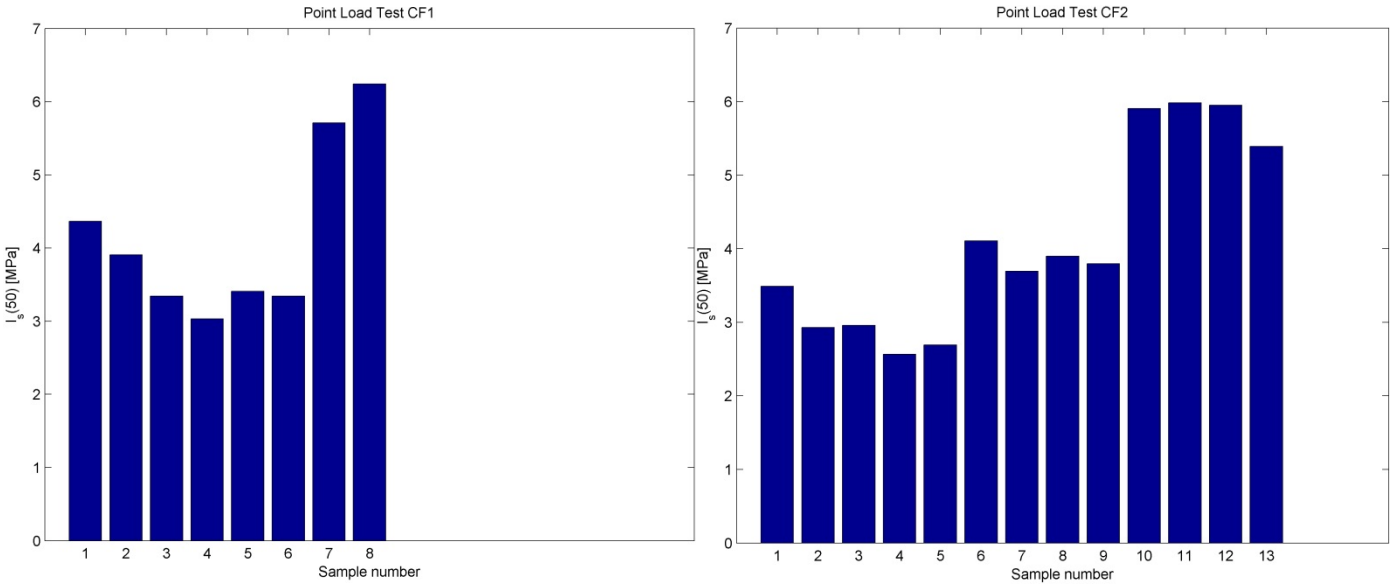

Figure 52 : Is(50) of CF1 and CF2 samples

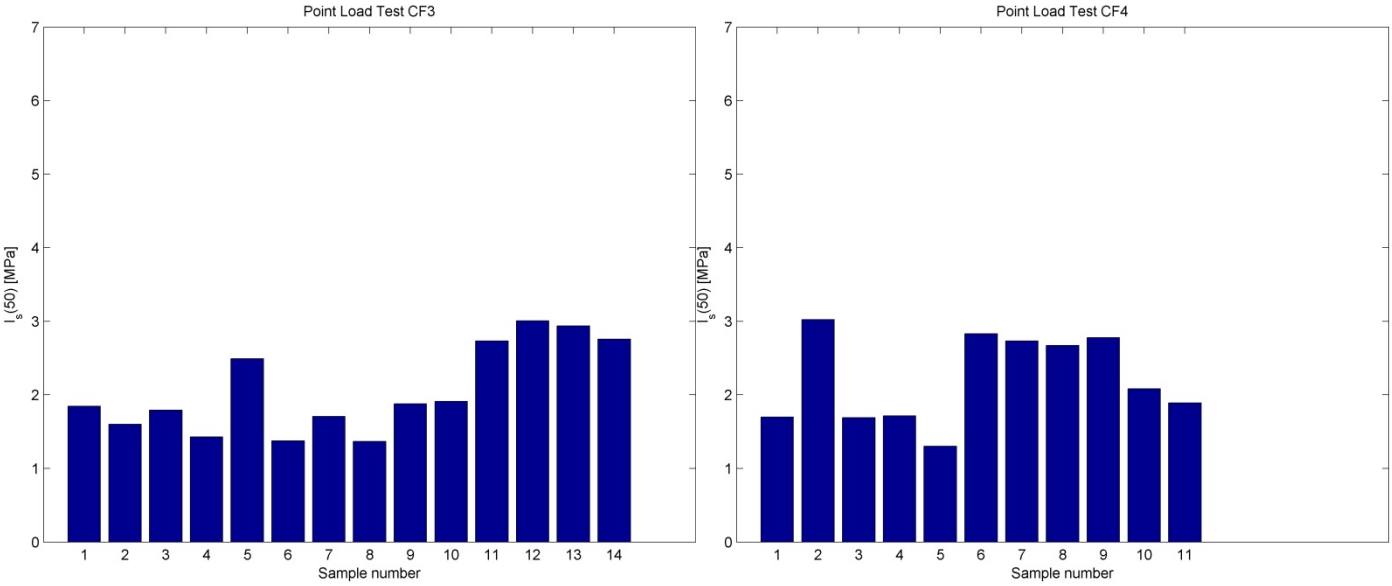

Figure 53 : Is(50) of CF3 and CF4 samples

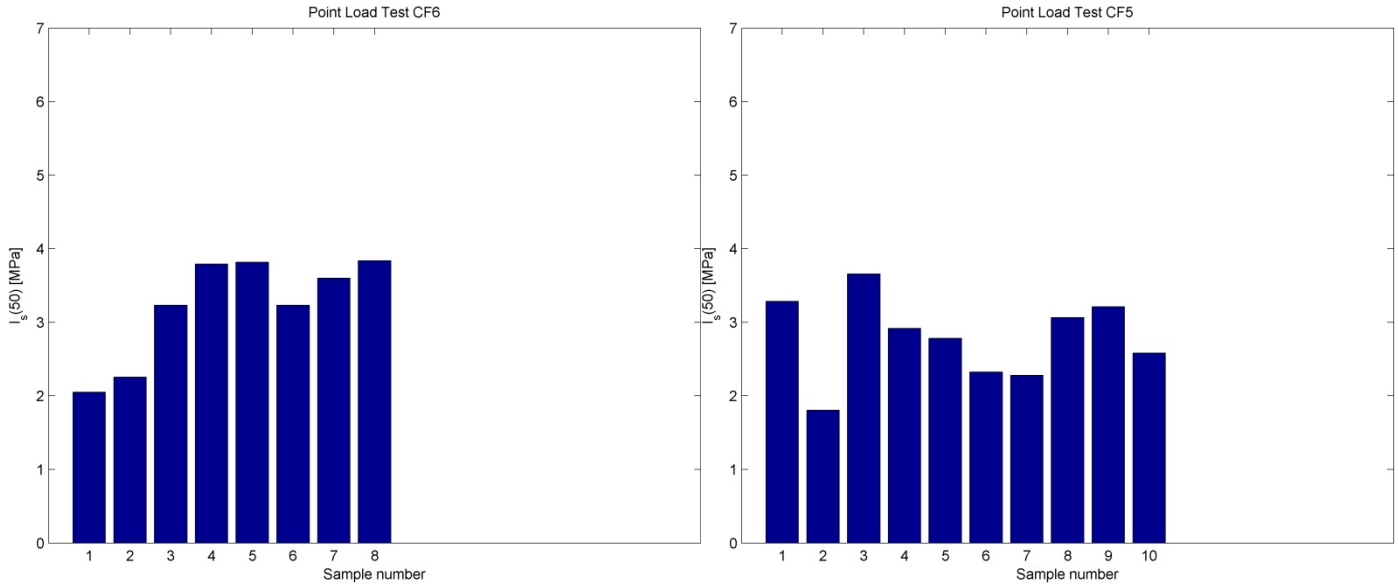

Figure 54 : Is(50) of CF5 and CF6 samples

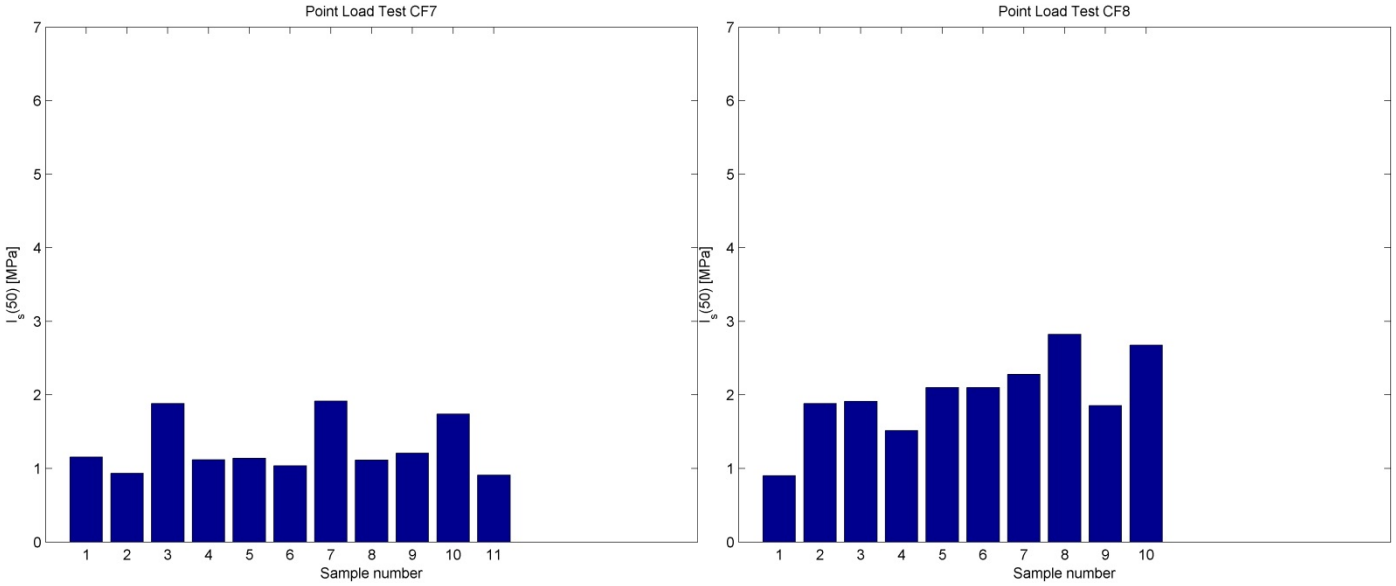

Figure 55 : Is(50) of CF7 and CF8 samples

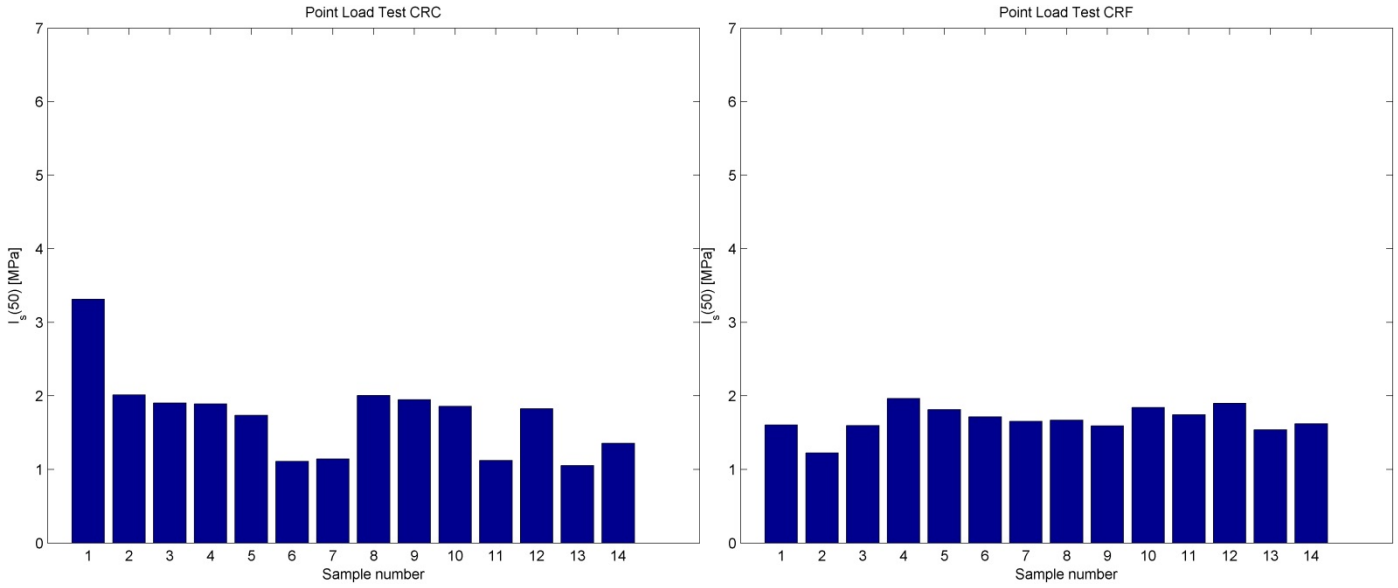

Figure 56 : Is(50) of CRC and CRF samples

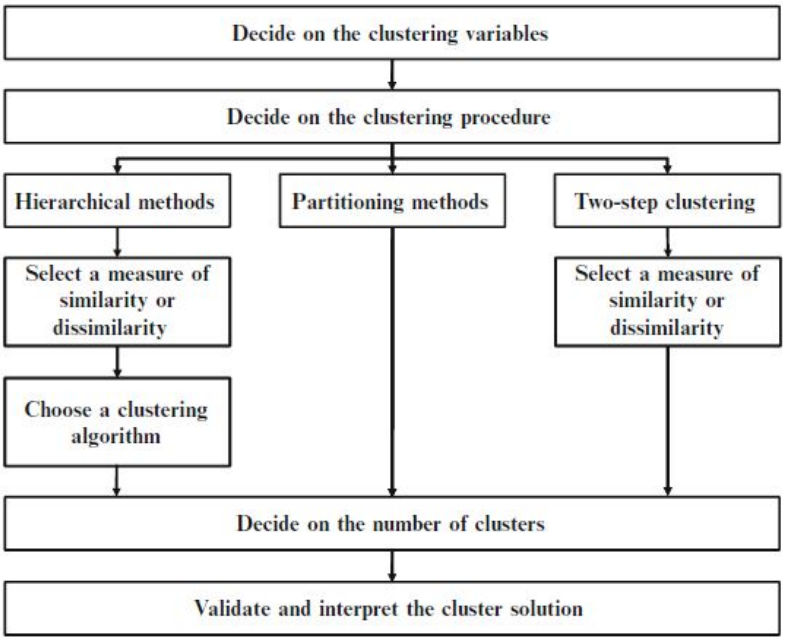

Figure 57 : General clustering process (Mooi E. 2011)

Figure 58 : Jaw crusher (left) and Ball mill (right) used in this work

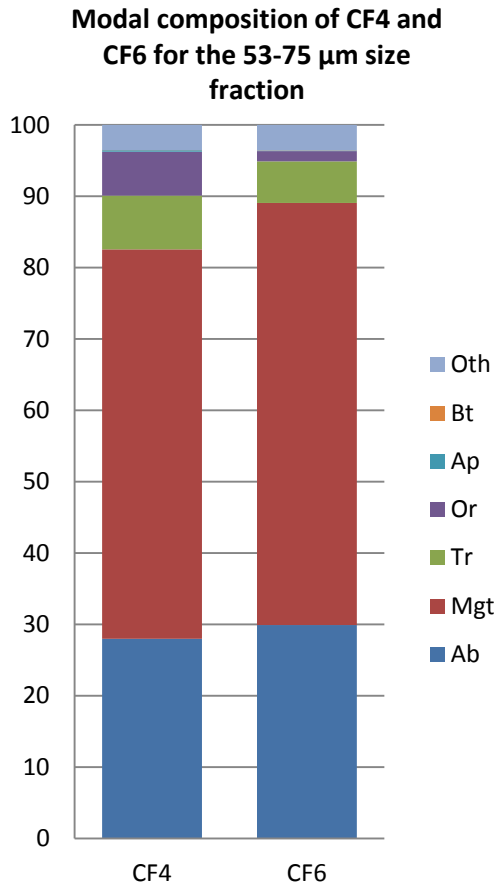

Figure 59 : Modal composition of CF4 and CF6 for the 53-75 µm size fraction

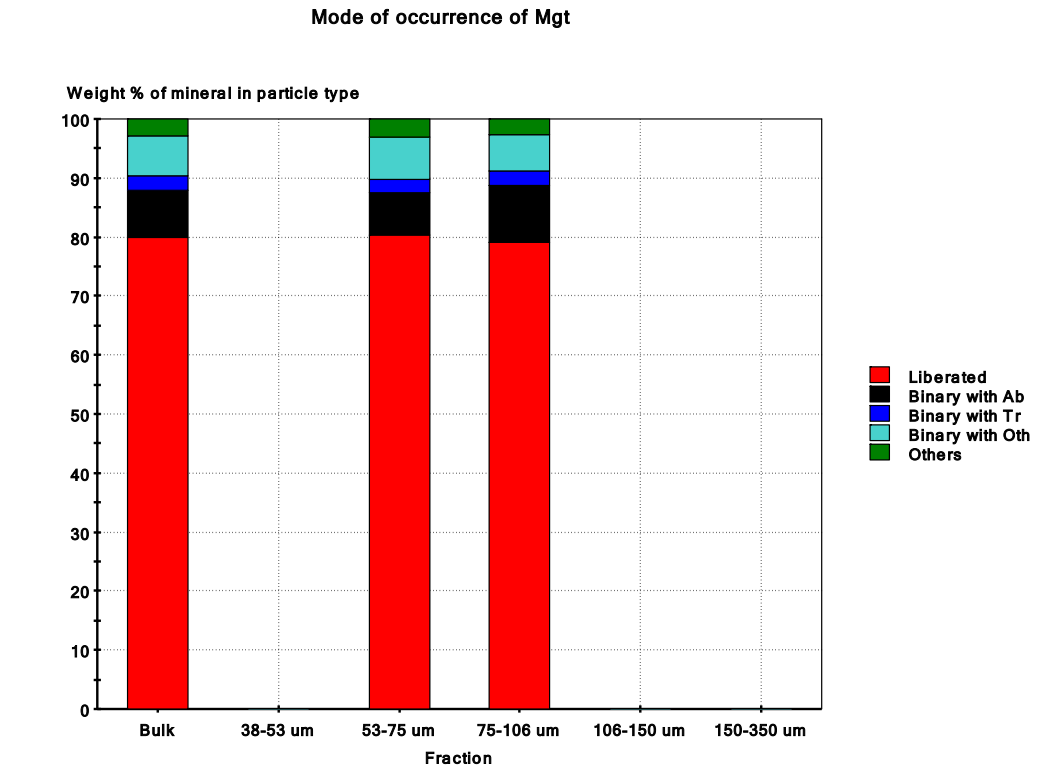

Figure 60 : Mode of occurrence of magnetite in CF2

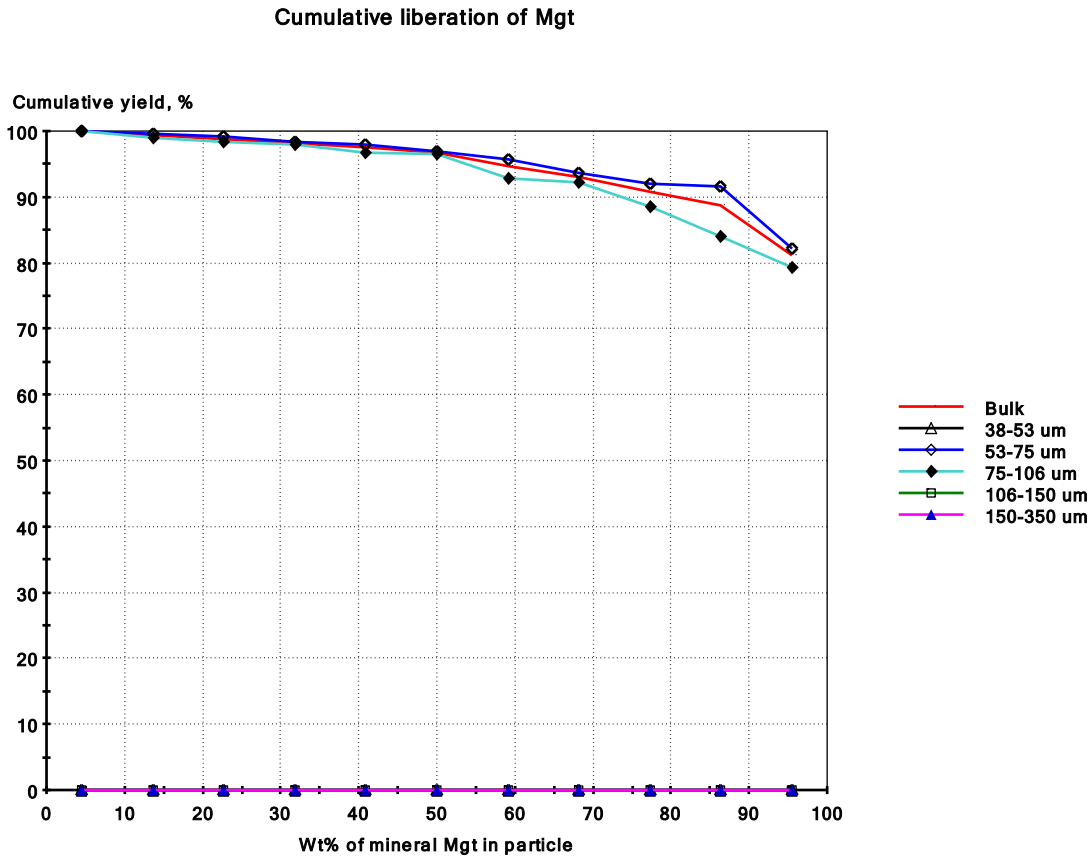

Figure 61 : Cumulative liberation curve of magnetite in CF2

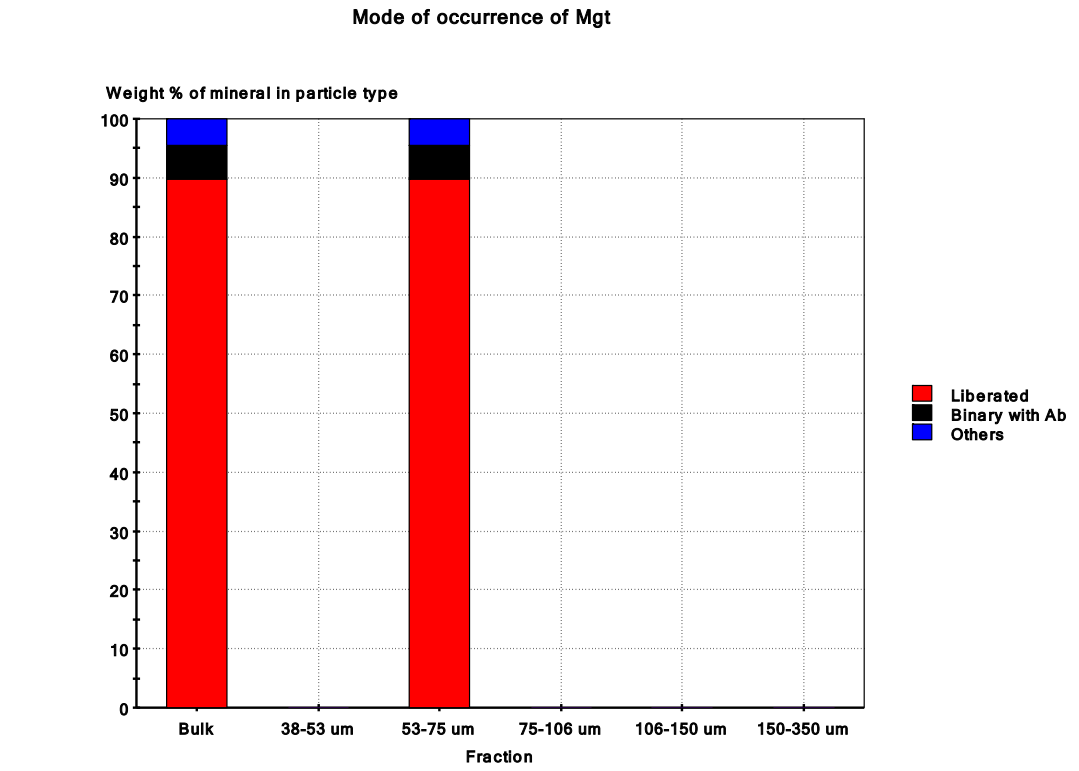

Figure 62 : Mode of occurrence of magnetite in CF4

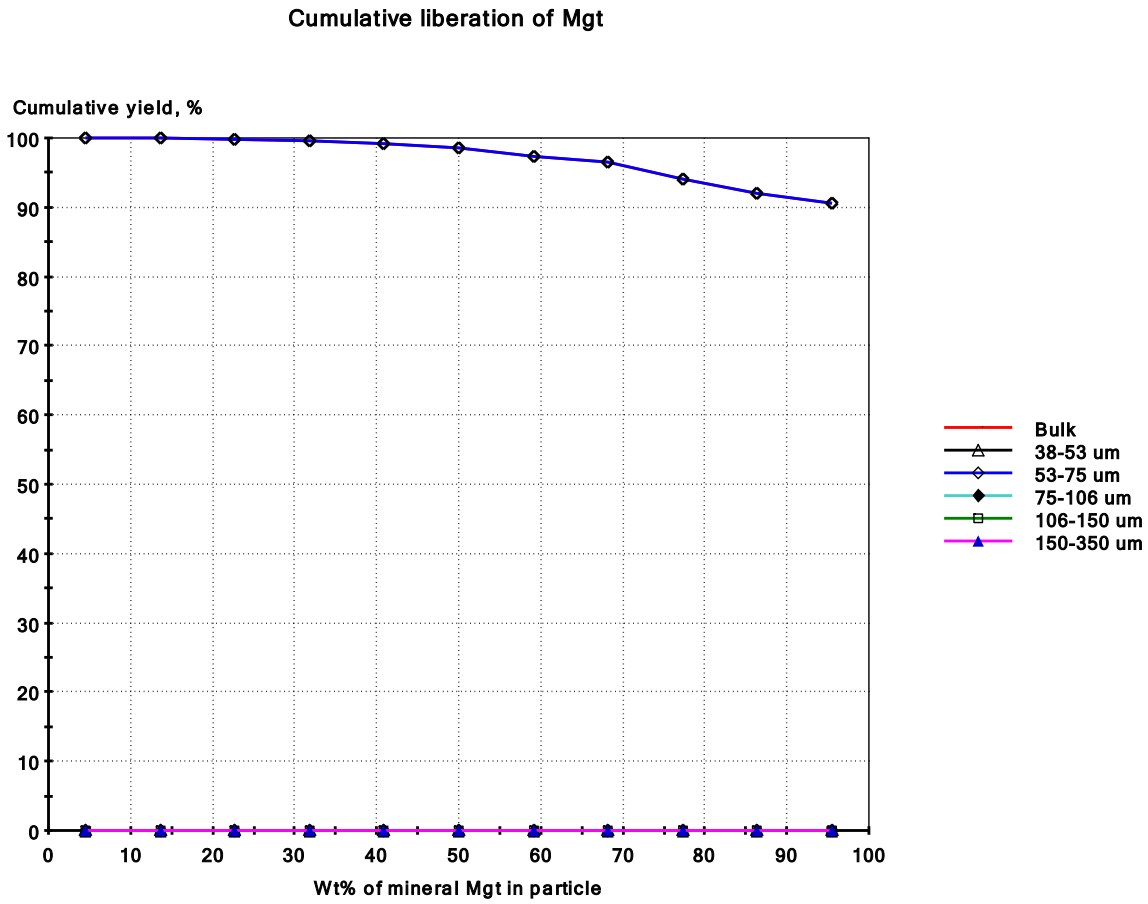

Figure 63 : Cumulative liberation curve of magnetite in CF4,

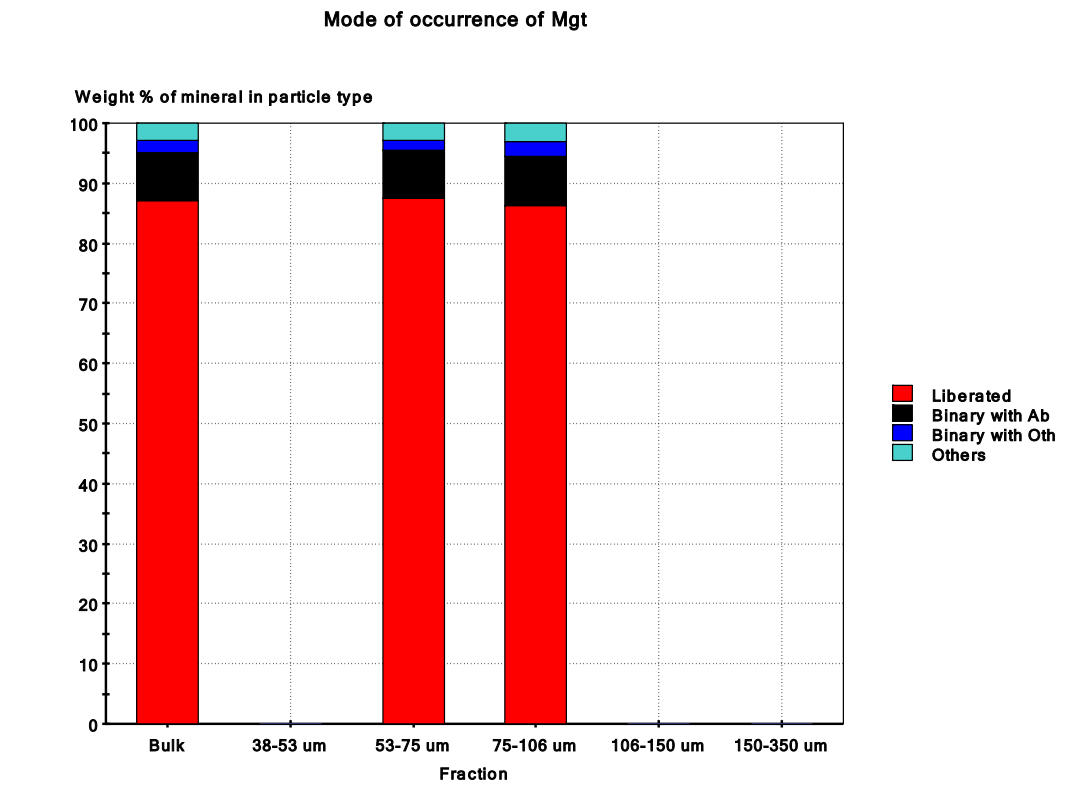

Figure 64 : Mode of occurrence of magnetite in CF6

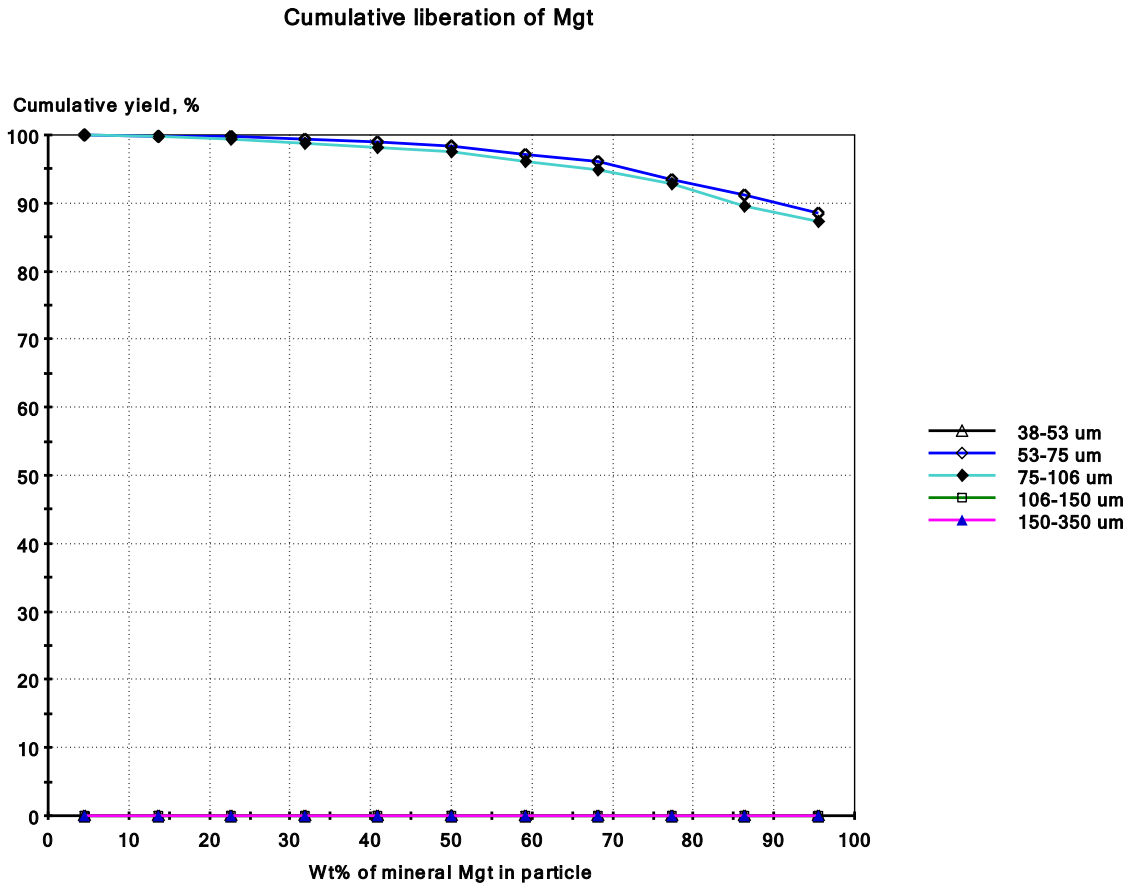

Figure 65 : Cumulative liberation curve of magnetite in CF6

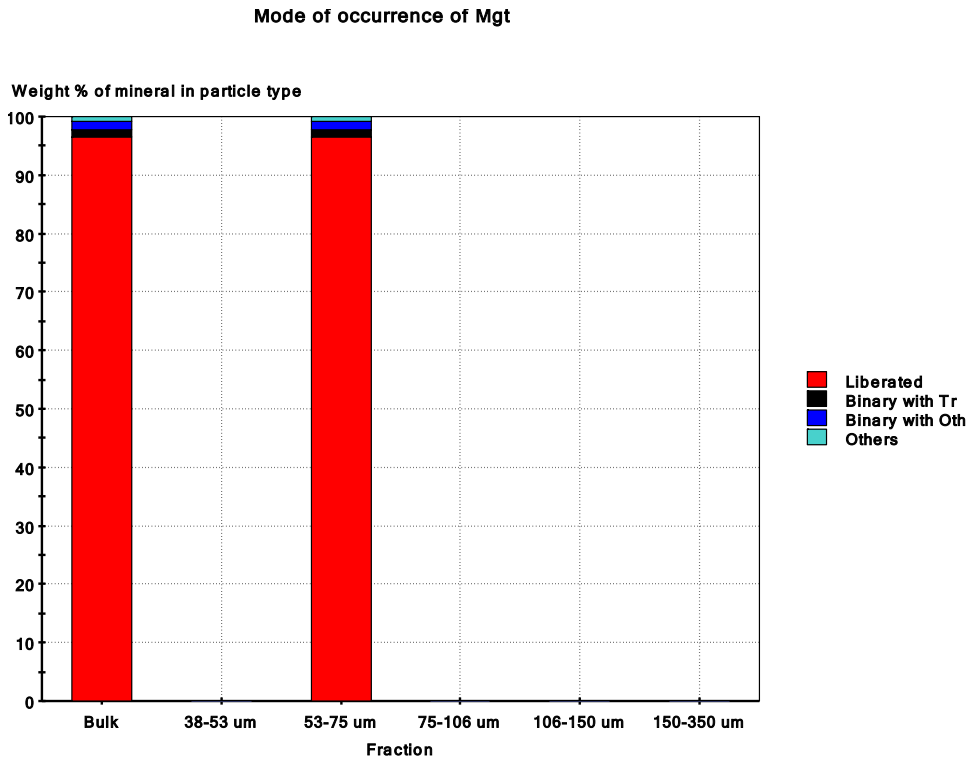

Figure 66 : Mode of occurrence of magnetite in CRC

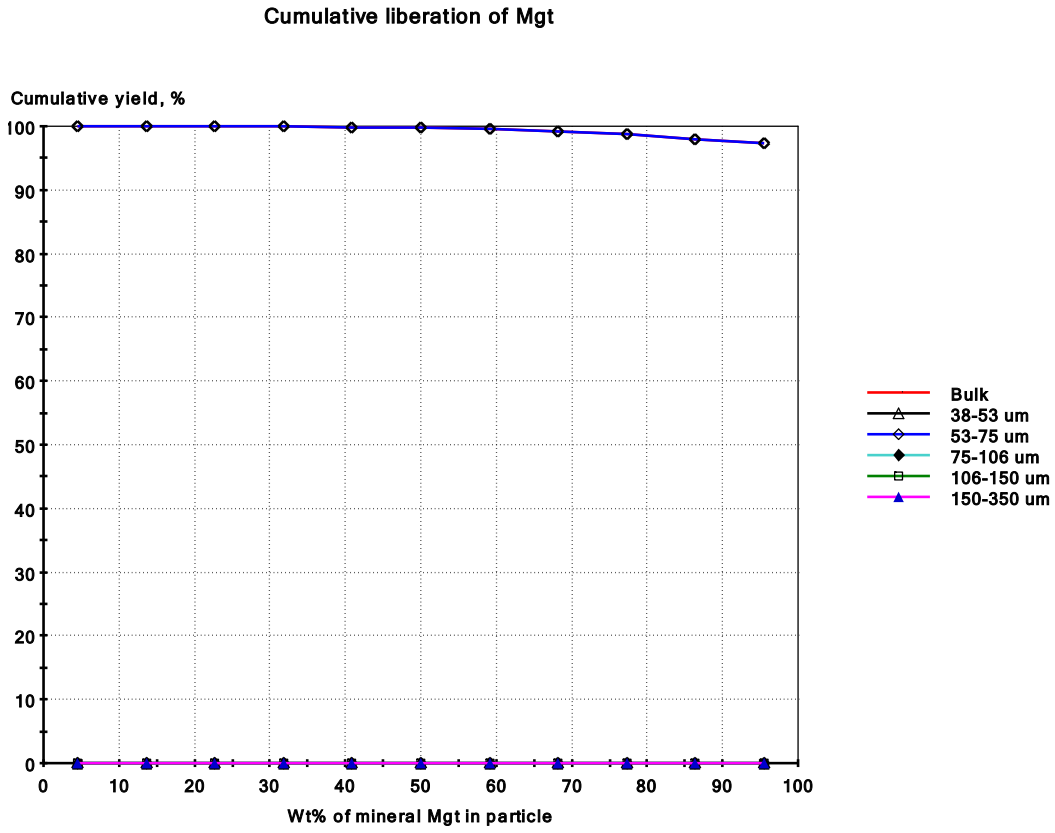

Figure 67 : Cumulative liberation curve for magnetite in CRC

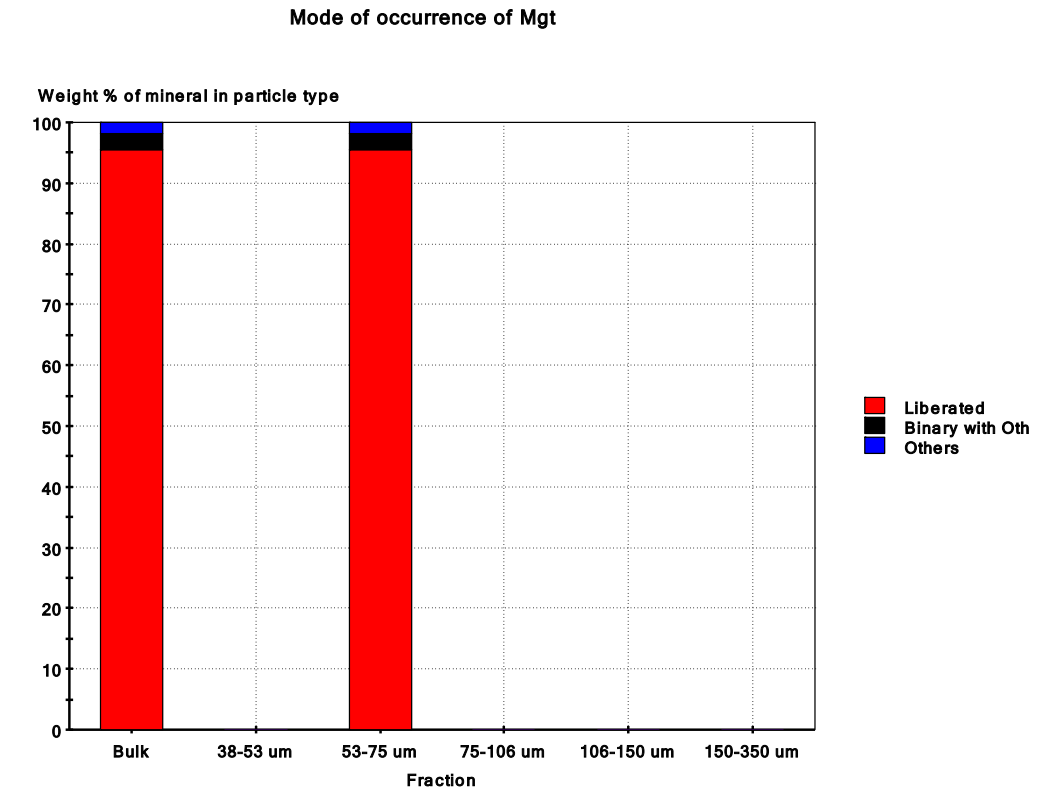

Figure 68 : Mode of occurrence of magnetite in CRF

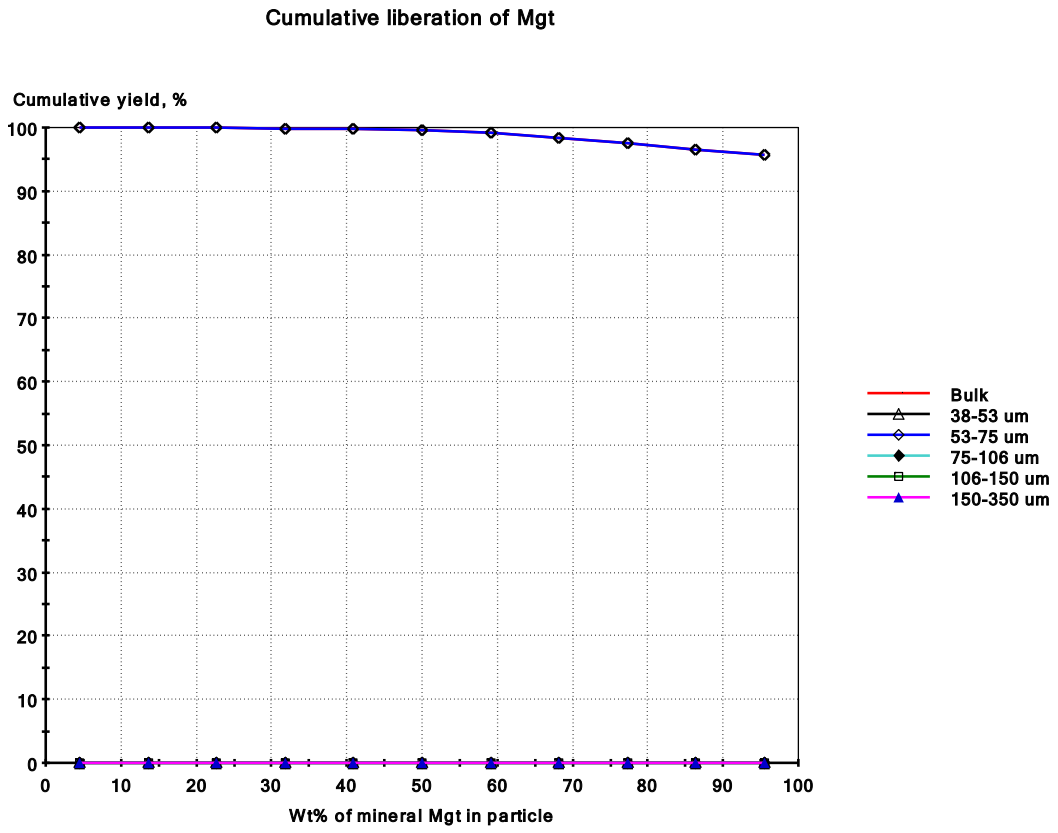

Figure 69 : Cumulative liberation curve for magnetite in CRF

b. Appendix B : data files

Table 13 : Composites and samples

Composite ID	Sample ID	Drillhole ID	Start [m]	End [m]	Weight [g]
CF1	CF1001	6500	103.2	103.2	137.9
CF1	CF1002	6496	382.3	382.4	180.7
CF1	CF1003	6496	587.7	587.9	336.1
CF2	CF2001	6496	159.0	159.2	253.4
CF2	CF2002	6496	195.1	195.3	233.2
CF2	CF2003	6496	610.2	610.4	355.0
CF3	CF3001	6852	148.1	148.5	275.7
CF3	CF3002	6496	367.3	367.5	262.7
CF4	CF4001	6533	125.9	127.0	820.0
CF4	CF4002	6500	128.8	129.7	765.0
CF5	CF5001	6496	107.1	107.3	274.0
CF5	CF5002	6500	870.7	871.3	352.0
CF6	CF6001	6496	334.8	335.8	1021.7
CF7	CF7001	6839	397.4	397.8	413.8
CF7	CF7002	6839	342.2	342.5	307.5
CF8	CF8001	6533	47.9	48.1	190.3
CF8	CF8002	6533	66.3	66.5	170.4
CF8	CF8003	6533	166.4	168.6	422.0
CRC	CRC001	6500	424.5	426.9	1927.0
CRC	CRC002	6500	424.5	426.9	412.0
CRF	CRF001	6533	62.4	63.5	920.5
CRF	CRF002	6496	262.5	263.7	550.6

Table 14 : PLT and CS measurements for all samples

Sample	PLT Press. [MPa]	Corr PLT [N/mm²]	CS [non-calibrated kp]	CS [N/mm²]
CF10011	4.85	4.37		
CF10012	4.25	3.91		
CF10013			2600.00	99.591
CF10014			2700.00	105.098
CF10015			1600.00	68.128
CF10016	3.65	3.34		
CF10021	invalid	invalid		
CF10022	3.45	3.03		
CF10023			1200.00	54.159
CF10024	3.85	3.41		
CF10025			1180.00	65.806
CF10026			1520.00	81.888
CF10027	3.80	3.34		

Sample	PLT Press. [MPa]	Corr PLT [N/mm²]	CS [non-calibrated kp]	CS [N/mm²]
CF10031	6.20	5.71		
CF10032			2000.00	74.053
CF10033			2640.00	95.453
CF10034	6.80	6.24		
CF10035			2850.00	112.539
CF20011	3.80	3.49		
CF20012			1400.00	62.181
CF20013	3.20	2.93		
CF20014			1720.00	83.198
CF20015	3.20	2.96		
CF20016			1400.00	63.356
CF20017	2.80	2.57		
CF20018			1280.00	60.494
CF20019	3.00	2.69		
CF20111			1400.00	65.056
CF20021	4.40	4.11		
CF20022			1640.00	69.255
CF20023	4.00	3.69		
CF20024			1680.00	71.337
CF20025	4.20	3.90		
CF20026			2420.00	99.983
CF20027	4.00	3.80		
CF20028			1720.00	70.715
CF20031	6.20	5.90		
CF20032			1860.00	54.679
CF20033	6.30	5.98		
CF20034			2340.00	74.763
CF20035	6.20	5.95		
CF20036			2320.00	70.501
CF20037	5.80	5.39		
CF20038			2140.00	78.451
CF30011	2.00	1.85		
CF30012	1.80	1.55		
CF30013			1000.00	62.814
CF30014	2.00	1.81		
CF30015			280.00	10.613
CF30016	1.60	1.44		
CF30017			760.00	39.613
CF30018	2.80	2.48		
CF30019			960.00	49.555
CF30111	1.60	1.44		
CF30112			1040.00	57.391
CF30113	2.00	1.82		

Sample	PLT Press. [MPa]	Corr PLT [N/mm²]	CS [non-calibrated kp]	CS [N/mm²]
CF30114			400.00	20.158
CF30115	1.60	1.36		
CF30116			575.00	30.304
CF30117	2.00	1.78		
CF30021			1200.00	48.975
CF30022	2.20	1.97		
CF30023			640.00	28.199
CF30024	3.00	2.76		
CF30025			1200.00	57.734
CF30026	3.20	2.78		
CF30027			1700.00	70.016
CF30028	3.20	2.90		
CF30029			2600.00	122.635
CF30121	3.00	2.74		
CF30122			3120.00	137.236
CF30123	1.80	1.64		
CF40011				
CF40012			2900.00	94.556
CF40013	3.20	3.02		
CF40014			1800.00	67.564
CF40015	4.00	3.78		
CF40016			1020.00	36.397
CF40017	1.80	1.69		
CF40018			2100.00	84.820
CF40019	1.80	1.71		
CF40111			2100.00	73.926
CF40112	1.40	1.30		
CF40113			800.00	26.900
CF40114	3.00	2.83		
CF40115			1600.00	60.573
CF40116	3.10	2.73	700.00	19.795
CF40021				
CF40022			1800.00	57.454
CF40023	2.80	2.68		
CF40024			600.00	15.908
CF40025	2.90	2.80		
CF40026			1000.00	32.755
CF40027	2.20	2.12		
CF40028			1080.00	32.393
CF40029	2.00	1.89		
CF50011			820.00	40.762
CF50012	3.60	3.34		
CF50013			1000.00	60.707

Sample	PLT Press. [MPa]	Corr PLT [N/mm²]	CS [non-calibrated kp]	CS [N/mm²]
CF50014	2.00	1.83		
CF50015			1820.00	92.710
CF50016	4.00	3.64		
CF50017			900.00	45.659
CF50018	invalid(0.6)	invalid		
CF50019			1600.00	88.250
CF50111	3.20	2.87		
CF50112			1000.00	45.007
CF50113	3.00	2.73		
CF50021			1700.00	59.088
CF50022	2.40	2.27		
CF50023			2000.00	78.755
CF50024	2.40	2.32		
CF50025			2000.00	65.899
CF50026	3.20	3.04		
CF50027			1600.00	49.529
CF50028	3.30	3.17		
CF50029			1800.00	63.091
CF50121	2.70	2.58		
CF60011			960.00	38.709
CF60012	2.20	2.08		
CF60013			1000.00	39.878
CF60014	2.40	2.23	1400.00	54.015
CF60015				
CF60016				
CF60017	3.40	3.22	1220.00	45.120
CF60018	4.00	3.80		
CF60019			1440.00	50.984
CF60111	invalid(2.2)	invalid		
CF60112			1380.00	50.728
CF60113	invalid(2)	invalid		
CF60114			1070.00	39.515
CF60115	invalid(2)	invalid		
CF60116			980.00	36.255
CF60117	4.00	3.81		
CF60118			1140.00	39.454
CF60119	3.40	3.16		
CF60120			1340.00	45.640
CF60121	3.80	3.60		
CF60122			1420.00	58.605
CF60123	4.20	3.84		
CF60124			1620.00	60.920
CF60125	invalid(0.8)	invalid		

Sample	PLT Press. [MPa]	Corr PLT [N/mm²]	CS [non-calibrated kp]	CS [N/mm²]
CF60126			680.00	26.478
CF70011	1.25	1.15		
CF70012			680.00	26.719
CF70013	1.00	0.93		
CF70014			540.00	17.950
CF70015	2.00	1.88		
CF70016			560.00	19.585
CF70017	1.20	1.12		
CF70018			440.00	13.862
CF70019	1.20	1.14		
CF70111				
CF70112	1.20	1.04	400.00	12.719
CF70021	2.00	1.92		
CF70022			500.00	19.581
CF70023	1.20	1.11		
CF70024			320.00	11.745
CF70025	1.30	1.21		
CF70026			800.00	35.731
CF70027	1.80	1.74		
CF70028			320.00	11.064
CF70031	1.00	0.91		
CF70032			580.00	32.981
CF80011	1.00	0.90		
CF80012			820.00	31.355
CF80013	2.00	1.88		
CF80014			540.00	19.305
CF80015	2.00	1.91		
CF80016			1040.00	42.427
CF80021	1.60	1.51		
CF80022			380.00	12.580
CF80023	2.20	2.10		
CF80024			1900.00	69.404
CF80031	2.20	2.10		
CF80032			840.00	29.422
CF80033	2.40	2.28		
CF80034			880.00	27.913
CF80035	3.00	2.82		
CF80036			1400.00	53.364
CF80037	2.00	1.86	920.00	33.268
CF80038			1410.00	50.021
CF80039				
CF80311			920.00	31.890
CF80312	2.90	2.72		

Sample	PLT Press. [MPa]	Corr PLT [N/mm²]	CS [non-calibrated kp]	CS [N/mm²]
CRF0011			1140.00	43.334
CRF0012	1.70	1.60		
CRF0013			840.00	31.444
CRF0014	1.30	1.18		
CRF0015			1000.00	34.010
CRF0016	1.70	1.48		
CRF0017			580.00	20.002
CRF0018	2.10	1.97		
CRF0019			880.00	31.423
CRF0111	1.90	1.80		
CRF0112			960.00	33.456
CRF0113	1.80	1.70		
CRF0114			820.00	34.580
CRF0115	1.80	1.71		
CRF0116			800.00	29.847
CRF0117	1.80	1.67		
CRF0118			1100.00	40.953
CRF0119	1.70	1.58		
CRF1111			1180.00	41.729
CRF0021	2.00	1.92		
CRF0022			1710.00	51.966
CRF0023	1.80	1.69		
CRF0024			420.00	11.809
CRF0025	2.00	1.92		
CRF0026			2310.00	73.311
CRF0027	1.60	1.54		
CRF0028			960.00	28.515
CRF0029	invalid(1.8)	invalid		
CRF0211			320.00	7.658
CRC0011	1.70	1.67		
CRC0012			1410.00	42.049
CRC0013	3.40	3.27		
CRC0014			930.00	27.228
CRC0015	2.10	2.00		
CRC0016			400.00	10.603
CRC0017	2.00	1.93		
CRC0018			420.00	11.559
CRC0019	2.00	1.90		
CRC0111			580.00	16.356
CRC0112	1.80	1.72		
CRC0113			480.00	13.381
CRC0114	1.20	1.14		
CRC0115			600.00	17.240

Sample	PLT Press. [MPa]	Corr PLT [N/mm²]	CS [non-calibrated kp]	CS [N/mm²]
CRC0116	1.20	1.15		
CRC0117			800	22.31
CRC0118	2.00	1.92		
CRC0119			380	9.23
CRC1111	2.00	1.93	1140	34.15
CRC1112				
CRC1113			650	18.36
CRC1114	1.90	1.85		
CRC1115			1440	42.44
CRC1116	1.20	1.16		
CRC1117			280	6.118
CRC1118	1.90	1.81		
CRC1119			320	7.49
CRC1211	invalid (0.8)	invalid		
CRC1212			780	25.24
CRC1213	1.10	1.06		

Table 15 : Correction factor for the laboratory ball mill

Appropriate correction factors for the experimental results	
Different sample	
Diameter of mergan mill(mm)	184
f3(diameter factor)	1.677
f5(fineness of grind factor)	0.919
ball mill factor f7	
R< 6?	1.855
	4.962
Average R	**3.408**
f 7(ball mill factor)	1.036
Appropriate product factor(F)	1.597

Table 16: MERLIN scanning electron microscope specification sheet (Zeiss 2011)

MERLIN® Essential Specifications		
Probe current	10 pA up to 300 nA (depending on system configuration)	
Resolution (optimal WD) *All resolution specifications are dependent on the system configuration.*	0.8 nm @ 15 kV 1.4 nm @ 1 kV 3.0 nm @ 20 kV at 10 nA, WD = 8,5 mm 0.6 nm @ 30 kV (STEM mode)	
Acceleration voltage	0.02 – 30 kV	
Magnification	12 – 2000000 x in SE mode 100 – 2000000 x with EsB® detector	
Emitter	Thermal field emission type, stability >0,2 %/h	
Specimen stage	5-Axes Motorised Eucentric Specimen Stage X = 130 mm Y = 130 mm Z = 50 mm T = -3° to 70° R = 360° (continous) Further additional optional stage systems available	
Detectors	Standard:	High efficiency in-lens SE detector Everhart Thornley Secondary Electron detector
	Optional:	EsB® detector with filtering grid, filtering voltage 0 – 1500 V Integrated AsB® detector
Chamber	330 mm (Ø) x 270 mm (h) 15 accessory ports for various options including STEM, 4QBSD, EBSD, EDS, WDS CCD-Camera with IR-illumination Charge compensation with in-situ cleaning (optional)	
Image processing	Resolution: Up to 6144 x 4608 pixel (32 k x 32 k pixel optional available) A large number of integration and averaging modes available	
Image display	Single 19'' TFT monitor with SEM image displayed at 1024 x 768 pixel	
System control	Intergrated SmartSEM® user interface based on Windows® operating system controlled by mouse keyboard, joystick and control panel (optional)	

Table 17 : Microprobe analysis of magnetite and ilmenite of Fabian ore body (Lund et al., 2009)

	Fabian Ore						
Mineral	Magnetite						Ilmenite
Sample no.	V35-1-259	584A-7	V20-1-294	BC6-3-800	V40-1-372	586C-478	V40-1-376
Texture	Fine grain	Fine grain	Fine grain	Coarse grain	Coarse grain	Coarse grain	
FeO (tot)	94.436	93.569	93.144	94.118	93.452	93.881	41.95
Al_2O_3	0.014	0.112	0.096	0.134	0.471	0.24	0.047
TiO_2	0.021	0.059	0.014	0.012	0.506	0.14	47.256
V_2O_3	0.172	0.146	0.128	0.031	0.105	0.043	0.322
MgO	0	0.11	0.067	0.104	0.288	0.203	2.609
P_2O_5	0	0	0	0	0	0	0
CaO	0	0	0	0	0	0	0
SiO_2	0	0	0	0	0	0	0
MnO	0	0.053	0	0.009	0	0.009	0.286
NiO	0	0	0.009	0	0	0	0
Cr_2O_3	0.033	0.005	0.044	0	0.034	0.004	0
ZnO	0	0.024	0	0	0	0.036	0
CuO	0.024	0.067	0	0.051	0.008	0	0.021
Total	94.7	94.145	93.502	94.459	94.864	94.556	92.491
Fe_2O_3 (calc)	70.016	69.496	69.105	69.958	68.789	69.631	-
FeO (calc)	31.435	31.036	30.963	31.169	31.555	31.226	-

Fe^{2+} and Fe^{3+} recalculated

Table 18 : Microprobe analysis of magnetite and ilmenite from Fabian ore breccia (Lund et al., 2009)

	Fabian Ore breccia							
Mineral	Magnetite							Ilmenite
Sample no.	V38-1-2	V11-1-648	V17-2-503	H20-1-704	V29-3-186	V49-2-126	AP1-8 729	V38-1-4
Type	Massive	Massive	Massive	Inclusion	Inclusion	Inclusion	Inclusion	
FeO (tot)	93.876	93.282	94.25	93.507	94.01	93.676	93.191	46.431
Al_2O_3	0.178	0.055	0.069	0.063	0.069	0.002	0.059	0.018
TiO_2	0.026	0.024	0.019	0.054	0.009	0.021	0.009	52.282
V_2O_3	0.125	0.03	0.004	0.023	0.248	0.133	0.031	0.392
MgO	0	0.106	0.057	0	0	0	0	0.262
P_2O_5	0	0	0	0	0	0	0	0
CaO	0	0	0	0	0	0	0	0
SiO_2	0	0	0	0	0	0	0	0
MnO	0	0	0	0	0.016	0.032	0	2.016
NiO	0	0.003	0	0	0	0.003	0.009	0
Cr_2O_3	0.025	0.062	0.045	0.025	0.019	0.047	0.009	0.001
ZnO	0	0.021	0.022	0.035	0	0	0.009	0.01
CuO	0.021	0.017	0.054	0.055	0.058	0.082	0.03	0.036
Total	94.251	93.6	94.52	93.762	94.429	93.996	93.347	101.448
Fe_2O_3 (calc)	69.502	69.301	70.008	69.323	69.688	69.527	69.143	-
FeO (calc)	31.337	30.924	31.256	31.129	31.304	31.115	30.975	-

Fe^{2+} and Fe^{3+} recalculated

Table 19 : statistics and t-test for magnetite between SEM and EMC

t, F and Kolmogorov-Smirnov tests of difference in means, variances and distribution							
Basic statistics							
	Case	Modal.Mgt IN	Modal.Fe oxi	Rel.diff.%			
	N	14.	14.	0.00			
	Average	52.4	51.6	-1.51			
	Standard deviation	26.94	28.21	4.73			
	Variance	725.6	796.0	9.69			
	CV%	51.4	54.7	6.34			
	MIN	9.16	8.45	-7.78			
	MAX	90.5	90.5	0.0			
	MEDIAN	51.6	51.1	-0.92			
T-test (to test are the averages significantly different when variances are equal)							
	T	0.08					
	PROB% (significance)	93.8	Difference is not statistically significant				
T-test (to test are the averages significantly different when populations have unequal variances)							
	T	0.08					
	PROB% (significance)	94.0	Difference is not statistically significant				
F-test (to test are the variances significantly different)							
	F	1.10					
	PROB% (significance)	87.0	Difference is not statistically significant				
Paired T-test (to test are the averages significantly different in paired samples)							
	T	1.22					
	PROB% (significance)	24.36	Difference is not statistically significant				
Kolmogorov-Smirnov test (to test if continuous distributions are equal)							
	D	0.14					
	PROB% (significance)	99.9	Difference is not statistically significant				

Table 20 : statistics and t-test for specific gravity between SEM and EMC

t, F and Kolmogorov-Smirnov tests of difference in means, variances and distribution							
Basic statistics							
	Case	name.EMC	name.mea	Rel.diff.%			
	N	5.	5.	0.00			
	Average	3.81	3.75	-1.62			
	Standard deviation	0.79	0.76	-3.19			
	Variance	0.62	0.58	-6.29			
	CV%	20.65	20.32	-1.60			
	MIN	2.87	2.74	-4.40			
	MAX	4.76	4.71	-0.89			
	MEDIAN	3.49	3.62	3.72			
T-test (to test are the averages significantly different when variances are equal)							
	T	0.14					
	PROB% (significance)	89.1	Difference is not statistically significant				
T-test (to test are the averages significantly different when populations have unequal variances)							
	T	0.13					
	PROB% (significance)	90.3	Difference is not statistically significant				
F-test (to test are the variances significantly different)							
	F	1.07					
	PROB% (significance)	95.1	Difference is not statistically significant				
Paired T-test (to test are the averages significantly different in paired samples)							
	T	1.02					
	PROB% (significance)	36.5	Difference is not statistically significant				
Kolmogorov-Smirnov test (to test if continuous distributions are equal)							
	D	0.20					
	PROB% (significance)	100.0	Difference is not statistically significant				

Table 21 : Statistics for model 1

Modeled	Explains	R	Eq	Multipl.	Constant	VAR	%Variance
[Sheet1].[Rc]					9.060	0.345	
	[Sheet1].[CS]	-0.807	-2.367957E-02*x + 1.001035	-0.024	1.001	0.120	65.207
	[Sheet1].[Grain size µm]	-0.937	-6.033543E-03*x + 0.5939118	-0.006	0.594	0.015	30.552
							95.760
5 rows analysed							
Following variables used	**R**						
[Sheet1].[CS]	-0.808						
[Sheet1].[Grain size µm]	-0.283						

Table 22 : Statistics for model 2

Modeled	Explains	R	Eq	Multipl.	Constant	VAR	%Variance
[Sheet1].[Rc]					9.060	0.345	
	[Sheet1].[Tr wt%]	-0.918	-9.070167E-02*x + 0.9786878	-0.090	0.979	0.054	84.270
	[Sheet1].[Ap wt%]	-0.310	-0.2024837*x + 7.613894E-02	-0.202	0.076	0.049	1.513
	[Sheet1].[Ab wt%]	-0.373	-4.41276E-03*x + 8.921862E-02	-0.004	0.089	0.042	1.985
							87.768
5 rows analysed							
Following variables used	**R**						
[Sheet1].[Ab wt%]	-0.915	5					
[Sheet1].[Tr wt%]	-0.918	5					
[Sheet1].[Ap wt%]	0.67	5					

Table 23 : Statistics for model 3

Modeled	Explains	R	Eq	Multipl.	Constant	VAR	%Variance
[Sheet1].[Wi[kWh/t]]					5.0834	0.020	
	[Sheet1].[PLT]	0.780	0.1048348*x - 0.2717945	0.105	-0.2728	0.008	60.927
	[Sheet1].[Grain size [µm]]	0.874	1.429517E-03*x - 0.1407145	0.001	-0.141	0.002	29.839
							90.766
5 rows analysed							
Following variables used	R						
[Sheet1].[Grain size [µm]]	0.544	5					
[Sheet1].[PLT]	0.781	5					

Table 24 : Statistics for model 4

Modeled	Explains	R	Eq	Multipl.	Constant	VAR	%Variance
[Sheet1].[Wi]					5.083	0.020	
	[Sheet1].[Ab wt%]	0.795	5.968641E-03*x - 0.1206757	0.006	-0.121	0.007	63.174
	[Sheet1].[Ap wt%]	0.371	0.0888279*x -3.340153E-02	0.089	-0.033	0.006	5.066
	[Sheet1].[Or wt%]	0.379	7.551853E-03*x - 4.116171E-02	0.007	-0.041	0.005	4.576
							72.816
5 rows analysed							
Following variables used	R						
[Sheet1].[Ab wt%]	0.795	5					
[Sheet1].[Tr wt%]	0.739	5					
[Sheet1].[Or wt%]	0.781	5					
[Sheet1].[Ap wt%]	-0.498	5					

Table 25 : Statistics for model 5

Modeled	Explains	R	Eq	Multipl.	Constant	VAR	%Variance
[Sheet1].[Lib %]					89.328	36.291	
	[Sheet1].[Tr wt%]	-0.991	-1.004174*x + 10.83521	-1.004	10.835	0.5984	98.351
	[Sheet1].[Ap wt%]	0.363	0.7877654*x -0.2962199	0.787	-0.296	0.5193	0.218
	[Sheet1].[Or wt%]	0.390	7.053095E-02*x - 0.3844321	0.0705	-0.384	0.44	0.218
							98.787
5 rows analysed							
Following variables used	R						
[Sheet1].[Ab wt%]	-0.955	5					
[Sheet1].[Tr wt%]	-0.992	5					
[Sheet1].[Or wt%]	-0.919	5					
[Sheet1].[Ap wt%]	0.904	5					